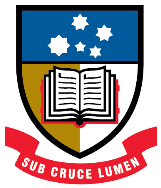

THE UNIVERSITY of ADELAIDE

Ionic Liquids for High Performance Solid-state Lithium Metal Batteries

Tianhua Chen

Thesis submitted for the degree of Doctor of Philosophy

School of Chemical Engineering and Advanced Materials

Faculty of Engineering, Computer and Mathematical Sciences

The University of Adelaide, Australia

April 2023

BLANK PAGE

TABLE OF CONTENTS

ABSTRACT

The quest for high energy storages has driven the growth of high-performance lithium metal batteries, but this has also raised serious safety concerns. In response, ionic liquids (ILs) have become a popular choice due to their high ionic conductivity, non-flammability, and ability to facilitate the formation of stable solid electrolyte interphase (SEI) layer. Understanding the challenges faced by lithium metal batteries and the role of ILs in them is vital to improving their performance. This study examines how ILs affect key factors such as ionic conductivity, Li^+ ion transference number, electrochemical stability window, and the lithium metal anode/electrolyte interface. It also investigates the use of ILs with different types of cathodes, such as, including $LiFePO_4$ (LFP), $LiNi_{0.6}Co_{0.2}Mn_{0.2}O_2$ (NCM622), $LiNi_{0.8}Co_{0.1}Mn_{0.1}O_2$ (NCM811), and $LiCoO_2$ (LCO).

A comparative study was made on the development of ionic liquid involved solid-state electrolyte to achieve high performance solid-state lithium metal batteries. Three key aspects are addressed in this thesis:

Firstly, an ionic liquid was injected into metal-organic framework (MOF-5) nanomaterials to improve the poly(ethylene oxide) (PEO) solid electrolyte and enhance the performance of solid-state lithium batteries. The results show that the formed nano-wetted interface structure can greatly improve the interface stability, reduce the interface impedance, and inhibit the Li dendrite growth. The MOF structure accelerates the transport of lithium ions by ion confinement effect on anions inn the IL and large-size cations, thereby improving the lithium transference number.

As a consequence, the overall performance of solid-state Li metal battery has been improved.

Secondly, using electrospun polyacrylonitrile (PAN) membranes, the ionic liquid and liquid electrolyte monomers are combined and in-situ polymerized to form a polymer electrolyte. In this system, the decomposition of the ionic liquid is involved in the formation of the solid electrolyte interface (SEI) membrane. Through analysis at different current densities of the Li symmetric cell, it was found that the ionic liquid can significantly suppress the formation and growth of lithium dendrites. Moreover, due to the increased lithium affinity of the ionic liquid, Li-ion transport is accelerated, resulting in a high lithium transference number, which improves conductivity and allows the battery performing within a wide temperature range. Additionally, $LiFePO_4$/Li batteries can run steadily for 1000 cycles at high rate of 2 C.

Thirdly, through the combined action of fluorine-containing additives and ionic liquids, the in-situ formed polymer lithium battery can operate stably at high voltage. Analysis has shown that the SEI membrane in this system is rich in LiF, which effectively increases interface stability. The ionic liquid enhances the electrochemical window of the polymer electrolyte, allowing this system to match high-voltage cathodes. Moreover, IL is beneficial to improve the interfacial contact and provide stable components for the interfacial layer. Results show that at room temperature, the NCM811/cell can perform at 1C, and the LCO/Li cell has good cycling performance at 4.45 V, increasing the battery energy capacity.

This project contributes to the understanding of the application of ionic liquids in solid-state electrolytes, the knowledge of which can be used to design the solid-state electrolyte. The

chemical compositions of the SEI layers formed on the surface of Li anode from this experimental work also provide valuable data that can be used in the future studies.

HDR THESIS DECLARATION

I certify that this work contains no material which has been accepted for the award of any other degree or diploma in my name, in any university or other tertiary institution and, to the best of my knowledge and belief, contains no material previously published or written by another person, except where due reference has been made in text. In addition, I certify that no part of this work will, in the future, be used in a submission in my name for any other degree or diploma in any university or other tertiary institution without the prior approval of the University of Adelaide and where applicable, any partner institution responsible for the joint award of this degree.

The author acknowledges that copyright of published works contained within this thesis resides with the copyright holder(s) of those works.

I also give permission for the digital version of my thesis to be made available on the web, via the University's digital research repository, the Library Search and also through web search engines, unless permission has been granted by the University to restrict access for a period of time.

I acknowledge the support I have received for my research through the Beacon of Enlightenment PhD Scholarship to undertake PhD at the University of Adelaide and Institute of Process Engineering, Chinese Academy of Sciences.

20/04/2023

Tianhua Chen | Date

ACKNOWLEDGEMENTS

I express my sincere appreciation to all those who have accompanied and assisted me during my PhD journey at The University of Adelaide and Institute of Process Engineering of Chinese Academy of Sciences. I would like to express my heartfelt gratitude to my supervisor, Prof. Dusan Losic, whose unwavering passion, exceptional guidance, and motivational influence have been instrumental in pushing me beyond my limits and helping me achieve my goals. I appreciate greatly to my supervisors in China, Shimou Chen, Haitao Zhang and Suojiang Zhang for supporting me sail so far away. I sincerely thank Jian Wang for giving me some good ideas on improving my deep understanding on the research.

I would like to extend special thanks to Jiaxin Liu for helping me conduct my experiment. My sincere gratitude also goes to Thanks the support from Beijing Key Laboratory of Ionic Liquids Clean Process, and School of Chemical Engineering and Advanced Materials supporting staff, ECMS technical staff as well as the experts from Adelaide Microscopy and Biogeochemistry and Stable Isotope Facility for their technical support.

I gratefully acknowledge the Australian and Chinese Government for providing me research training with Beacon of Enlightenment PhD Scholarship to undertake PhD at the University of Adelaide and Institute of Process Engineering, Chinese Academy of Sciences. This work was partly supported by National Natural Science Foundation of China (Grant No. 51922099), Innovation Academy for Light duty Gas Turbine, Chinese Academy of Sciences (Grant No. CXYJJ20-MS-05), Natural Science Foundation of Hebei Province for Distinguished Young

Scholars (E2020103052).

I would like to thank my family for always being there to provide a stable foundation for my life and future. I thank them for their encouragement, patience and faith in me throughout my PhD study. I would also like to thank my friends for their emotional support and encouragement. Thanks to those who have made contributions in safeguarding the health of people around the world during the past three years of the COVID-19 virus. Finally, I thank myself for always cheering up and have faith in the future.

PREFACE

This thesis is submitted as a portfolio of publications according to the 'Specifications for Thesis 2023'of the University of Adelaide. This thesis contains the following list of publications during my PhD candidature. The outcomes generated during my PhD candidature include 14 publications, 11 accepted for publication and 3 under reviewed journal articles (4 first-authored; 9 co-authored).

The journals in which the articles were published and to be submitted are given in the following tables.

The main body of this work is listed in the following journal papers:

1. **Chen, T.**, Chen, S., Chen, Y., Zhao, M., Losic, D., Zhang, S. Metal-organic frameworks containing solid-state electrolytes for lithium metal batteries and beyond. *Materials Chemistry Frontiers* **(IF=8.683)**, 2021. 5(4): p. 1771-1794. (Chapter 2)

2. **Tianhua Chen**, Jian Wang, Simeng Wang, Jin Li, Dusan Losic, Shimou Chen. Incorporating Metal-Organic Framework with Ionic Liquid as Ion Diffusion Booster for Flexible Solid-State Lithium Metal Batteries, *Nano Research* (**IF=8.897,** to be submitted) (Chapter 3)
3. **Tianhua Chen**, Jian Wang, Jin Li, Dusan Losic, Haitao Zhang. Ionic Liquid Boosting the Electrochemical Stability of a Poly(1,3-dioxolane) Solid Electrolyte for High-voltage Solid-state Lithium Batteries, *ChemSusChem* (**IF=9.140**, to be submitted) (Chapter 4)

4. **Tianhua Chen**, Jiaxin Liu, Jian Wang, Dusan Losic, Haitao Zhang, Suojiang Zhang, Ionic liquid boosting the electrochemical stability of a poly(1,3-dioxolane) solid electrolyte for

high-voltage solid-state lithium batteries, *Journal of Power Sources* (**IF=9.794,** to be submitted) to be submitted) (Chapter 5)

5. Yong Chen, Kaihua Wen, **Tianhua Chen**, Xiaojing Zhang, Michel Armand, Shimou Chen, Recent progress in all-solid-state lithium batteries: The emerging strategies for advanced electrolytes and their interfaces, *Energy Storage Materials* **(IF=20.831)**, 2020, 401-433

6. Kaihua Wen, Xin Tan, **Tianhua Chen**, Shimou Chen, Suojiang Zhang, Fast Li-ion transport and uniform Li-ion flux enabled by a double–layered polymer electrolyte for high performance Li metal battery. *Energy Storage Materials* **(IF=20.831)**, 2020. 32: p. 55-64

7. Jin Li, Feng Huo, **Tianhua Chen**, Hanwen Yan, Yaxi Yang, Suojiang Zhang, Shimou Chen. In-situ construction of stable cathode/Li interfaces simultaneously via different electron density azo compounds for solid-state lithium metal batteries. *Energy Storage Materials* **(IF=20.831)**, 2021. 40: p. 394-401

8. Jin Li, Feng Huo, Yaxi Yang, **Tianhua Chen**, Yingyue Cui, Yingjun Cai, Haitao Zhang, Constructing stable lithium interfaces via coordination of fluorinated ether and liquid crystal for room-temperature solid-state lithium metal batteries. *Chemical Engineering Journal* **(IF= 16.744)**, 2022. 433: p. 133562.

9. Shuxin Yan, Yanlei Wang, **Tianhua Chen**, Zhongdong Gan, Shimou Chen, Yuwen Liu, Suojiang Zhang, Regulated interfacial stability by coordinating ionic liquids with fluorinated solvent for high voltage and safety batteries, *Journal of Power Sources* **(IF=7.467)**, 2021. 491: p. 229603.

10. Yingyue Cui, Yanlei Wang, Shijie Gu, Cheng Qian, **Tianhua Chen**, Shimou Chen, Jianling Zhao, Suojiang Zhang, An effective interface-regulating mechanism enabled by non-sacrificial additives for high-voltage nickel-rich cathode. *Journal of Power Sources* **(IF=7.467)**, 2020. 453: p. 227852.

11. Xiaoyang Wang, Kaihua Wen, **Tianhua Chen**, Shimou Chen, Suojiang Zhang, Supercritical fluid-assisted preparation of Si/CNTs@FG composites with hierarchical conductive networks as a high-performance anode material. *Applied Surface Science* **(IF=7.392)**, 2020. 522: p. 146507.

12. Rumeng Wang, Dongjin Feng, **Tianhua Chen**, Shimou Chen, Yuwen Liu, Mussel-inspired polydopamine treated Si/C electrode as high-performance anode for lithium-ion batteries. *Journal of Alloys and Compounds* (**IF=6.371)**, 2020. 825: p. 154081.

13. Dongjin Feng, Shimou Chen, Rumeng Wang, **Tianhua Chen**, Shijie Gu, Jielong Su, Tao Dong and Yuwen Liu, Mixed Lithium Salts Electrolyte Improves the High-Temperature Performance of Nickel-Rich Based Lithium-Ion Batteries. *Journal of The Electrochemical Society* **(IF=7.392)**, 2020. 167(11): p. 110544.

CHAPTER 1:

Introduction

1.1 Background

As lithium-ion batteries continue to advance from their use in consumer electronics to electric vehicles and industrial energy storage systems, there is an increasing demand for improved energy density, power density, cycling life, and safety.[1-3] In particular, the use of organic electrolytes in traditional lithium-ion batteries has led to significant safety hazards in new energy vehicles, with frequent reports of battery-related fires and explosions due to issues such as flatulence, leakage, and thermal runaway.[4-6] Organic electrolytes are prone to decomposition, which can cause overheating of the electrolyte due to abnormal events such as overcharging and internal short circuits, ultimately resulting in spontaneous combustion or explosion. Therefore, the safety issues of lithium-ion batteries must be urgently addressed to promote their practical applications in portable devices and larger-scale energy storage systems. The industry's pressing need for high battery safety has greatly accelerated the research and development of solid-state lithium metal batteries (SSLMB), which have gained increasing attention in recent years.

In contrast to traditional lithium-ion batteries, SSLMBs do not rely on excess organic electrolytes in their preparation process. Instead, SSLMBs mainly use solid-state electrolytes (SSEs), which are more stable and do not pose a risk of danger due to overcharging, damage, or overuse as is the case with organic electrolytes. The new generation of SSLMBs is also more malleable in shape, greatly increasing the flexibility of styling design, making it easier to match product requirements and effectively optimize product performance. The use of solid electrolytes in lithium batteries can also inhibit the growth of dendrite lithium and avoid issues such as liquid leakage by dissolving the plasma.[7-9] By using SSLMB technology, it is possible to create thinner

batteries with higher energy density and smaller form factors (below 0.1 mm thick). [10-14]

ASLMBs have gained increasing attention in both industry and academic research and are seen as cutting-edge technology for the next generation of power batteries. They are expected to address two major issues currently affecting the power battery industry: safety risks and limited energy density.[15-17] Automakers and battery suppliers are leading the way in research, development, and testing of solid-state batteries, and are even announcing schedules for mass production. Material manufacturers, such as Mitsubishi Gas Chemical, Toray, and Sumitomo Chemical, are also optimistic about the market potential of solid-state batteries and are accelerating their research and development efforts in related materials. Mitsubishi Gas Chemical aims to develop a solid-state electrolyte for solid-state batteries by 2020 and bring the next generation of battery materials to market as soon as possible. In 2018, Japan's New Energy Industry Technology Development Organization (NEDO) plans to invest 10 billion yen over five years to support solid-state battery development projects for Toyota and other companies. Overall, solid-state batteries are seen as the next generation of battery technology with broad optimism among researchers in both industry and academia field.

Ionic liquids (ILs) exhibit great potential for use in lithium metal batteries and have versatile roles due to their distinct physicochemical properties compared to molecular solvents and inorganic salts.[18] They can act as electrolyte solvents, replacing carbonate solvents, to enhance battery safety as they are non-volatile and non-flammable.[19] Alternatively, they can be added to conventional electrolytes with low viscosity to create composite electrolytes with both high conductivity and safety.[20] Furthermore, they can be incorporated into polymer frameworks,

ionic gels or porous networks to produce solid electrolytes that possess exceptional electrical conductivity and mechanical properties.[21] ILs can also take part in reactions with lithium metal electrodes as an electrolyte component, forming a functional solid electrolyte interphase (SEI) film containing specific elements like F and N.[22] IL-derived polymers can form a protective film on the electrode surface directly to safeguard the lithium metal anode.[23, 24] Lastly, ILs can serve as wetting agents to stabilize the interfacial properties between solid-state electrolytes and electrodes.[25]

1.2 Scope and structure of the Thesis

This thesis is structured into six Chapters. The following is a summary of the topics covered in each chapter.

In the first chapter, the introduction of the thesis and chapter summary is presented summary is presented. Chapter 2 presented as the first published journal paper (review) chiefly summarizes strategies toward constructing advanced solid-state electrolyte and improving the interfacial compatibility of all batteries with the optimizations of every battery component, which are related to energy densities as well as rate densities. Secondly, it illuminates strategies toward coupling matched electrodes for long cycling; Thirdly, the review concisely some integrated strategies for enhancing rate property. Moreover, some possible research directions, useful guidance and insights for the development of new strategies have been proposed by in-depth discussion and reasonable analysis, which played a crucial guiding role in the future research tendency.

Chapter 3 presented as the second journal paper (to be submitted to Nano Research) comprehensively discuss the role of ionic liquids on wetting the interface contact between electrolyte and electrodes of solid-state lithium metal batteries. The research involved creating a composite electrolyte (pDOL-py electrolyte) by incorporating anion-immobilized IL@MOF-5 nanoparticles into a PEO/LiTFSI matrix using a universe blade method. This resulted in an electrolyte with a low active energy and conductivity level that was ten times higher than that of PEO electrolytes. The pDOL-py electrolyte prevented dendrite formation on Li anodes during Li deposition and promoted stable interfacial contact. The anion-immobilized electrolytes also formed a stable CEI layer in Li metal cells with $LiFePO_4$ and NCM622 cathodes, exhibiting excellent rate and long cycling performances. The findings suggest that anion-immobilized electrolytes have great potential for developing high-performance lithium metal batteries.

Chapter 4 presented as the third journal paper (to be submitted to ChemSusChem) investigate the effect of IL ($Py_{13}TFSI$) on improving the cycling stability of lithium metal batteries. This study also investigated the contributions of IL on the SEI layer and the working temperature range.

Chapter 5 presented as the fourth journal paper (to be submitted to Journal of Power Sources), studies the application of IL ($PP_{14}TFSI$) in enhancing the voltage and capacity of lithium metal batteries matched with $LiCoO_2$ (4.45 V) and $LiNi_{0.8}Co_{0.1}Mn_{0.1}O_2$ (4.3 V) cathode at room temperature.

Chapter 6 comprises the conclusions of this study, together with recommendations for future

directions, based on the research findings.

References for Chapters 3, 4 and 5 are listed at the end of each chapter. References for Chapter 2 are listed at the end of the chapter and the attached journal paper.

CHAPTER 2:

Literature Review

2.1 Introduction

Resolving the stability issues of the lithium metal anode is crucial for achieving safe and practical use of metal lithium batteries. Ionic liquids, which consist of organic cations and inorganic/organic anions, exhibit highly desirable properties such as low volatility, high ionic conductivity, good thermal stability, low flammability, and electrochemical stability. Poly(ionic liquids), ionic gels, and related derivatives also possess similar properties to ionic liquids, making them highly promising for protecting the lithium anode and receiving significant attention, as shown in Fig. 1. A thorough understanding of the role of ionic liquids in safeguarding the lithium anode is essential for expanding the practical applications of ionic liquids in lithium metal batteries. This literature review provides practical guidance in this area by systematically summarizing the current challenges of lithium metal anodes and the efforts made to overcome them using ionic liquids. In addition, an article published in this part displays the influence of MOF-based electrolytes, including ionic liquid@MOF- based system, on the lithium metal batteries.

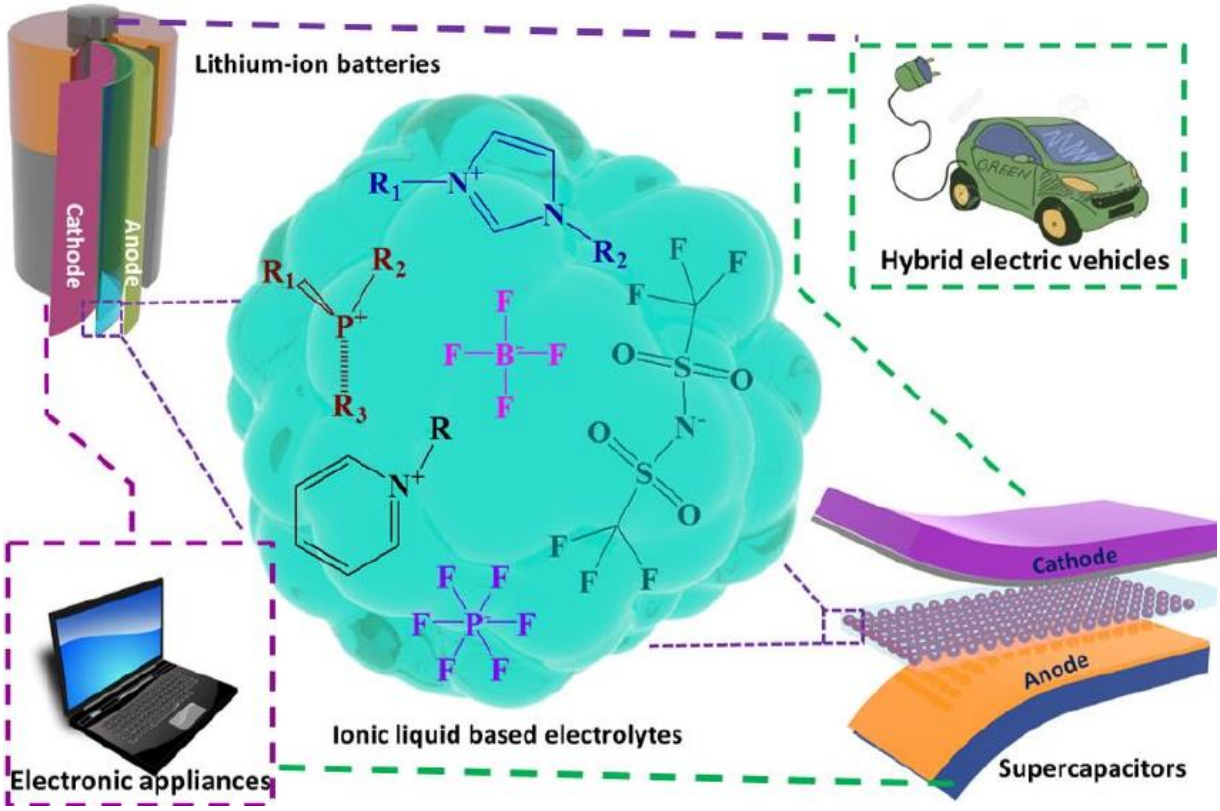

Figure 1. Schematic representation of ionic liquid (IL)-based electrolytes applications in energy storage devices[26]

2.2 Solid-state electrolyte

Solid-state electrolytes offer several advantages, including good film formation, stability, flexibility, high safety, and low cost. These solid-state electrolytes can be used as a separator between the cathode and anode electrodes, as well as an electrolyte for transmitting ions. As a result, SSLMBs offer several advantages, including:

(1) High working voltage, long cycling life, and high energy capacity[27, 28], as shown in Table 1.

Table 1 Comparison of SSLB and other batteries

Battery type	Output voltage (V)	Energy capacity ($Wh \cdot kg^{-1}$)	Energy density ($Wh \cdot L^{-1}$)	Cycling life (h)
Lead-acid	2.0	35	70	200~250
Nickel-chrome	1.2	50	80	400~500
Lithium-ion	3.6	150	240	>1000
ASSLMB	4.0	200	450	>4000

(2) Batteries of almost all shapes or sizes can be made and can be directly integrated into circuits by different processing methods, such as in-situ preparation and the 3D printing technology that has emerged in recent years. [29-32] This technology can process the electrolyte into the desired shape, saving raw materials with improved performance. However, the technology is not sophisticated yet.

(3) It can be charged and discharged thousands of times with slow self-discharge rate, accompany with no memory effect.

(4) Stable electrochemical performance feather with high safety.

(5) Wide operation temperature range, and it can be stable between -40 ~ 150 °C or even wider.[33]

According to the aforementioned analysis, the stability of the lithium metal anode is significantly impacted by the electrolyte used. In particular, the use of carbonate-based liquid electrolytes results in thermodynamic instability of the lithium metal anode, which leads to the growth of

lithium dendrite, the formation of dead lithium, and the consumption of the electrolyte in an irreversible process. These issues can cause serious safety concerns and result in a decrease in capacity over time. To mitigate these concerns, solid-state electrolytes have been proposed as an alternative to liquid electrolytes due to their reduced risk of leakage and flammability. Additionally, high-concentration electrolytes have shown promise in suppressing the growth of lithium dendrite and enhancing cycling stability. Another approach to stabilizing the lithium metal anode is through the use of electrolyte additives, which can aid in the formation of a stable SEI film or affect the behavior of Li^+ ion plating and stripping. Additives are widely used and considered to be a convenient method for stabilizing lithium metal anodes.

2.3 Ionic liquids

Ionic liquids (ILs) are a type of molten salts that remain in liquid state at room temperature, and they consist of cations and anions. The first known IL, which was discovered by Walden in 1914, was a nitroethylammonium ($C_2H_5NH_4NO_3$) ionic liquid with a low melting point of 12 °C. However, this IL was not widely recognized at the time due to its unstable properties.[34] Until to the 1980s and 1990s did researchers begin to focus on ILs. In 1992, Wilkes and Zaworotko discovered the 1-ethyl-3-methylimidazolium tetrafluoroborate ($EMIBF_4$) ionic liquid, which was stable in air and water. This was followed by Bonhote et al.'s introduction of the trifluoromethylsulfonimide ($TFSI^-$) anion in 1996, which significantly expanded the selection of cations available for ionic liquids.[35, 36] Currently, there are thousands of types of ILs available, and research and applications related to their properties are constantly expanding. These include separation and purification, polymer dissolution and regeneration, organic catalytic synthesis

reactions, and electrochemical electrolytes, among others.[37, 38]

The diversity of ILs is made possible by the abundance of available anions and cations. Figure 2 below displays some of the commonly used anions and cations in ILs.[38] Common cations used in ILs include ammonium salts (such as imidazole and pyrrolyl groups, as well as saturated alkane groups), phosphine salts, and sulfur salts. Anions used in ILs include $(RSO_2)_n^-$, $CF_3SO_3^-$, RSO_4^-, $(CN)_{2n}$, $PF_6BF_4^-$, $AlCl_4^-$, $CuCl_2^-$, etc. By adjusting the composition and structure of the anions and cations in ILs, their physicochemical properties can be finely tuned to exhibit different desirable characteristics.

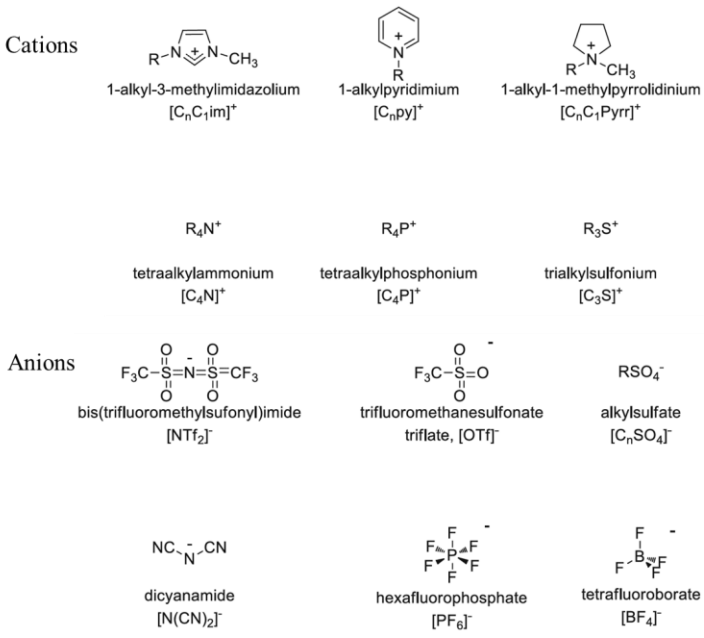

Figure 2. Some cations and anions of commonly used ionic liquids[38]

The design flexibility of ILs allows for the creation of "task-specific" or "tailor-made" ILs by adjusting the combination of anions and cations, or by grafting appropriate functional groups. These ILs have shown promising applications in areas such as separation and purification,

nuclear waste recycling, and special optical materials. Additionally, the combination of ILs with existing technologies such as supercritical fluids, electrochemistry, and microelectronics has expanded their development space and improved their functionalities. Research on ILs has rapidly expanded beyond the development of "clean" or "green" chemistry and chemical fields to include functional materials such as electro-optical and optoelectronic materials, lubricating materials, energy storage such as lithium-ion/metal batteries and beyond, key materials for solar cells, and resources and environment-related applications like natural gas purification and lignin degradation.[39] In addition, interdisciplinary research at the intersection of life sciences and ILs has also emerged as a promising area for the development of science and technology.

2.4 Applications of ionic liquids in solid-state lithium metal batteries

The electrochemical properties include electrochemical stabilities, Li plating/stripping, Li^+ transference number, and interfacial contact between electrolyte and electrodes.[40] It is essential to achieve high ionic conductivity and Li^+ ion transfer number at room temperature when using ionic liquid electrolytes. The ionic conductivity of ionic liquids is a little lower than organic liquid electrolytes.[41] In liquid electrolytes, the ionic liquid's high viscosity can be reduced by adding an organic solvent, which increases its ionic conductivity. In composite quasi-solid-state electrolytes, the interaction between the ionic liquid and inorganic or organic materials enhances ion conductivity and migration number. Fig. 3 displays the overall properties of the ionic liquid based lithium metal batteries.[42]

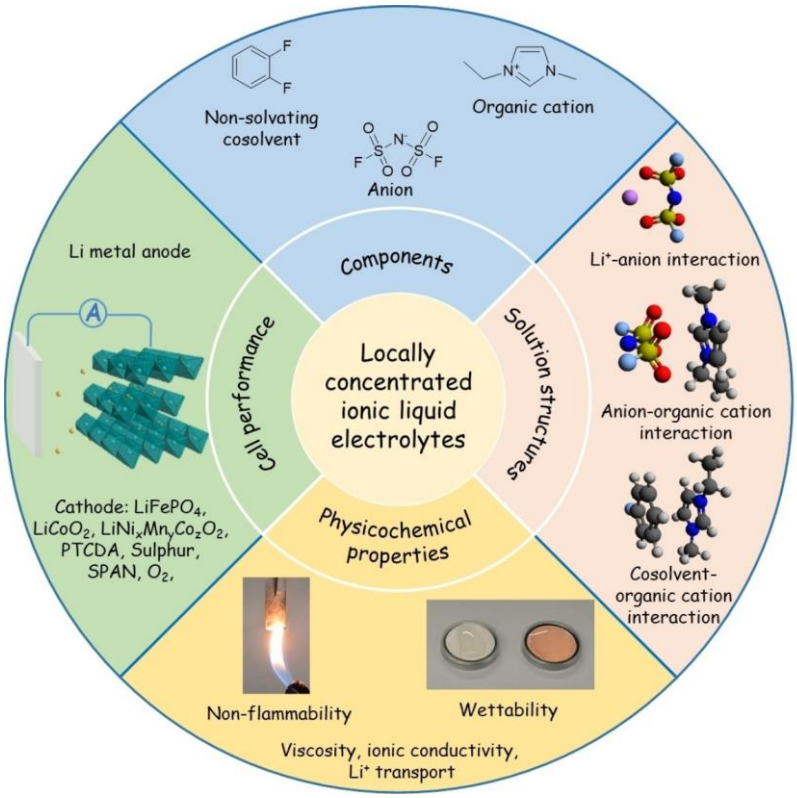

Fig. 3 Illustration of the progress of the recently developed locally concentrated ionic liquid electrolytes (LCILEs), including their physicochemical properties, solution structures, and applications in lithium-metal batteries with a variety of high-energy cathode materials.[42]

To improve the transfer number of Li-ion, various techniques have been explored in electrolyte systems. Grafting nanoparticles with ionic liquids has proven to be the most effective approach.[43] This creates a unique -like structure that forms a special Li-ion migration channel, resulting in a Li-ion transference number approximate to 1.0, much higher than other systems.[44] One method involves a composite electrolyte system consisting of PVDF-HFP and an ionic liquid.[45] The negatively charged fluorine atoms in PEO interact with the positively charged imidazole cations in the ionic liquid, resulting in the formation of a 3D cross-linked network that binds TFSI- ions, leading to improved ionization of the lithium salt and facilitating the Li^+ ion

transport. Infused of the ionic liquid electrolyte into MOF materials further enhances the migration of free Li^+ by $TFSI^-$ interacting with the unsaturated MOF metal atoms. Polymerized ionic liquids can also promote Li^+ ion transport, the movement of $TFSI^-$ is confined due to chemical interactions between groups of polymer monomer and $TFSI^-$.[25]

2.5 Research gaps

Although the application of ionic liquids in solid-state electrolytes has shown promising results, there are still some research gaps that need to be addressed. Here are a few examples:

1. Further research is needed on the interface reactions between ionic liquids and solid-state electrolyte materials. The chemical composition and properties of solid-state electrolyte materials may cause unnecessary chemical reactions with ionic liquids, affecting the stability and performance of the battery. Therefore, a deeper understanding of the interface reaction mechanism between ionic liquids and solid-state electrolyte materials is needed, and effective interface engineering strategies should be developed to address electrode interface issues.

2. An important issue facing the application of ionic liquids in solid-state electrolytes is the improvement of their thermal stability, chemical stability, and renewability. Under high-temperature or high-voltage conditions, ionic liquids may decompose or undergo chemical reactions, leading to a decline or failure in battery performance. Therefore, it is necessary to search for ionic liquids with better thermal and chemical stability, or improve their stability by adding stabilizers or other methods.

The application of ionic liquids in solid-state electrolytes is a relatively new field, and although some progress has been made, there is still some uncertainty about their ion transport mechanisms and interactions. Ionic liquids are liquids composed of ions and in solid-state electrolytes, they play a role in ion transport, making the study of ion transport mechanisms particularly important.

2.6 Aims and objectives

This study aimed to understand the effect of ionic liquids on improving the performance of solid-state lithium metal batteries, including ionic conductivity, cycling stability, Li^+ transfer number and so on. The detailed objectives are as the following:

❖ Objective 1: To identify limitations and research gaps of the stable solid-state electrolyte for solid-state lithium metal batteries with high chemical and electrochemical performance.

❖ Objective 2: To establish fundamental understanding on the effect of ILs in the solid-state electrolyte for the lithium metal batteries.

❖ Objective 3: To conduct suitable IL-based solid-state electrolytes and optimize the electrolyte system.

❖ Objective 4: To evaluate the application of IL in improving the performance of solid-state lithium metal batteries in the aspects of interfacial contact, high-voltage, energy capacity and so on.

2.7 Statement of Authorship

Statement of Authorship

Title of Paper	MOFs Containing Solid-state Electrolytes for Lithium Metal Batteries and Beyond
Publication Status	☑ Published ☐ Accepted for Publication ☐ Submitted for Publication ☐ Unpublished and Unsubmitted work written in manuscript style
Publication Details	Tianhua Chen, Shimou Chen, Yong Chen, Ming Zhao, Dusan Losic, Suojiang Zhang, MOFs Containing Solid-state Electrolytes for Lithium Metal Batteries and Beyond. Mater. Chem. Front., 2021, 5, 1771-1794

Principal Author

Name of Principal Author (Candidate)	Tianhua Chen		
Contribution to the Paper	Prepared, edited and revised the review manuscript.		
Overall percentage (%)	85%		
Certification:	This paper reports on original research I conducted during the period of my Higher Degree by Research candidature and is not subject to any obligations or contractual agreements with a third party that would constrain its inclusion in this thesis. I am the primary author of this paper.		
Signature		Date	2023/04/18

Co-Author Contributions

By signing the Statement of Authorship, each author certifies that:

i. the candidate's stated contribution to the publication is accurate (as detailed above);
ii. permission is granted for the candidate in include the publication in the thesis; and
iii. the sum of all co-author contributions is equal to 100% less the candidate's stated contribution.

Name of Co-Author	Shimou Chen		
Contribution to the Paper	Co-supervised and revised manuscript, and acted as the corresponding author.		
Signature		Date	2023/04/19

Name of Co-Author	Yong Chen		
Contribution to the Paper	Edited and revised the review manuscript.		
Signature		Date	2023/04/18

Please cut and paste additional co-author panels here as required.

Name of Co-Author	Ming Zhao		
Contribution to the Paper	Edited and revised the review manuscript.		
Signature		Date	2023/04/18

Name of Co-Author	Dusan Losic		
Contribution to the Paper	Supervised the development of work, edited and revised the review manuscript, and acted as the corresponding author.		
Signature		Date	2023/04/19

Name of Co-Author	Suojiang Zhang		
Contribution to the Paper	Co-supervised and revised manuscript, and acted as the corresponding author.		
Signature		Date	2023/04/19

2.8 Metal-organic frameworks containing solid-state electrolytes for lithium metal batteries and beyond

This section is presented as a review article as **Tianhua Chen,** Shimou Chen, Yong Chen, Ming Zhao, Dusan Losic and Suojiang Zhang, *Metal-organic frameworks containing solid-state electrolytes for lithium metal batteries and beyond*, Materials Chemistry Frontiers, 2021. Reproduced with permission.[46] Copyright (2021) Royal Society of Chemistry.

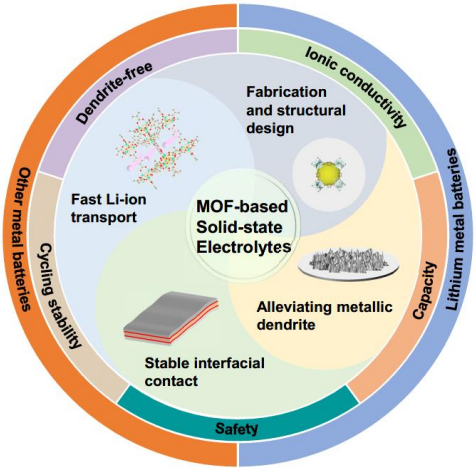

Figure 4 Graphical abstract of "*Metal-organic frameworks containing solid-state electrolytes for lithium metal batteries and beyond*". Reproduced with permission.[46] Copyright (2021) Royal Society of Chemistry.

MATERIALS CHEMISTRY FRONTIERS

REVIEW

View Article Online
View Journal | View Issue

Cite this: *Mater. Chem. Front.*, 2021, **5**, 1771

Metal-organic frameworks containing solid-state electrolytes for lithium metal batteries and beyond

Tianhua Chen,[a] Shimou Chen, *[bc] Yong Chen,[d] Ming Zhao,[c] Dusan Losic *[a] and Suojiang Zhang *[b]

Received 26th October 2020,
Accepted 13th December 2020

DOI: 10.1039/d0qm00856g

rsc.li/frontiers-materials

For solid-state Li and other metal batteries, solid-state electrolytes (SSEs) are a bridge between electrodes, and are significant in determining the behavior of batteries. Thus, constructing stable and excellent SSEs is vital for the feasible application of metal batteries. Because of their unique and multifunctional properties, namely unsaturated metal sites, tunable structure, and high specific surface area, porous metal–organic frameworks (MOFs) have been applied to SSEs to enhance the performance of metal batteries. In this review, the mechanisms of MOFs within polymer electrolytes on improving the Li-ion movement, stabilizing the solid/solid interfacial contact, and prohibiting the Li dendrite are briefly summarized. The multiple factors of MOF-based SSEs, including MOF structures, unsaturated metal sites, incorporation with ionic liquids, different organic ligands, pore size and nano/micro hierarchical structure that affect the battery performance are comprehensively discussed. Moreover, the mechanism and advancement of MOF-based SSEs for other metal batteries, including Na, Zn, and Mg batteries, are also illustrated. Eventually, new insights and future prospects in terms of MOF-based SSEs are proposed to stimulate more innovative approaches for the commercial applications of Li and other metal batteries.

[a] *School of Chemical Engineering and Advanced Materials, The University of Adelaide, Adelaide, SA 5005, Australia. E-mail: dusan.losic@adelaide.edu.au*
[b] *Institute of Process Engineering, Chinese Academy of Sciences, 100190, Beijing, China. E-mail: chenshimou@ipe.ac.cn, sjzhang@ipe.ac.cn*
[c] *State Key Laboratory of Organic–Inorganic Composites, Beijing University of Chemical Technology, Beijing, 100029, China*
[d] *School of Chemical & Environmental Engineering, China University of Mining & Technology, 100083, Beijing, China*

Tianhua Chen

Tianhua Chen received her BS degree from the University of Jinan in 2012, and Master's degree from the Institute of Process Engineering, Chinese Academy of Sciences in 2016. She is currently pursuing PhD in the School of Chemical Engineering and Advanced Materials, the University of Adelaide. Her research mainly focuses on exploring the design and applications of solid-state electrolytes for lithium metal batteries.

Shimou Chen

Prof. Shimou Chen received his BS degree from Zhengzhou University in 2002, and his PhD degree from the Shanghai Institute of Applied Physics, Chinese Academy of Sciences in 2007. In April 2008, he moved to Nagoya University as a JSPS postdoctoral fellow. From 2011 to 2012, he was a Research Associate at the National Institute for Materials Science (NIMS), Japan. In April 2012, he joined the Institute of Processing and Engineering as a professor funded by the "Hundred Talent Project" of the Chinese Academy of Sciences. His research interests include lithium-ion battery, lithium metal battery, Zn ion battery, and other advanced energy storage systems.

View Article Online

Review Materials Chemistry Frontiers

1. Introduction

The booming development of portable electronics, electric vehicles and stationary energy storage systems are calling for batteries with high energy/power densities. In consideration of the high theoretical capacity of lithium metal (3860 mA h g^{-1}) and lowest negative reduction potential (−3.04 V *vs.* standard hydrogen electrode), lithium metal batteries (LMBs) hold a promise for the next generation of energy storage technologies.[14–16] Nevertheless, the flammable and toxic commercial organic liquid electrolytes have caused safety hazards, such as several explosion accidents. In addition, the leakage of organic liquid electrolytes hinders the realization of flexibility and stretchability for some soft applications.[18–21] The solid-state electrolytes (SSEs) with inorganic materials or polymers as matrices are one of the key components in LMBs that determine the performance of LMBs. During past decades, manifold efforts have been made to enhance the electrochemical behavior of SSEs, for instance, improving the ionic conductivity,[24–27] stabilizing the interfacial contact between electrodes and SSEs[29–31] and the prevention of lithium dendrites.[32–34] However, substantial improvements on the SSEs properties are still urgent, driven by the ever increasing high energy/power requirements for practical applications.

Metal–organic frameworks (MOFs) are a kind of porous crystalline solids consisting of metal ions linked through various multi-functional organic ligands to build a vigorous multi-dimensional skeleton.[36,37] Due to their outstanding properties, such as high crystallinity, uniform pore sizes, large surface area, uniform and controllable morphologies, and excellent thermal stability, MOFs and their derivatives are widely investigated and applied in the realms of gas storage and separation, water purification, catalysis, energy storage systems (such as electrodes of the rechargeable batteries),[39,40] modification of separators,[11,41] supercapacitors,[42,43] oxygen electrocatalysts,[46] solar cells[47] and sensors.[49] They can be manageably converted into multicomponent systems, such

Yong Chen

Yong Chen obtained his BS degree from the University of South China in 2012. He is currently working as a graduate student (towards a Master's degree) at the School of Chemical & Environmental Engineering, China University of Mining & Technology. His research interests mainly focus on the design, synthesis and applications of novel composite polymer electrolytes for lithium metal batteries.

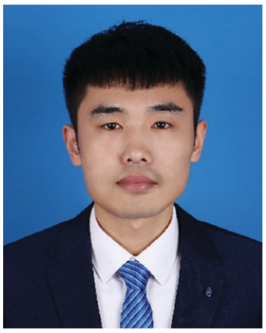

Ming Zhao

Ming Zhao received his MS degree in the College of Chemical Engineering from China University of Petroleum. He is now pursuing a PhD degree under the supervision of Prof. Jieshan Qiu in Beijing University of Chemical Engineering. His research focuses on the development of novel electrode materials, structures and electrolytes for rechargeable lithium-sulfur batteries and solid-state lithium batteries.

Dusan Losic

Prof. Dusan Losic completed his PhD degree in Nanoscience and Nanotechnology at Flinders University, followed by a one-year postdoctoral position at Monash University. He then spent 3 years as a Research Fellow at Flinders University, and was the ARC Future Fellow from 2012 at the University of Adelaide. Since 2017, he has been leading the Graphene Research Hub for Industry Transformation, the first Australian integrated research program for the translation of graphene research. His interdisciplinary research encompassing several disciplines focuses on applying nanoscience and nanotechnology to engineer new nanomaterials, processes and devices to address fundamental, health, environmental, energy and agriculture problems.

Suojiang Zhang

Prof. Suojiang Zhang obtained his Bachelor's degree from Henan University in 1986, Master's degree from Henan Normal University in 1989, and received his PhD from Zhejiang University in 1994. He is now the Deputy Director at the General of Institute of Process Engineering, Chinese Academy of Sciences. He is also the winner of the National Science Foundation for Distinguished Young Scholars (China), Chief Scientist of "973", and member of the Royal Society of Chemistry. His research interests focus on the fundamental applications of ionic liquids, which include molecular design, structure–properties, large scale preparation, industrial applications, and green integrations.

View Article Online
Materials Chemistry Frontiers Review

as carbon materials and metal-doped hybrid solid polymer systems, which often show excellent electrochemical performance. Since Long and co-workers first reported the possibility of MOFs as an addition to modify electrolyte separators for lithium batteries in 2011,[50] MOFs have been considered as a kind of functional material as fillers or ionic sieves in SSEs to realize the application of SSEs. As multifunctional materials, the special structure of MOFs enables the high performance of SSEs: (i) the porous structure as Li-ion channels can also help to fix the anions, and improve the Li-ion transference numbers (t^+). In liquid electrolytes, the cations and anions are all mobile; thus, the t^+ is usually lower (0.2–0.4).[51] On the contrary, anions can be locked in the pores or integrated with the unsaturated metal site (such as Zn_4O^{6+}) of MOFs, as a function of 'cage' to immobilize anions to improve the t^+ during cycling. Furthermore, the long-range ordered, controllable and uniformly distributed pores can host trace gases and liquids. The pores trap the byproducts generated during the battery operation process, and therefore increase the lifetime of the batteries. (ii) In particular, the MOFs components barely provide high-density mobile electrons or holes, which endow the materials with excellent electrical insulation. This insulation feature is instrumental in the electrolyte in order to separate the electrodes and prevent short circuits. (iii) The tunable synthesis of MOFs, such as the controllability to design the pore size, feasibility of grafting various functional ligands, and the expected particle size and density, is beneficial to meet the standards of a variety of specific devices.[52,53]

1.1 Principles and challenges of SSEs for Li metal batteries

Coexisting with the advantages of SSEs, the Li metal anode is considered as 'unsafe' and 'unstable' in commercial application due to the formation and growth of dendritic and mossy metal deposits, unstable interfacial contact and subsequent degradation process during the charging/discharging progress. Generally, SSEs are classified into two kinds: solid polymer electrolytes (SPEs) and inorganic ceramic electrolytes. Featured on the basis of the current progress in this field, the challenges and principles are summarized as below.

1.1.1 Principles. Tremendous strides have been made to address the issues mentioned above. However, there is still a huge room for advancement in terms of SSEs. In order to implement LMBs into practical application, efforts on the SSEs must be made in the following areas:

(i) *Effective ionic channels* to support the Li-ion transport.[54] For solid polymer electrolytes (SPEs), the relatively low ionic conductivity and narrow electrochemical window restrict their high-voltage applications. Designing effective ionic channels to bestow the SPEs with highly ionically conductive and electronically insulating properties is needed in this system.[55]

(ii) *Suitable Young's modulus*. SSEs are a key factor affecting the dendrite formation and growth. To some extent, mechanically robust SSEs with a shear modulus higher than 6 GPa can mechanically block the dendrite formation and growth on a macro level.[56,57]

(iii) *Stable interfacial contact with electrodes*.[58,59] Although inorganic ceramics have favorable ionic conductivity and high modulus, the lack of compatibility with Li has an adverse effect on the homogeneous electrodeposition of Li during cycling. How to design a fully contacted interface between electrolyte and electrode, as well as keep the contact stable, is the key for LMBs. The SPEs have the same issues to some degree.

(iv) *Stable chemical and electrochemical property of SSEs*. For the ceramic based SSEs with a high Li ionic conductivity, such as $Li_7La_3Zr_2O_{12}$ (LLZO) and $Li_{10}GeP_2S_{12}$ (LGPS), the materials tend to be oxidized and decomposed. Thus, the battery performances are compromised. The polymer SSEs are easy to be decomposed at high voltage, and lead to severe capacity decay.[60,61] Thus, stable materials are developed, and other protective strategies are explored to realize stable SSEs for high performance LMBs. The chemical and electrochemical stability of SSEs highly affect the long cycling stability and capacity of LMBs.[62]

In addition, the favorable SSEs require fillers or conductors with properties, such as the abundant surface charge, strong compatibility with electrodes, high mechanical stability, and high specific surface area, among others.

1.1.2 Challenges of SSEs

Low ionic conductivity. The function of the electrolyte is to build a channel for the lithium ion to move between the cathode and anode electrodes in the charging and discharging process. The indicator that determines the lithium ion transmission is the ionic conductivity. The level of ionic conductivity directly affects the overall impedance and rate performance of the battery.[63] For single element polymer electrolyte systems, the ionic conductivity is 10^{-5}–10^{-9} S cm^{-1}, and their stabilities at high voltage are unsatisfactory, although they possess low resistances at the electrode/electrolyte interfaces.[64] The conductivity of the sulfide electrolyte is relatively high, which is only limited to the comparison with the lowest ones. Inorganic ceramics possess higher ionic conductivities of 10^{-4}–10^{-2} S cm^{-1}.[65] Obviously, compared to commercial LIBs, the low ionic conductivity of SSEs is a tricky problem that hampers the advancement of LMBs, especially at room temperature and below.

Lithium dendrite growth. The uneven charge distribution and inevitable defects on the surface of Li metal cause the unstable Li electrodeposition, which eventually evolves into the formation of the Li dendrite.[33,34] The unexpected Li dendrite can penetrate separators or soft SPEs and cause an internal short circuit. This leads to a low coulombic efficiency and severe safety risk, thus hindering the capacity of high energy density. Furthermore, the nucleation and growth of the dendrite have a close relationship with the surface contact between the SSE and Li metal anode.[66] That is, the Li dendrites covered by the reaction outcomes of solid electrolyte interface (SEI) films during the repeated Li insertion and deinsertion process increases the interfacial resistance, which conversely accelerates the Li dendrites. Dendrite growth can be relieved by tailoring the surface of the Li metal and delicate structural design of SSEs. However, there is a long way to go to suppress the dendrite growth.

Unstable interfacial contact. Another major issue that hinders the practical applications of solid-state batteries is the large

interfacial resistance rising from the poor interfacial contact between the SSEs and the electrodes.[29,67] Because of their high crystallization, high rigidity and poor compatibility with the Li metal, SSEs present unexpected wettability towards the lithium anode on the surface. The hard interfacial solid-to-solid contact substantially prevents the overall Li-ions transport, and causes the uneven deposition of the Li metal, which could cause the formation of a dendrite that penetrates the separators and finally leads to the short circuit of batteries. As a result, the energy capacity is substantially decreased, which accelerates the cell failure.

1.2 Mechanism of MOFs-based electrolytes for Li metal batteries

Due to their low electrical conductivity, the ability to be easily structurally tailored, and the porous structure providing a channel for Li-ion transport and ion-sieving capability, MOFs have proven to be promising materials for Li^+ conductors in SSEs by inhibiting the recrystallization of the polymer. Meanwhile, by maintaining a good distribution in the polymer matrix, MOFs are in favor of more interaction sites to stabilize the interfacial contact between solid interfaces.[68] During the last decades, endeavors have been made to explore the performance of MOFs as solid hosts for Li salts to benefit Li^+ transport and thus improve the ionic conductivity, or serve as active fillers for SPEs to improve their mechanical robustness during the charging/discharging process. This review covers the mechanism of MOFs used as solid-state electrolytes, the structural fabrication and modification of MOF-based SSEs, and the future directions in terms of this field.

1.2.1 Li-ion transport. Two mainly accepted mechanisms are developed to illustrate the function of MOFs to immobilize anions in a three-dimensional pore framework: the combination of anions with the coordinatively open metal sites in charge-neutral skeletons, and directly binding negatively charged ingredients; and the intrinsic nanoporous structure of the MOF material to restrain the large size anions to facilitate Li ions transport.[22,69,70] The metallic centre of the MOF materials can bind the anions of the Li salt, leaving the cation to move comparatively freely along the pores. Also, due to the fact that the anions of the Li salt are much larger than the Li-ions, the porous structure of MOFs is considered as a 'cage' or 'host' to trap anions, thus facilitating Li ion transport. The Chen group confirmed the mechanism by Fourier transform infrared spectroscopy (FTIR).[9] The S═N═S and O═S═O peaks of the $TFSI^-$ anion in the FTIR spectra indicate the strong interactions between the MOF metallic centre and the anion of the Li salt in the electrolyte. Raman data also showed that the MOF stimulates the dissociation of the Li salt. Huang and coworkers further confirmed the interaction between Li^+ and the MOF through X-ray phosphorescence (XPS).[71] Long and co-workers pointed that in MOFs containing SSEs systems, the ionic transportation is determined by through-the-pore diffusion. Conversely, in polymer electrolytes, the ionic conductivity relies on the polymer chain mobility.[7,72] Therefore, the bifunctional MOF electrolytes can realize both high conductivity and mechanical properties.

DFT-based MD simulations are widely used to measure the ionic diffusivity in battery systems. The Zhou group conducted DFT-MD calculations to illustrate the diffusion kinetics of the original liquid electrolyte and MOF-tailored electrolyte,[5] as shown in Fig. 1(a–g). The results show the similarity of the ionic transport in the pristine electrolyte and MOF-modified electrolyte. For a traditional electrolyte, the rapidly diffused Li^+ and $TFSI^-$ ions reacted quickly to generate uneven Li peeling behavior on the surface of the Li metal caused by the random fluctuations during the lithium position, thus resulting in Li dendrite growth by self-amplification. On the contrary, in the MOF-modified electrolyte system, the MOF scaffolding with well-ordered and confined pore structure restricted the $TFSI^-$ diffusion spatially, which consequently led to a homogenous Li^+ flux and almost $TFSI^-$ "cage" (Fig. 1g). This opinion was consistent with that of the Chen group that the IL ions and anions were trapped inside the MOF pores. In addition, there was excessive ionogel electrolyte adsorbed on the outer surfaces of the MOF nanoparticles, thus the Li^+ ions are continuously conducted on the surfaces and within the nanopores of the MOF (Fig. 1h).[9]

On account of the electrostatic forces of Li^+ and $TFSI^-$ in the neutral LiTFSI and the confined $TFSI^-$ diffusion, the Li^+ ions are distributed homogeneously in the MOF-modified electrolyte, thus leading to a uniform electrodeposition on the Li-metal surface. As shown in Fig. 1(i), the nanoporous adsorption effect and Lewis acid derived from the highly ordered porous MOF nanoparticles are the keys to transporting Li^+ ions. The MOF material used is the sponge-like SSZ-13, which is an aluminosilicate that includes Si and Al linked by O atoms with a three-dimensional open structure. The absorption ability of the porous MOF surface can accelerate the dissociation of the Li salt (LiTFSI).[21] Meanwhile, the −25 mV zeta potential of the SSZ-13 nanoparticles suggested that the nanoparticles possess a Lewis acid property on the surface, and thus can disperse uniformly in a PEO suspension system without clustering. Thus, the interaction between LiTFSI and the surface groups on the MOF material are closely enhanced. As a plasticizer, the homogeneous SSZ-13 in the formed CPE can greatly decrease the PEO crystallinity and expand the amorphous polymer region. The charged silica group on the surface of SSZ-13 further enables the dissociation of LiTFSI to shape a Li^+-rich layer on the surface of the porous structure. Complexation between the Li^+ ions with the lone-pair electrons in the dissociated EO units endows the Li^+ ions to transport in a high speed. Also, the competition between SSZ-13 and PEO to react with Li^+ ions can lead to a high t^+. Simultaneously, the $[N(SO_2CF_3)_2]^-$ anions of the LiTFSI were restrained by the aluminol groups of the SSZ-13 nanoparticles, which can also increase the t^+ of the CPE. As a result, high ionic conductivity was realized and the t^+ of the SPE was 0.5, which was two times higher than the other PEO-based SSEs (0.25).

The Kitagawa group investigated the inclusion and dynamics of Li^+ from a polyethylene glycol (PEG)–$LiBF_4$ complex in the nanochannels of $[Zn_2(terephthalate)_2(triethylenediamine)]_n$.[68] The Li^+ complexation and mobility in the host pores were studied by ^7Li NMR and relaxation analysis, separately. The Lorentzian line shape between the +1/2 and −1/2 transition implied a liquid-shape movement pattern of the Li^+ in the PEG

View Article Online
Materials Chemistry Frontiers Review

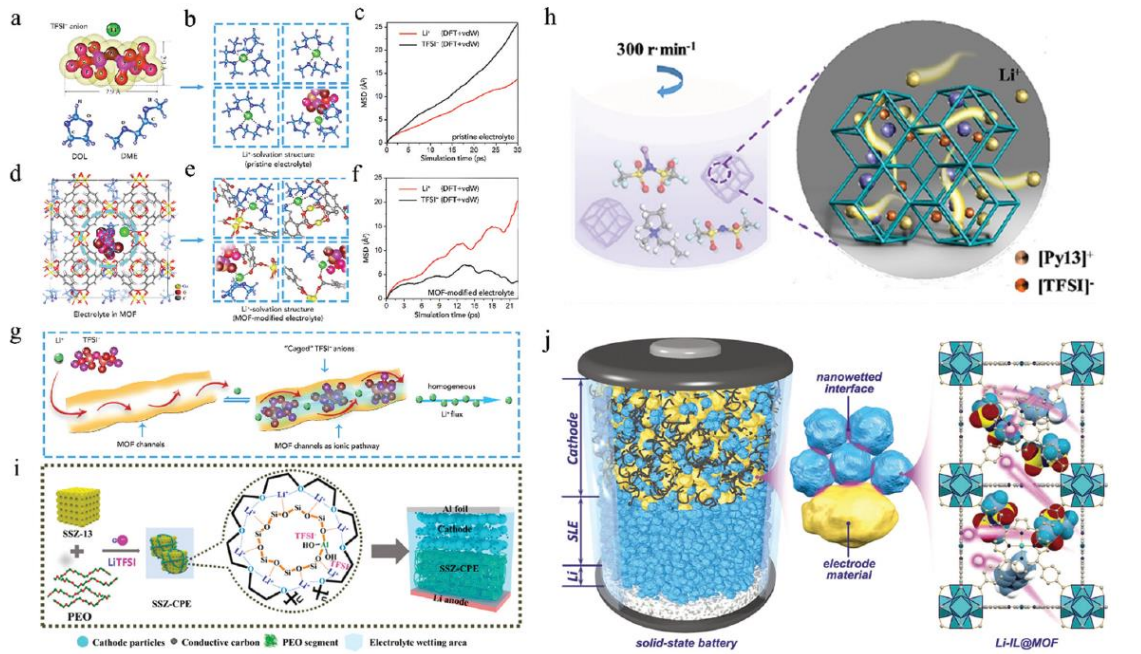

Fig. 1 Mechanism of MOF materials for Li^+ transport: (a–g) Molecular/crystal structures used in the MD simulation (reproduced with permission,[5] Copyright 2018 Elsevier B.V.). (a) Molecular structure of the LiTFSI salt and DOL/DME solvent. (b) Typical solvation structures of the LiTFSI@DOL/DME electrolyte during the MD operation. (c) Calculated mean square displacement (MSD) of Li^+ and $TFSI^-$ in the pristine electrolyte as a function of the simulation time. (d) Schematic illustration of the MOF-modified electrolyte, where the LiTFSI@DOL/DME electrolyte is incorporated into the MOF host. (e) Li^+-solvation structures of the MOF-modified electrolyte during the MD operation, wherein the MOF host participated in the Li^+ solvation process. (f) The MSD of Li^+ and TFSI ions in MOF-modified electrolyte as a function of the simulation time. (g) Schematic of the selective Li^+ ionic transport imposed by the MOF host. (h) A schematic representation of the synthesis method of ILE@MOF, and schematic illustration of Li^+ transport paths (reproduced with permission,[9] Copyright 2019 Royal Society of Chemistry). (i) Mechanism of SSZ-13 addition interaction with PEO and LiTFSI, improved ionic conductivity and schematic of the CPE-Li metal battery cell (reproduced with permission,[21] Copyright 2018 American Chemical Society). (j) Schematic illustration for the architecture and nanowetted interfacial mechanism of the solid-state battery with a magnification showing crystal structures of the MOF. $[EMIM]^+$and $[TFSI]^-$ ions in space-filling model are randomly displayed in the pores of the MOF. The migrating Li^+ ions are highlighted by glowing pink spheres. Hydrogen atoms are omitted in MOF structure for clarity (reproduced with permission,[2] Copyright 2018 John Wiley & Sons).

chains and MOF nanochannels. In addition, the low E_a (0.18 eV) value shows that the composite possesses high ionic mobility, which was similar to the values reported in other composite systems, such as bulk polymer–Li salt complexes, composites with inorganic nanoparticles, and composites with mesoporous alumina.

The ionic liquids (ILs) have been extensively employed in liquid/solid electrolytes as conductors or fillers due to their excellent properties of relatively high ionic conductivity, eco-friendliness, low interfacial resistance and high safety.[73–75] The Feng group designed a MOF-based solid-like electrolyte impregnated with ionic liquid (Li-IL@MOF), as Fig. 1j shows.[2] In this system, the sizes of $[EMIM]^+$ and $[TFSI]^-$ are much smaller than the pore size of MOF-525(Cu) (7.9 Å, 7.6 Å, 12 × 7 Å, respectively). Thus, the porous structure can confine the $[EMIM]^+$ and $[TFSI]^-$ ions inside the pores to slow down their movement, and simultaneously enable the Li-IL ions to smoothly pass through. The Li^+ ions migrate inside the pores and through the MOF's framework. Greenbaum reported that fillers with Lewis acid–base groups can improve the mobility of the Li^+ ions by strong interaction between the lithium salt and composite polymer electrolytes (CPEs).[76] Lately, the Kitagawa group studied the lithium ion diffusion in ZIF-8 mediated by an incorporated ionic liquid (IL)-$[EMI_{0.8}Li_{0.2}][TFSA]$, which is a mixture of [EMI][TFSA] and LiTFSA.[77] Results show that the ILs in the microchannels display quite different phase performance due to the nano size effect in microchannels or the interaction with the inner surface of ZIF-8. In the system, the movement of the $TFSA^-$ increases with increasing temperature, and the incorporated ILs in the porous structure were protected from freezing and unexpected glass transition. The movement of the Li^+ ions is not broken by the MOF due to the solvation and exchange effect. In addition, the Li^+ in the bulk spread with the exchange of the solvating $TFSA^-$ on account of the low comparable activation energies. The nano channels of MOFs are favorable for improving the ionic conductivity.

Overall, the Li^+ transport across the MOF-Li salt (IL) crystals can be concluded. In the system, the polyhedral nanostructured MOF-Li (IL) salt crystals are densely arranged. Thus, the open porous frameworks as Li^+ channels are tightly linked with each

other by face-sharing mechanism, and the anions of the Li salt are bonded and restricted by the unsaturated metallic centre and the apertures of the MOFs. Thus, the Li^+ can move easily from one crystal to another through the channels, and across the surface of MOF materials. The interactions between the MOF nanoparticles and other composites have multifunctional effects: significantly lower the crystallinity of polymers, improve mechanical strength of the SSEs, and greatly change the transmission pathway of Li^+ ions and meanwhile restrain the movement of Li salt anions.

1.2.2 Interfacial behavior. For Li metal batteries, the interfacial behavior determines the SEI film, cycling stability and battery life. Stephan *et al.*[11] supposed that the improved interfacial properties of MOF-based SSEs is due to the eliminating ability of the nano-porous structure in MOFs to track the solvent impurities. The large surface area and porous structure of the MOF nanoparticles facilitate the absorbing of trace impurities, thus preventing them from accumulating at the solid–solid interface and protecting the metal anode. To further explore the compatibility of the MOF-containing SSEs, the morphologies of the Li|Li-IL@MOF interfaces were clearly observed. Because of the irregularity and mismatching of the Li metal and the SSE layer, nano-gaps can be seen obviously between the two surfaces before cycling (Fig. 2a). While after the charging/discharging process, these gaps were eliminated and a seamlessly connected interface was formed with a slightly reduced resistance. As shown in Fig. 2(b), after cycling, the initial gaps were solid with a growth-inhibited "Li dendrite" layer, and a smooth and dense morphology was obtained on the Li anode surface. This is attributed to the nano-wetted interfaces (formed by the addition of IL) and high mechanical stability of the Li-IL@MOF SSE layer that facilitates the uniform Li deposition. Besides, in the SSEs with nanometer scale feather particle sizes, the specific surface area and surface tension are clearly higher than in those with larger particle sizes, thus leading to a tight solid-to-solid interfacial contact. The time-dependent voltage of the Li|Li-IL@MOF|Li cell shown in Fig. 2(c) displayed a small polarization voltage (less than 100 mV) under different current densities. In detail, the voltage of each cycle was quite flat and stayed stable during the cycling (1000 h).

Interfacial resistance is a significant factor that reflects the stability of contact. The EIS Nyquist plot shows the comparison of the Li|Li-IL@MOF|Li cell before and after Li plating/stripping (Fig. 2d).[2] After the cycling process, the total resistance is 10 Ω lower than that of the cell before cycling, which is about 130 Ω. The nano structural particles and Li^+ transport framework of SSEs explain the excellent compatibility of the Li-IL@MOF SSE with the Li metal anode, as well as the small interfacial resistance between them. In summary, the mechanism of the interfacial contact is schematically elaborated in Fig. 2e.

In terms of the interfacial stability, exploring the formation and composition of the solid electrolyte interface (SEI) layer is significant. Fig. 2(f) shows the schematic of the formation of SEI at the lithium and electrolyte interface. Fig. 2(g and h) shows the composition of the lithium surface in contact with Mg-TMA. The figures prove that Li_2CO_3 and LiF were formed on the surface of the lithium anode, which originated from various hydrocarbon species, and LiTFSI salt, separately. To be specific, F came from the contact of the lithium surface and CPEs. Meanwhile, the influence of the organic ligands of Mg-TPA and

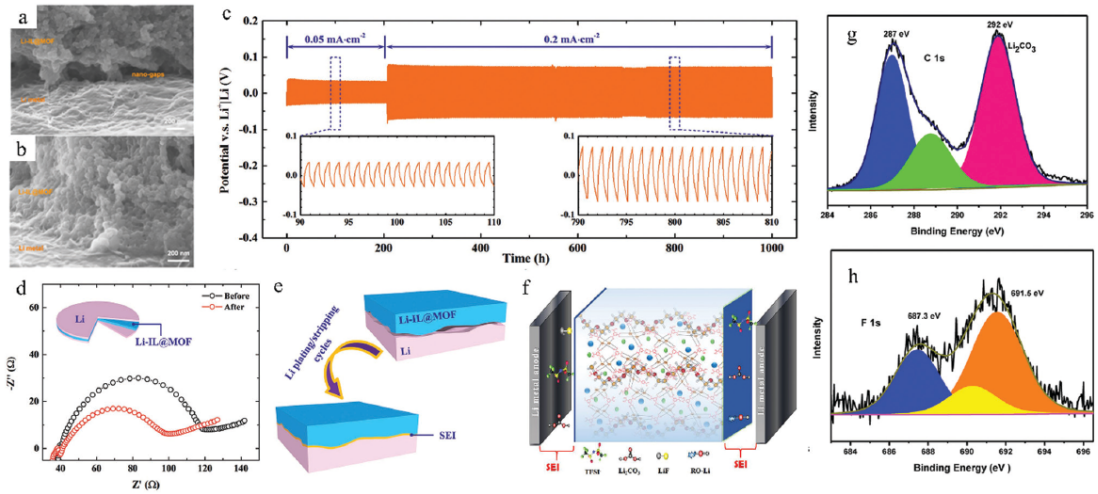

Fig. 2 SEM morphologies of (a) the as-synthesized MOF and (b) the cross-sectional of Li-IL@MOF pellet. The interface between the Li foil and the Li-IL@MOF (a) before and (b) after Li plating/stripping cycles. (c) Voltage profiles for the Li|Li-IL@MOF|Li symmetric cell at current densities of 0.05 and 0.2 mA cm^{-2}. (d) EIS of the Li|Li-IL@MOF|Li symmetric cell before and after the Li-plating/stripping cycles. (e) Schematic illustration for the improved interfacial contact after Li-plating/stripping cycles (reproduced with permission,[2] Copyright 2018 John Wiley & Sons). (f) Schematic of the SEI formation at lithium electrolyte interface. XPS spectra of the lithium surface in contact with Mg-TMA: (g) C 1s, (h) F 1s (reproduced with permission,[5,10,11] Copyright 2019 Elsevier B.V.).

View Article Online
Materials Chemistry Frontiers Review

Mg-TMA SSEs on the electrochemical and interfacial behaviors matching with LiTFSI as salt was studied and compared.[10] In their study, the Lewis-acid groups of the MOFs compete against the Lewis acidic Li^+ with the alkoxide of PEO chains and $TFSI^-$ to form complexes. To some extent, the specific actions of the polar surface groups lead to the structural modifications on the MOF surfaces. Also, by the formation of the 'ion-filler complex', the ionic coupling can be decreased and the salt dissolution is further improved. In addition, the Lewis acid center on the MOFs can react with the $TFSI^-$, and clearly reduce the crystallinity of PEO with the individual impregnating of Mg-TPA and Mg-TMA MOF. In this way, the interfacial impendence is highly decreased. In addition, the ambient condition has an influence on the physical/chemical stability of SSEs.

The stability between the MOF-containing SSEs with air or water was also studied. The Kitagawa group found that the MOF-PEG-$LiBF_4$ SSE was not steady in water vapor, but was integral in air and exhibits a thermal stability up to 220 °C.[68] As mentioned before, the thermal stability of MOFs-containing SSEs are much higher than practical requirements, which enables the solid-state batteries to work stably at changing temperatures without destructive deformation.

1.2.3 Lithium electrochemical deposition. In consideration of the inherently ordered pores of the crystalline MOF lattice being able to store various guest liquids and gaseous, the application of the compatible pores of MOF materials for SSEs may offer ordered ionic transport channels that consequently lead to homogeneous Li electrodeposition.

Fig. 3(a–e) displays the schematic illustration of the Li dendrite and dendrite-free Li growth of liquid electrolytes and MOF-modified electrolytes.[5] Due to the pore chemistry mentioned before, the introduction of the porous structure of the MOF species into the electrolyte highly improves the Li^+ transport, and subsequently realizes stable Li electrodeposition. In other words,

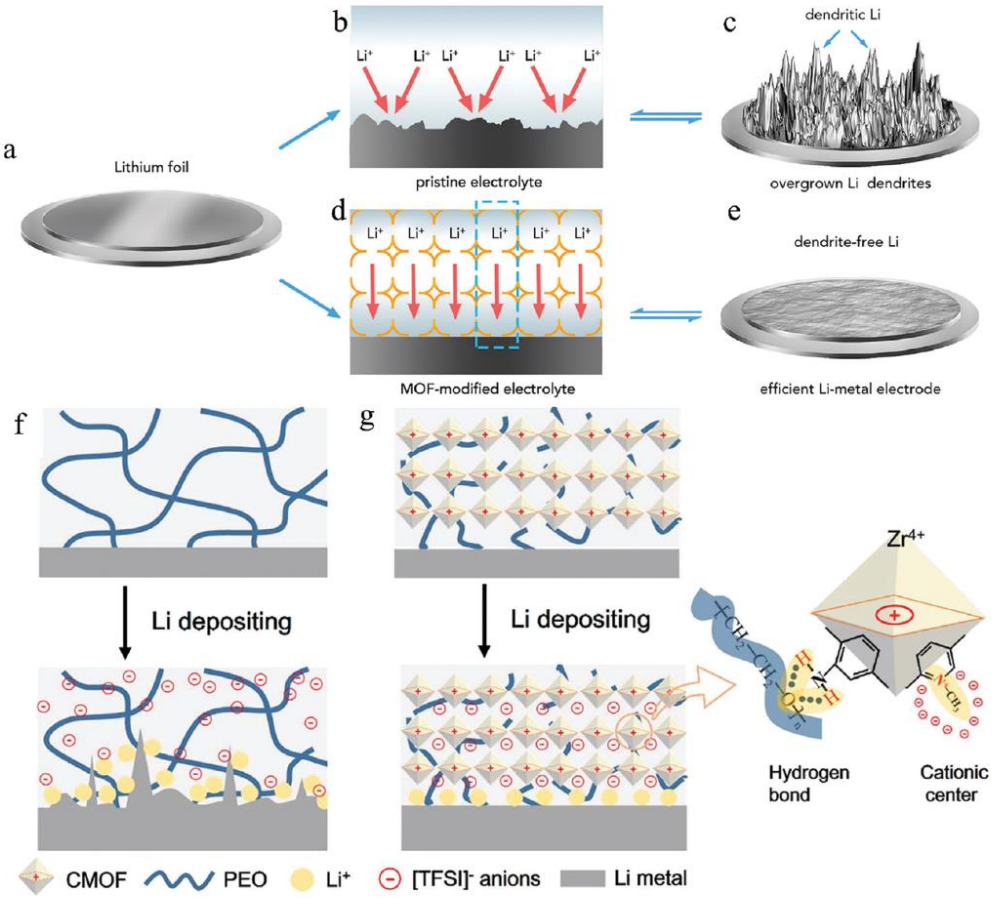

Fig. 3 Schematic showing the Li-metal electrode (a) with pristine electrolyte (b and c). The inhomogeneous Li-ion flux results in the overgrown Li dendrites. (d and e) Schematic of the Li-metal electrode (d) with MOF-modified electrolyte (e). The homogeneous Li-ion flux facilitating a uniform Li growth on the Li-metal surface enables an efficient Li-metal electrode. The cyan dashed region indicates the ionic transport pathway provided by the MOF host (reproduced with permission,[5] Copyright 2018 Elsevier B.V.). Schematic of the Li deposition behavior with the (f) PEO(LiTFSI) electrolyte and (g) anion-immobilized P@CMOF electrolyte (reproduced with permission,[28] Copyright 2019 American Chemical Society).

the caged anions in MOF generate uniform Li-ion flux, thus inhibiting the formation of harmful dendrites, and finally achieving stable Li electrodeposition. Fig. 3(f and g) compares the SSEs with and without MOF materials. Considering this, MOFs are applied as a protective layer to protect the Li metal anode.[25,78,79] During Li deposition, the coordination of the $-NH_2$ modified MOF with PEO within the SSE system led to dendrite-free Li anodes.[28] As shown in the figures, according to simulation, a small concentration gradient of Li^+ ions were formed in the anion-fixed CPE, restraining the formation of the dendrite in a large area, and thus displaying excellent rate and cycle behavior matched with the $LiFePO_4$ and $LiFe_{0.15}Mn_{0.85}PO_4$ cathodes. Another important factor that enables uniform lithium electrodeposition is the high lithium-ion transference number t_{Li^+} in MOF-based SSEs, which is due to the 3D polymer network crosslinking with the MOF framework.[80]

Owing to the special function of the MOF structure and properties, which facilitate the homogeneous lithium flux and stabilize the interfacial contact, the Li uniformly deposits on the surface of the Li metal without dendrite formation. In other words, the 'caged' anions within the MOF can enable a uniform Li-ion flux, inhibiting the formation and growth of detrimental dendrites. As a result, a stable Li electrodeposition can be realized.

2. Fabrication and modification of MOFs-based SSEs

2.1 Composition of electrolytes

Usually, the MOF-containing SSEs consist of a polymer matrix, lithium salt, MOF nanoparticles, and other fillers. To explore the benefits of the MOFs materials in SSEs, multicomponent systems are being developed, where single ingredients merging into higher complexity structures introduces new functionality. In the MOF-based SSEs, MOF materials serve as a cation cage to confine cations of the Li salt and boost the Li ions transport.[48,81,82] Apart from that, MOF materials also form the skeleton of the SSE to enhance the stiffness and mechanical strength of the soft polymer matrix in composite SSEs, with the polymer matrix offering the multidimensional Li ion pathway. Besides, there are additions like ILs that serve as 'wetting' agents to stabilize the solid/solid interfaces.[9,13] Other fillers, such as ceramic materials and inert oxides, are added to enhance the electrochemical performances of LMBs. Every component works in coordination with each other.

2.2 Gel to solid electrolytes

The polymer-based SSEs offer good flexibility and therefore excellent interfacial contact with the Li metal anode, while suffering relatively low ionic conductivity and narrow operation window. Ceramic-based SSEs have advantages of a higher modulus to alleviate the dendrite and higher ionic conductivity, but are rigid to achieve a better interfacial contact with Li. Thus, complex SSEs is a compromise to utilize both merits.[27]

2.2.1 Gel electrolytes. To stabilize the lithium anode, through the vacuum-filtration method, Gao's group explored a Mg-MOF-74-modified PVDF-based gel polymer electrolyte (GPE) with immobilized anions for a quasi-solid-state Li–S battery.[4] Matched with a sulfur–carbon composite cathode, cells with three different types of electrolytes were tested in the research: liquid electrolyte with Celgard separator, PVDF GPE, and MOF-modified PVDF (MOF-PVDF) GPE. As shown in Fig. 4a, the as-prepared MOF-PVDF GPE fully utilizing the abundant pores of the MOF skeleton to fix the polysulfide anions with large size. Meanwhile, the cages trap the electrolyte anions $TFSI^-$ into the pores, thus endowing a homogeneous transport of Li^+ effectively and advantageously to the even Li deposition. Thus, the lithium anode matched with MOF-PVDF GPE kept a uniform morphology and formed a stable SEI film. Because of the excessive consumption of soluble polysulfides towards the Li anode, the Celgard 2325 cell formed a solid electrolyte interphase (SEI) film with a thickness from 4 to 9 μm. The lithium anode with MOF-PVDF GPE exhibits a more dense and homogeneous SEI film with only 5 μm thickness (Fig. 4b). In addition, the patchy SEI film of the pristine PVDF. Supposedly, GPE can assist soluble polysulfides in corroding the surface of the Li anode. The sharp redox peaks in Fig. 4c suggest the cells with this MOF-tailored GPE deliver lower polarization and excellent reversibility. Moreover, the polarization voltage of the Li/Li symmetrical cell with the MOF-PVDF electrolyte is only 31 mV during 120 cycles without short-circuit (Fig. 4d). In addition, the cells with the MOF-PVDF GPE remain stable at a high current density of 2 mA cm^{-2}, which illustrates the advantage of the MOF material on Li electrodeposition. Also, the MOF-PVDF GPE improved the t^+ value from 0.37 to 0.66, which is consistent with the MOFs being capable of caging the counter anions of Li^+, leading to a fluent Li^+ pathway (Fig. 4e). XPS spectra were collected to investigate the chemical composition of the Li anode surface. The results show that the formation of the SEI film, containing inorganic components $-NSO_2CF_3$ (688.3 eV) and inorganic LiF (684.7 eV), is significant to prevent the deposition of Li_2S/Li_2S_2 on the surface of the Li anode, thus exhibiting high charge/discharge and high-rate capability. As Fig. 4f shows, in terms of the long-term cycling at 0.1C rate, the cell with the MOF-modified GPE delivers the lowest capacity decay after 200 cycles with a high capacity retention compared to the cells with the Celgard separator and PVDF electrolyte.

2.2.2 Hybrid solid-state polymer electrolyte (HSPE). HSPE is also called composite polymer electrolyte (CPE). Yuan *et al.* incorporated MOF-5 as a filler into the PEO matrix, highly improving the electrochemical performance of the CPE.[83] Mixed with PVDF by a 3 : 1 weight ratio, MOF-688 greatly improved the performance of HSPE.[22] In their work, Yaghi *et al.* developed a new three-dimensional MOF-688 by connecting ditopic amino functionalized polyoxometalate $[N(C_4H_9)_4]_3[MnMo_6O_{18}((OCH_2)_3CNH_2)_2]$ with 4-linked tetrahedral tetrakis(4-formylphenyl)-methane building units through imine condensation. The accessible void space of MOF-688 possesses a 3-layer interpenetrated structure, as Fig. 4g shows. TBA^+ of the MOF material can be exchanged with Li^+, leading to a high ionic conductivity of 3.4×10^{-4} S cm^{-1} at room temperature. The t^+ of MOF-688 is 0.87, which is enormously higher than that of conventional liquid electrolytes (0.2–0.4) and single-ionic polymer electrolytes. This implies that most of the

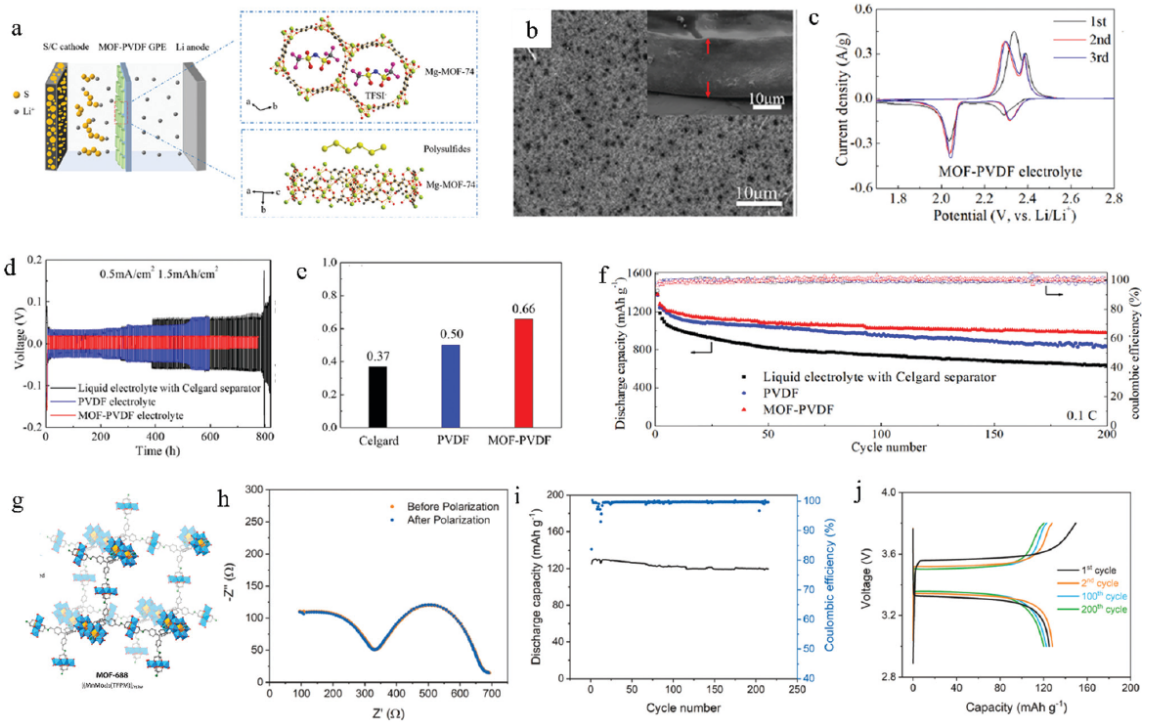

Fig. 4 (a) Schematic illustration of MOF-PVDF GPE with anions immobilized for the lithium-sulfur battery. (b) SEM images of the prepared MOF-PVDF film. (c) CVs of the cell using MOF-PVDF GPE. (d) Li plating/stripping behavior of Li/Li symmetrical cells using various electrolytes at a low current density of 0.5 mA cm^{-2}. (e) The t^+ values of Celgard, PVDF, and MOF-PVDF GPE. (f) The cycling ability at a rate of 0.1C with different electrolytes (reproduced with permission,[4] Copyright 2019 American Chemical Society). (g) Structure illustration of MOF-688. (h) Nyquist plots of the Li|MOF-688|Li cell before and after polarization. (i) Discharge capacity and coulombic efficiency of the Li|MOF-688|$LiFePO_4$ cell. (j) Charge and discharge profile of the Li|MOF-688|$LiFePO_4$ cell for the 1st, 2nd, 100th, and 200th cycle (reproduced with permission,[22] Copyright 2019 American Chemical Society).

charges in the MOF is transported by Li^+, confirming that the polyoxometalate anions are caged in the backbone of the framework. The low interfacial resistance of 353 Ω against the lithium anode in the measurements from the Li|MOF-688|$LiFePO_4$ cell before and after cycling shows that the material is a stable and suitable candidate as a solid-state electrolyte (Fig. 4h). Excluding the first cycle, the mean coulombic efficiency was about 99.6%, which indicates limited side reactions on both cathode and anode (Fig. 4i). In Fig. 4j, over the process of 200 cycles, the charge/discharge voltage gap remained stable. The improvement of the PVDF polymer electrolyte is due to the special structural framework. Carrying more than one charge, the triply interpenetrated diamond-based dia topology MOF-688 delivers excellent charge density, which is different from traditional building units of MOFs and COFs. In this framework, TBA^+ would fill the pores and simultaneously neutralize the charge of the anions.

2.2.3 Ionic liquid and MOFs composite electrolyte. Feng Pan's group developed a solid-like electrolyte consisting of MOF-525 (Cu) and ionic liquid [EMIM][TFSI].[2] The novel ionic-liquid-impregnated MOF nanocrystals (Li-IL@MOF) demonstrated excellent electrochemical properties, such as the amelioration of the interfacial issue and realization of high energy density. The pore size of MOF-525 (Cu) is about 12 × 7 Å, which enables the Li-IL ions to transport. Simultaneously, the structure can also lower the mobility of $[EMIM]^+$ and $[TFSI]^-$ ions by confining them into the pores, therefore improving the t^+ to 0.36. The electrochemical performance remained stable under a wide temperature range. In Fig. 5(a), we can see that the corresponding Arrhenius plot of ionic conductivity are 2.2×10^{-5}, 3.0×10^{-4}, and 4.9×10^{-3} S cm^{-1} at different temperatures: −20 °C, room temperature, and 100 °C, respectively. The UV-Vis result also confirms that by hot-pressing and with a high content of encapsulated Li-IL, the densely packed highly porous MOF nanocrystals exhibit the high ionic conductivity, which corresponds to a low interfacial resistance. The Li-IL@MOF SSE is further studied in the rechargeable Li|SSE|$LiFePO_4$ cell with a high active loading of 25 mg cm^{-2} from −20 to 150 °C. The charge/discharge capacity increased with the rising temperature from −20 °C to RM, and remained stable up to 150 °C, indicating that the electrolyte can operate well over a wide temperature range with remarkable performance, especially at high temperature (Fig. 5b). As a result, the nanowetted interfaces introduced by the addition of IL, the good mechanical stability of the Li-IL@MOF electrolyte and the nanoconfined Li-IL guests lead to the uniform Li deposition, improving the compatibility of the Li-IL@MOF electrolyte with the

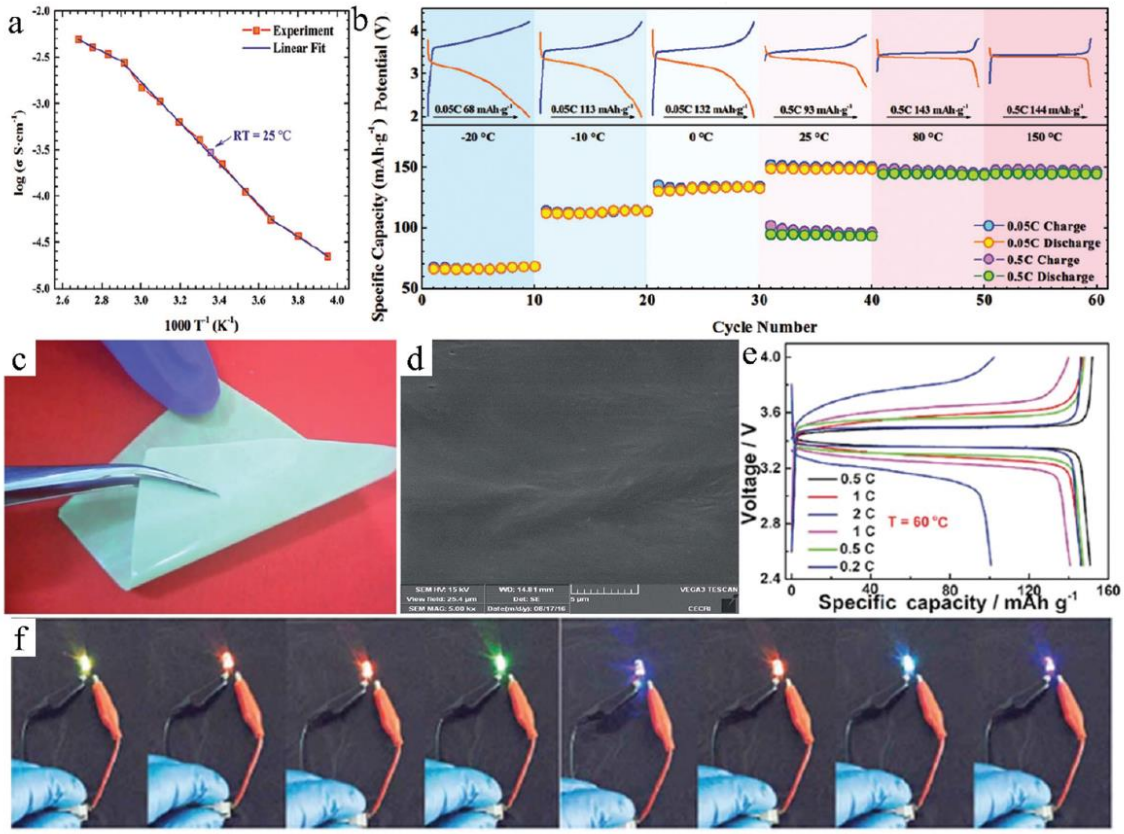

Fig. 5 (a) Corresponding Arrhenius plot of the ionic conductivity. (b) Temperature-dependent cyclability of the Li|Li-IL@MOF|LFP SSB with corresponding charge/discharge curves (reproduced with permission,[2] Copyright 2018 John Wiley & Sons). (c) Digital photograph of the CPE and (d) SEM image of the CPE (reproduced with permission,[11] Copyright 2016 Royal Society of Chemistry). (e) Cycle performance of the Li/HSPE-1–8/LFP. (f) Image of the cell of Li/HSPE-1–8/LFP powering LEDs of different colors at room temperature (reproduced with permission,[38] Copyright 2018 Royal Society of Chemistry).

Li metal. The effective 3D Li^+ conductive network created by the coordination throughout the whole battery determines the remarkable performance of this SSB system.

2.2.4 All solid electrolytes. All solid electrolytes were prepared without the attendance of solvents to suppress the growth of dendrites, and thus prevent the short circuit caused by the puncture of the dendrite with high ionic conductivity. However, the disadvantage of all solid-state electrolytes is that the interfacial contact still needs a long way to explore. Even neat MOF materials are used as SSEs at the earlier stage to propose the concept of MOF-based SSEs.[1,84] Fig. 5(c) and (d) show the visual appearance of the Ni_3-$(BTC)_2$-MOF SSE and the surface morphology of one sample, respectively. The seamless polymeric SSE is thin, bendable and nonsticking. The flat surface morphology membrane in Fig. 5(d) is ascribed to the uniform distribution of Ni_3-$(BTC)_2$-MOF particles.[11] By hot-pressing, Stephan and co-workers prepared a copper benzene dicarboxylate MOF (Cu-BDC MOF) and employed it in the PEO-LiTFSI electrolyte,[85] delivering a stable discharge capacity of 110 mA h g^{-1} at 70 °C with 1C rate, which is much higher and stable than most of the SSEs. In addition, the Li|CPE|$LiFePO_4$ cell could be cycled over a wide temperature range, which guaranteed its safety. Besides, other electrochemical performance, such as the ionic conductivity, compatibility and thermal stability of SSE were also improved by the incorporation of Cu-BDC MOF. Fig. 5(e) illustrates the charge and discharge performances of the Li/SSE-1–8 sample/LFP cell at various C rates. Stable and high discharge capacities are delivered at the corresponding rates, which imply the stable and sustainable interface of the cell at high current rates and long cycling conditions.[38] Notably, in Fig. 5(f), the cell of the Li/HSPE-1–8 sample/LFP can light LEDs of different colors at room temperature, practically supporting that the electrolyte is a potential solid-state electrolyte for commercial application. However, for batteries with all-solid-state polymer electrolytes, low ionic conductivity and poor solid/solid interfacial contact, especially at low temperature still prevent the operating of the cells.

2.3 Modification of MOFs-based SSE

To fully use the unique structure of MOFs, like the open metal centers, modifications are implemented *via* covalent modification

View Article Online
Materials Chemistry Frontiers Review

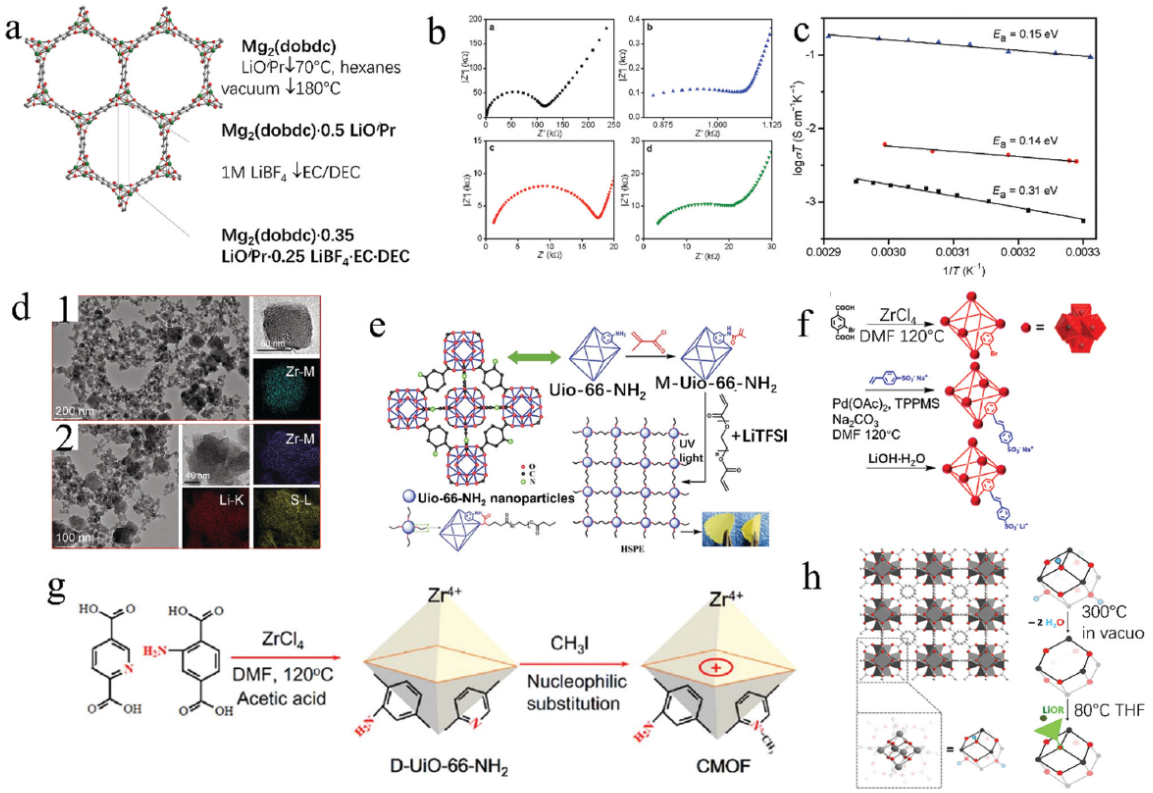

Fig. 6 (a) Structure of Mg_2(dobdc) and the scheme for its modification to form the solid electrolyte (reproduced with permission,[1] Copyright 2019 American Chemical Society). Different approaches of modifying the Uio-66 MOF: (d) TEM images of: (1) Uio-66 and (2) UIO/Li-IL, and the corresponding EELS element mappings of Zr, Li and S (reproduced with permission,[13] Copyright 2019 John Wiley & Sons). (e) Synthetic route of the hybrid covalently linked MOF PEGDA-based all-SSEs (reproduced with permission,[38] Copyright 2018 Royal Society of Chemistry). (f) Synthetic route and the schematic UiO-66-LiSS structure (reproduced with permission,[44] Copyright 2019 Elsevier B.V.). (g) Schematic illustration for the synthesis of Co-MOF (reproduced with permission,[21,45] Copyright 2019 Elsevier B.V.). (h) Representation of the grafting process, involving insertion of a lithium alkoxide in dehydrated UiO-66 (reproduced with permission,[48] Copyright 2013 John Wiley & Sons).

of organic ligands, grafting ligands on to open sites, or transplanting useful functional groups of organic liquids.

In 2011, Long and co-workers reported novel hybrid SSEs by tailoring the Mg_2(dobdc) through organic liquids.[1] In their work, three steps were taken to modify the initial Mg_2(dobdc): the grafting of lithium isopropoxide (LiO^iPr) in Mg_2(dobdc) ($dobdc^{4-}$ = 1,4-dioxido-2,5-benzenedicarboxylate), followed by infiltrating with $LiBF_4$ in a typical ethylene carbonate (EC), and with diethyl carbonate (DEC) electrolyte solution. As a result, the new solid lithium electrolyte $Mg_2(dobdc)\cdot 0.35LiO^iPr\cdot 0.25LiBF_4\cdot EC\cdot DEC$ was formed. As shown in Fig. 6(a), the grifted Mg_2(dobdc) shows a framework with one-dimensional hexagonal pores (mean diameter of ~14 Å) and the lined coordinatively unsaturated Mg^{2+} cation sites. These open sites preferentially coordinate with the lithium alkoxide ions, and pin the ions in the framework, while smoothing the transportation of Li^+ along the channel. The delicate design improves the ionic conductivity to 3.1×10^{-4} S cm^{-1} at 300 K, as shown by the two-point AC impedance data (Fig. 6b). The novel isopropoxide-grafted MOFs can be considered as a superionic conductor since the variable-temperature measurements displays a low activation energy of just 0.15 eV, as shown in Fig. 6c. A pellet with only this grifted MOFs delivered a much lower ionic conductivity of 10^{-7} S cm^{-1}. Clearly, without the existence of additional lithium salts, it is hard to realize the excellent interparticle ionic conductivity and good interfacial contacts between the compact MOFs pellet and the electrodes. Lithium salts offer Li^+ ions that can move effectively in the SSE system. Their work significantly implied the function of the unsaturated metal sites of MOFs and micropore channels in the dissociation of Li salts and Li^+ transportation in MOF-based SSEs. However, more systematic investigations including both theoretical modeling and experimental study, such as testing of the behavior of MOF material upon cycling within a lithium metal battery, were absent to further support the novel system. The grifting strategy paved the way for the use of MOFs as SSEs for the next-generation Li batteries, and could be extended to exploit other ionic conductors, such as Na, Mg, Zn metal batteries.

Nanostructured Uio-66 and its derivative are widely used in the SSEs, owing to their abundant nanopores, large specific area and long-term performance stability properties.[2,13,38,44,45,48,86,87]

The transition metals in this kind of MOFs does not provide redox-active centers, and the Zr^{4+} ions are difficult to decrease. Therefore, it avoids the induction of electronic conduction, while forming a contact with the Li metal anode.[13] At the structural level, Uio-66 is easily tailored by various functional groups, and can retain a stable structure for a relatively long time period. The morphologies of Uio-66 and UIO/Li-IL were observed by TEM images in Fig. 6d. The crystallite sizes of Uio-66 are about 50 nm, which holds the nanostructure after incorporation with Li-IL (UIO/Li-IL). The nanoparticles of pristine Uio-66 and UIO/Li-IL are mostly octahedral, which belong to the face center cubic lattice structure. By face-sharing, the quadrate structure is prone to be densified seamlessly with each crystal connected closely. In Fig. 6(e), the MOF with –C═C– bonds (M-UiO-66-NH_2) was synthesized by the combination of UiO-66-NH_2 and methacryloyl chloride (MC).[38]

The Wu group synthesized a single lithium-ion conductor by covalently immobilizing 4-styrenesulfonate anions to the skeleton of Uio-66 structures (Fig. 6f).[44] The functionalized UiO-66 containing SSE delivered a wide electrochemical stability window to 5.2 V *vs.* Li|Li^+, and higher ionic conductivity at a wide temperature range. Further characterizations of the UiO-66-NaSS and UiO-66-LiSS suggested that the crystallinity of the MOF structure is still stable with the grafting of sodium *p*-styrenesulfonate and after exchanging the Na^+ ions with Li^+ ions. Notably, the tailored single-ion conductor achieved a super high t^+ of 0.90 at 25 °C without any plasticizer. Benefiting from the incorporation of EC and propylene carbonate (PC) into the modified Uio-66 MOF structure, the ionic conductivity even reached 7.8×10^{-4} S cm^{-1} at room temperature. The MOF SSE has been investigated with all-solid-state Li|SSE|$LiFePO_4$ batteries at room temperature, displaying remarkable rate capacity and stable cycling properties. Sun *et al.* gifted the –NH_2 group to UiO-66 by exchanging a guest and removing the DMF and $CHCl_3$ solvents. The D-UiO-66-NH_2 was activated before synthesis, followed by being soaked in fresh DMF and $CHCl_3$ solvents (Fig. 6g).[45] After further dipping and dying process, the cationic D-UiO-66-NH_2 (CMOF) was obtained. Through hydrogen bonds, the –NH_2 group would boost the successive linking with effective EO branches in PEO chains to obtain a stable structure of SSE and widen the electrochemical window. Moreover, the pyridine N with unsaturated electrons as the nucleophilic reagent was easy to replace the I in CH_3I and bind with the –CH_3 group. Once the nucleophilic substitution was completed, the charging center –N^+CH_3 was formed and thus the CMOF was successfully prepared. It is known that the small amount of free I^- from CH_3I penetrated into the SSEs has no adverse effect because LiI was also adopted as an additive into SPEs before.

Long's group adopted lithium salt, *tert*-butoxide (Li*O*t*Bu*), to grift a dehydrated UiO-66 by a two-step modification procedure, as Fig. 6(h) shows.[48] Simultaneously, propylene carbonate (PC) was also added to Uio-66 to solvate the Li^+ ions in the channels of MOFs. By adding the free Li^+ salt together with the introduction of PC at room temperature, the Li*O*t*Bu*-grafted UiO-66 delivers an ionic conductivity of 1.8×10^{-5} S cm^{-1}, which is two orders of magnitude higher than the pristine UiO-66 material. The improvement can be explained by the hypothesis of the effective pinning of Li–salt anions by the open Zr^{4+} sites. The bulky aliphatic group delocalized the negative charge of tBuO$^-$, which consequently weakens the interaction of Li^+-*t*BuO, resulting in the fast movement of dissociated Li^+ in the channels and high Li-ion transference number. This hypothesis of open metal sites in the Li-ion conduction was validated by synthesizing hydrated UiO-66 after being grifted without open metal sites. Although the Li^+ content in the deprotonated UiO-66 was four times the amount of the grifted unsaturated one, it delivered a much lower ionic conductivity of 3.3×10^{-6} S cm^{-1} when measured as the Li^+ conductor under room temperature. Notably, the activation energy of Li^+ transport of the hydrated-grafted UiO-66 is about two times higher than that of the dehydrated-grafted UiO-66 (0.35 eV, 0.18 eV, separately), which implies that the different coordination situation of the Li^+ ions in MOFs play a crucial role in the movement of Li^+. By the addition of a SiO_2 precursor, UiO-66-NH_2@SiO_2 was prepared and applied in SSE, enabling more uniform Li-ion flux and enhanced solid–solid interfacial properties.[87] Thus, the overall performance was highly enhanced. Although it delivered high ionic conductivity, the electrochemical windows of Uio-66s are supposed to be confined by the redox-active Cu(II) center.

3. MOFs-based SSEs in lithium metal batteries

3.1 Enhancement of ionic conductivity

As mentioned in the mechanism of Li^+ transport dominated in the MOF-containing SSEs systems, the special properties of nanosized MOF particles are considered to boost the ionic conductivity. To deal with the large interfacial impendence of materials in the LMBs caused by the unstable solid/solid contact, assistant ionic conductors are implemented to speed up the Li^+ transport of interfacial SSEs. One strategy of improving the ionic conductivity is by embedding an ionic liquid and Li salt (Li-IL) into the porous MOF channels. MOFs are also adopted as an addition in the oxide-based SSEs to highly enhance the interfacial Li^+ transport kinetics. The Pan group found that when coordinated with LLZO SSEs, the solidified Li-IL composite enabled a close contact with the LLZO particles directly due to the open and well-confined channels in the MOF nanoparticles.[88] The original unstable solid/solid contact changed into "nanowetted" interfaces, which boosted the Li^+ transport. With these closely connected interfaces, the SSE delivers a high ionic conductivity of 10^{-4} magnitude S cm^{-1} with a wider electrochemical window (reaches to 5.2 V). Simultaneously, the compatibility of SSE with the Li metal anode is highly improved. Moreover, the unique $LiCoO_4$ and $LiFePO_4$ SSBs obtained a low capacity decay of only 3% after 150 cycles at 0.1C. In this system of SSEs, the IL acts as a function of moisturizing, which enhances the stability between the electrolyte and electrodes. Through the nanostructured MOF-derived SSEs, the low resistances of the Li/SSE and cathode/SSE interfaces guarantee the fast Li^+ transportation kinetics in the LMBs.

View Article Online
Materials Chemistry Frontiers Review

The room temperature conductivity reached 2.0×10^{-4} S cm^{-1} due to the bilayer heterostructure solid electrolyte.[89]

3.2 Interfacial compatibility and stability of SSE with Li metal

The Li symmetrical cells were packaged to investigate the long-term electrochemical stability of MOF SSE against the Li metal.[9] The morphology is shown in Fig. 7(a). A layer was formed on the surface of the Li metal to protect the anode. Fig. 7(b) displays the interfacial compatibility between the SSEs and Li metal anodes. Over the first 4 days, the interfacial resistance decreased. During the subsequent evaluation period of 10 days, the resistance remained constant. This constant interface impedance illustrates that under high-temperature, a stable interface was formed between the Li and the electrolyte. At the same time, the electrolyte can stop the successive side reaction between the Li metal and the electrolyte. The electrochemical window can be broadened to a high voltage of 5.4 V (Fig. 7c). Fig. 7(d–f) shows the small changes under different current density, flat and even lithium deposition and small polarization voltage, which indicates that the adoption of this MOF containing gel electrolyte is a potential strategy to further suppress Li dendrite formation and growth, and thus enhance the effective and high-temperature durability of Li metal batteries. The Huang group also tested the Li plating/stripping stability.[71] In their work, the Li|MOF|Li symmetric cell had an initial overpotential of only 46 mV, and the final overpotential slightly increased to 100 mV after 600 h. The voltage profiles remained even, and no sign of short circuit occurred during the process, indicating a stable and uniform Li plating/stripping process and suppressed Li dendrite growth. The Sun group reported that the discharge/charge voltage profiles of the MOF-based gel SSE remained stable even after long-time cycling at a high current density.[90] In addition, the pouch cell worked

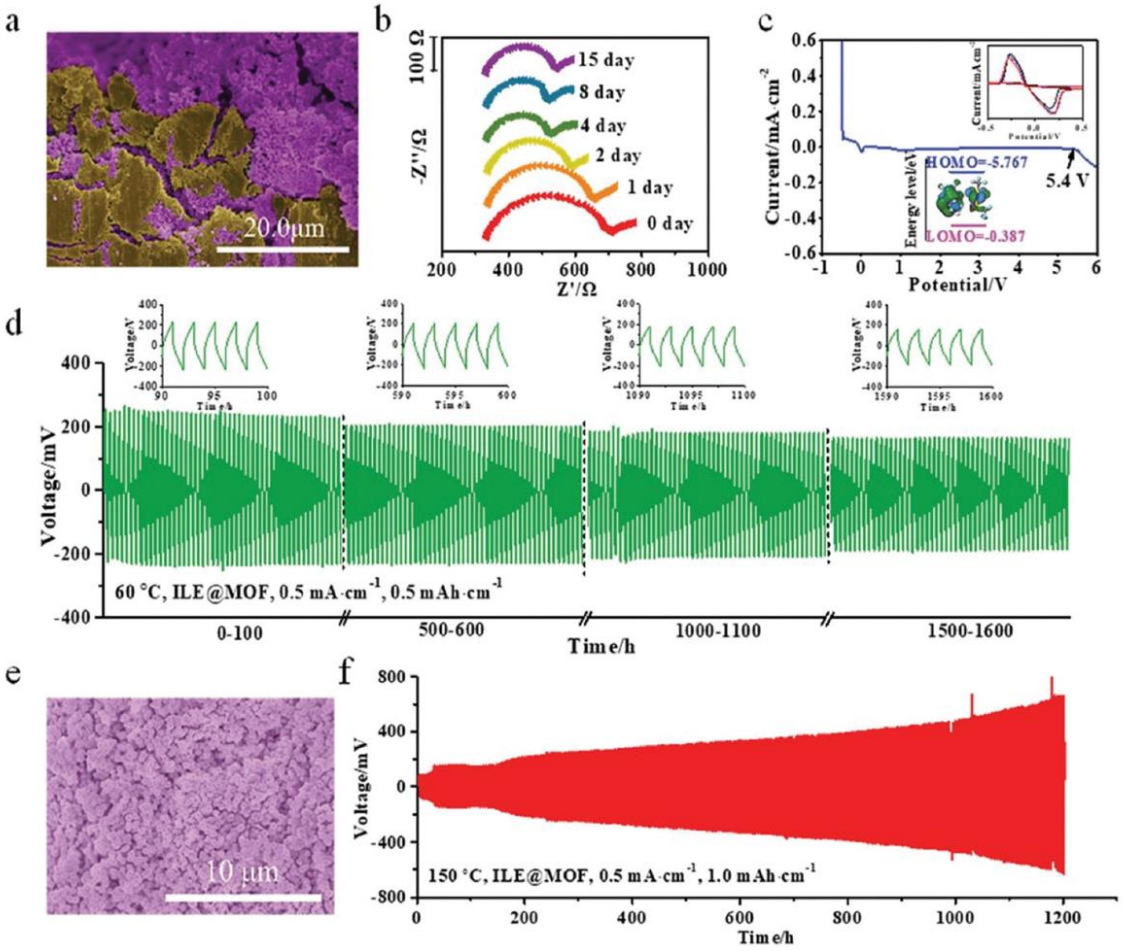

Fig. 7 (a) SEM morphology of the contact area of the Li metal and ILE@MOF. (b) Time evolution of the impedance response of a symmetrical Li/ILE@MOF/Li cell. (c) LSV curve of a Li/ILE@MOF/stainless steel (SS) cell. (d) Voltage profiles of the Li/ILE@MOF/Li cell cycling. (e) SEM morphology of the Li anode in the Li/ILE@MOF/Li cell. (f) Voltage profile of the Li/ILE@MOF/Li cell cycling (reproduced with permission,[9] Copyright 2019 Royal Society of Chemistry).

well after folding with different angles. Considering the potential safety concerns of LMBs, the battery abuse test of the pouch cells was performed by a destructive cutting experiment. The folding test and safety evaluation can also confirm the interfacial compatibility and stability between SSE and electrodes.

3.3 Suppressing of Li dendrite

According to the formation and growth mechanism of Li dendrites, it is significant to deposit the Li ions uniformly on the Li metal to eliminate the dendrite Li. By forming a particle-rich layer on the solid/solid contact side of the lithium anode, the introduction of MOF highly suppressed the formation of dendrite Li.[9] The protective layer markedly prevented the anode from generating dendrite at high temperatures. In detail, the Zhou group characterized Li electrodeposition by top-scanning electron microscopy using a MOF electrolyte with pristine electrolyte for comparison.[5] The SEM images confirmed that the MOF-based electrolyte can regulate the Li deposition, and effectively suppress the formation and growth of dendritic Li. Fig. 8(a and b) shows that for the symmetric cell with pristine electrolyte, the contiguous delithiation led to obvious breaks on the Li metal surface. The spikes represent Li dendrites, which are randomly orientated with a large portion having a length of ~10 mm. These overgrown Li dendrites can pierce the separator easily and pose severe safety problems, significantly hindering the application of LMBs. Fig. 8(c and d) displays the Li metal anode of the symmetric cell using the MOF-modified electrolyte. It can be observed that the surface of the Li metal anode is flat with low roughness even at high areal capacity. Almost no Li dendrite was observed on the surface of the Li metal anode after 2000 cycles. The Li metal surface still remained smooth and intact after 800 h with the increasing of the current density (Fig. 8e and f). Fig. 8(g and h) demonstrate that when the areal capacity and cycling time were increased, only a slight morphological roughness was seen on the Li metal surface, while no obviously substantial Li dendrites and excessive cracks occurred. The set of SEM images show the process of the function MOF served. Benefiting from the HKUST-1 containing SPE, a stable interfacial contact was obtained, which illustrated the Li deposition with the modification of MOF material.[89] Instead of Li dendrites, many flake-shaped structures with nanoscale thickness can be observed, as compared in Fig. 8(i and j). Instead of dendritic deposition, Li tended to deposit in a flaky form in the cells under the suppression of Li-IL@MCM-41.[35]

3.4 Lithium–sulfur batteries

For solid state lithium–sulfur batteries, there are other several issues:[91–93] (i) the polysulfide shuttle effect, which lies in the

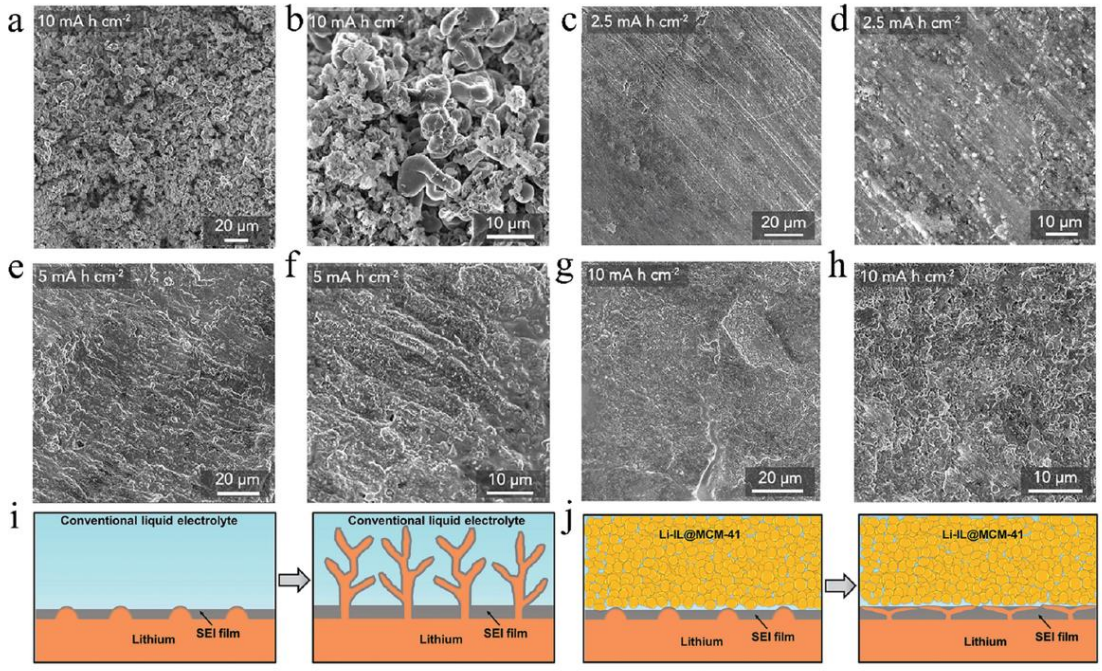

Fig. 8 Surface morphologies of the cycled Li-metal electrode at different current densities: (a and b) top-view scanning EM images of the Li-metal electrode with pristine electrolyte at the areal capacity of 10 mA h cm^{-2} after 120 h. (b) The overgrown Li dendrites (a) can be clearly observed in the enlarged view. (c–h): Top-view scanning EM images of the Li-metal electrode with MOF-modified electrolyte (c and d) at the areal capacity of 2.5 mA h cm^{-2} after 1000 h, (e and f) 5 mA h cm^{-2} after 800 h, and (g and h) 10 mA h cm^{-2} after 800 h. (i) Schematic illustration of the dendritic Li growth (reproduced with permission,[5] Copyright 2018 Elsevier B.V.). (j) Schematic illustrations of the Li deposition process in conventional liquid electrolytes (upper panel) and the Li-IL@MCM-41 SSE (lower panel) (reproduced with permission,[35] Copyright 2018 Royal Society of Chemistry).

View Article Online
Materials Chemistry Frontiers Review

high solubility of lithium polysulfides (LiPSs) in the matrixes, especially in the liquid electrolytes and polymer involved solid-state electrolyte systems. Once the concentration gradient and electric field force in the battery were close to their critical values, the polysulfide shuttled between the electrodes, resulting in the fading of the fast capacity, low coulombic efficiencies, and the corrosion of the Li metal anode. (ii) The chemical/electrochemical instabilities. The vulnerable sulfide-based SSEs are sensitive to the ambient environment. Ineluctable exposure to O_2 and H_2O can generate hazardous H_2S, followed by the decomposition of SSEs.[94] (iii) Insulating properties of S and Li_2S. In SSLSBs systems, the charge/discharge end products generated by active materials (S, LiPSs, or Li_2S) are S and Li_2S, offering high electrical conductivities and insulating ionic conductivities, and extremely slow Li^+ transportation. The conversion between S and Li_2S is quite limited, leading to inefficient active material utilization and low discharge availability.[95] (iv) Large volumetric changes during lithium insertion and extraction process caused by different densities of Li_2S and S, which can induce the cathode and cathode fracture, as well as separate the active materials from the Li^+/e^- conductors, finally giving rise to fast capacity decay.

MOF materials have been used to fabricate the electrodes and separators of Li–S batteries for their excellent performance.[96–98] There are several approaches to block the polysulfide shuttle. One strategy is through the utilization of the size difference of the MOF channels and polysulfides. Another way is the chemical interactions produced by the active unsaturated metal sites of MOFs. According to these strategies, Zhou *et al.* reported a MOF coating graphene oxide (MOF@GO) separator to ease the shuttling problem of the Li–S batteries.[99] Within the tailored separator, the small pore of MOF can significantly inhibit the pierce of the long chain polysulfides through the separator. The free-standing HKUST-1@GO separator was fabricated by the *in situ* growth method through vacuum filtration. For solid Li–S batteries, these strategies are also suitable.

Mg-MOF-74 was used in a quasi SSE to stabilize the Li anode for the Li–S battery.[4] Fig. 9(a) shows the ion transport in the electrolyte. Results show that the polysulfide shuttle was inhibited due to the porous structure and Lewis acid effect mentioned before. For the long cycling performance at 0.1C rate during 200 cycles, the MOF-PVDF GPE batteries delivered a comparatively low capacity fading with a slight capacity decay. In Fig. 9(c), the mobile $TFSI^-$ from the electrolyte with smaller t^+ traveled easily to the direction opposite to the Li^+ ions, thus plaguing the Li^+ transportation. On the contrary, the Mg-MOF-74 material can effectively restrain the $TFSI^-$ anions within the well-ordered pores, based on the steric hindrance effect and Lewis acid-based effect. According to the space charge theory, once the large $TFSI^-$ anions are immobilized, the Li-ions can transport smoothly from the electrolyte to the Li metal anode within the channels. Thus, due to the influence of anions, the MOF fabricated GPE is more stable and compatible for the Li anode. The shuttle effect of the polysulfide seriously affects the performance of the battery. They also found that after 7 days, the polysulfide was still inhibited by the MOF SSE, indicating a chemical stability and excellent polysulfide inhibiting effect. This was first ascribed to the confinement ability of the nanopores of MOF, which can suppress the penetration of the polysulfide species. In addition, the negatively charged polysulfides can bond with the positive charged metallic centre, thus boosting the Li ion mitigation. Fig. 9(c) illustrates the fabrication of SSE using Uio-66.[17] The results of the Li symmetric cells suggested the stable solid/solid interfacial contact.

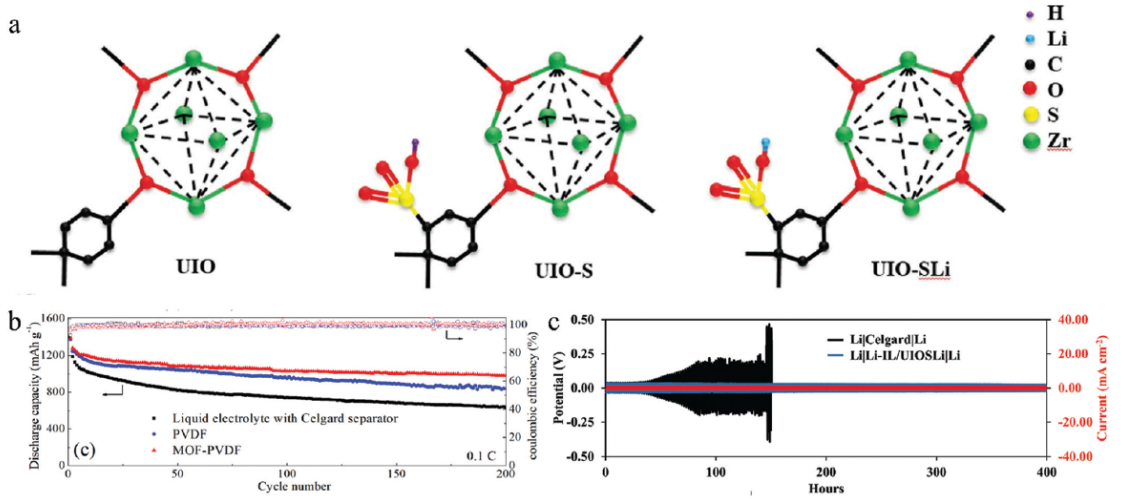

Fig. 9 (a) Schematic illustration of MOF-PVDF GPE with anions immobilized for the lithium–sulfur battery. (b) The cycling ability at a rate of 0.1C of the cells with various electrolytes (reproduced with permission,[4] Copyright 2019 American Chemical Society). (c) Schematic structures of UIO (Universitetet i Oslo) material, UIOS (UIO grafted with SO_3H), and UIOSLi (UIO grafted with SO_3Li). The results of the Li symmetric cells suggested the stable solid/solid interfacial contact.

The Gao group developed a GPE to stabilize the lithium–sulfur battery.[4] With the bi-functional MOF-based GPE, the rate capability and cycle life span of the Li–S battery were highly improved.

3.5 Li–oxygen batteries

Because of their large theoretical energy density of 3505 W h kg^{-1}, numerous efforts have been put into the rechargeable lithium oxygen batteries (LOBs).[100–102] However, there are several factors that plague the practical applications of the Li–O_2 batteries, including the unexpected high overpotential, poor cycling stability and relatively low rate capacity. Besides, the electrolytes and byproducts deposited on the surface of the cathode lead to the poor O_2 diffusion, severely deteriorating the battery performance.[103,104] Hollow materials are adopted to advance the catalysts of the O_2 electrodes for the Li–O_2 batteries with high performance.[105,106]

In consideration of the great potential of MOFs as adsorbents and separators for CO_2 capture and other gas separation, constructing a MOF-based film that can highly permeate O_2, while blocking the moisture and CO_2 are is promising. To block the moisture and CO_2, Lu and colleagues first set up a mixed matrix membrane (MMM) by coating Al-based MOF (CAU-1-NH_2) with polydopamine (CAU-1-NH_2@PDA) and polymethylmethacrylate (PMMA) for the Li–air batteries.[6] In the system, CO_2 is fully absorbed by the extensive –NH_2 from CAU-1-NH_2. In addition, the PMMA confers the film with highly hydrophobic property. Results show that under an ambient atmosphere, the Li–air battery with this MMM film exhibited a much better cycling stability and significantly higher charge/discharge capacity than those without the MMM film, as Fig. 10(a) shows. The structures of CAU-1-NH_2@PDA-PMMA are displayed in Fig. 10(b and c). This would render the well-defined MOF coatings as a promising application, because the MOF materials have abundant ion transport channels, which could promote ion movement and therefore increase the electrode capacity. In addition, the amount of CO_2 molecules entering the cell can be significantly decreased by the abundant functional groups (–NH_2, –OH and –C═O groups) within the MOF@PDA structure and PMMA matrix. Thus, the formation of lithium carbonates that can be reversible are inhibited, resulting in enhanced cycling performance and efficiency. A Grotthuss-like single-ion and versatile SSE was prepared by

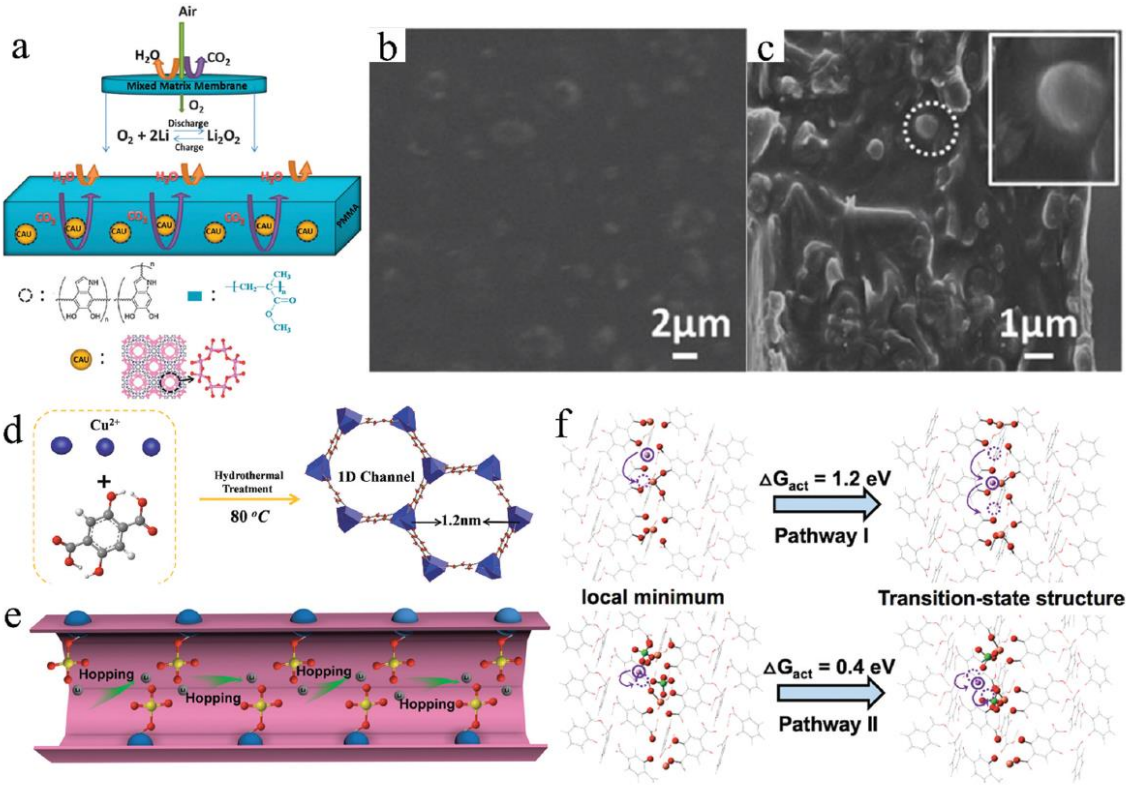

Fig. 10 (a) The schematic illustration of the MMM based on CAU-1-NH_2@PDA (PDA = polydopamine) and PMMA polymer for repelling H_2O and CO_2 molecules. The framework of CAU-1-NH_2 viewed along the *c* axis (f) and symbol: Al, pink; O, red; C, gray; H, blue. (b and c) Top and side view of the MMM based on CAU-1-NH_2@PDA-PMMA. The inset image in d is the 25 times magnified MOF particle indicated in the circle[6] (reproduced with permission, Copyright 2015 Royal Society of Chemistry). Synthesis and characterization of the single-ion electrolyte: (d) schematic illustration of the structure of Cu-MOF-74. (e) Schematic illustration of the Li diffusion path in the pore of the MOF (O atoms: red, Cl atoms: yellow; Cu atoms: blue; Li atoms: grey). (f) Quantum chemistry investigation of Li migration in the single-ion electrolyte (reproduced with permission,[23] Copyright 2020 Royal Society of Chemistry).

View Article Online
Materials Chemistry Frontiers Review

Wang and coworkers for dendrite-free LMBs.[23] As Fig. 10(d) shows, the Cu^{2+} ions can coordinate with the Li salt anions ClO^{4-}, and then be confined in the one-dimensional pores of Cu-MOF-74. The Li-ion transport is shown in Fig. 10(e), as discussed in Section 1.2.1. Fig. 10(f) displays the single-ion mechanism for Li^+. The low active energy for the hopping of Li ions between the ClO^{4-} anchored onto the open metal sites of Cu-MOF-74 indicate that the Li^+ hooping mechanism dominates the Li^+ migration, leading to an improved cycle life with reduced overpotential for the dendrite-free Li–O_2 batteries.

In summary, besides the great potentials as electrocatalysis or MOF-derived carbon coating layers, MOFs also exhibit an effective O_2 selective separator for both Li–O_2 and Li–air batteries. As separators for Li–air batteries, MOFs are favored because of the high CO_2 absorption ability and the hydrophobic quality. To date, only limited efforts were put into exploring MOFs on Li–O_2 batteries. The various organic ligands, adjustable pore structure of MOFs show great opportunities to enable Li–O_2 batteries with high performance.

4. MOFs-based SSEs for other metal batteries

Although the inherent properties, such as high theoretically energy capacity and reversible redox activity of the Li metal, enable Li and Li-ion batteries as the most promising energy sources, safety issues and Li abundance are still obstacles that need to be resolved in order to optimize the cell performance. In a comprehensive view of the safety, electrochemical performance, and abundance, other metals, namely Na, Mg, Al, K, Ca and Zn, have attracted increasing exploration for battery applications in the past few decades.

4.1 Sodium–metal batteries

Except for the Li-metal batteries, the research of Na-metal batteries are also booming because of their theoretical capacity of 1166 mA h g^{-1}, low redox potential ($E_{Na^+/Na}$ = −2.71 V *vs.* standard hydrogen electrode), low cost of abundant metallic Na, and can meet with large-scale energy storage application.[107] The similar storage mechanisms as Li metal batteries enable Na metal batteries as one of the most promising generation for commercial and large-scale applications.[108] However, the large size of Na^+ ions hinders their insertion and extraction from the active materials.[109] Although the MOF materials are adopted to fabricate the electrodes for better performance,[110,111] the use of MOF-based SSEs on Na metal batteries is not widely developed.

Liu first reported the adoption of MOF in SPE for sodium-sulfur batteries.[3] In their work, a flexible PEO-$NaCF_3SO_3$-MIL-53(Al) SSE was prepared. Fig. 11(a) shows that the SSE film was flexible enough for preparing batteries with special shape requirements. In addition, the ionic conductivity of the MOF-modified SSE was higher than the SSE without MOF from 40 to 100 °C (Fig. 11b and c). This improvement is mainly caused by the existence of MIL-53(Al) that improves the segment motion of PEO units through lowering the crystallization. Besides, the Lewis acidity on the surface of MIL-53(AL) enhanced the dissociation of sodium salts as well. Fig. 11(d–f) shows that the

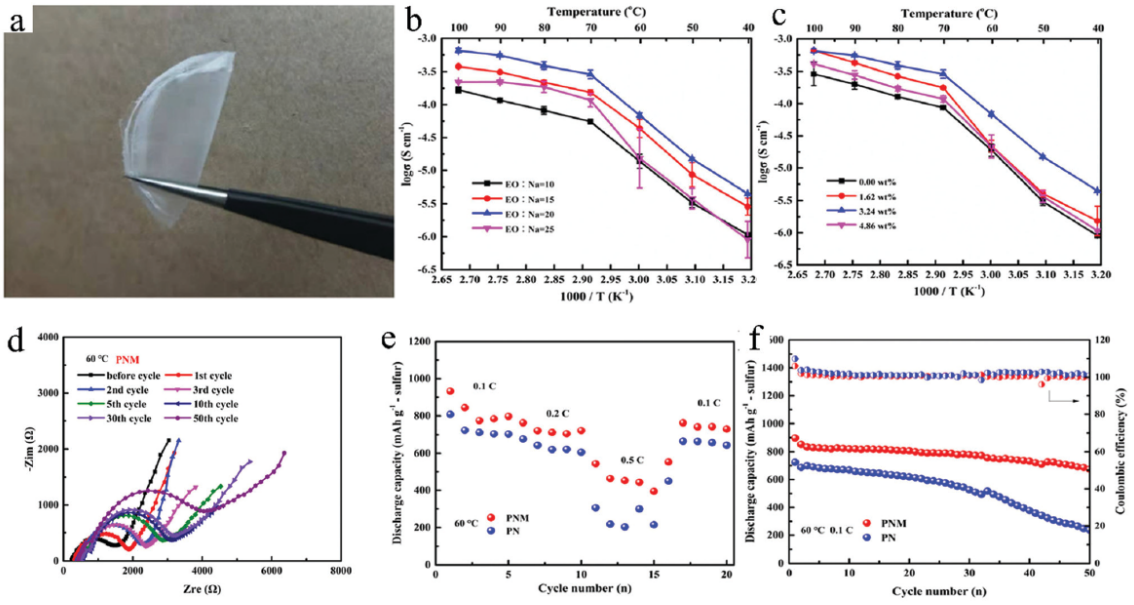

Fig. 11 (a) A photo of the PNM membrane. (b) Ionic conductivities of PNM with the EO : Na ratios of 10 : 1, 15 : 1, 20 : 1, and 25 : 1. (c) Ionic conductivities of PNM with 0.00, 1.62, 3.24, and 4.86 wt% of MIL-53(Al). (d) Nyquist profiles of PNM-based ASSBs. (e) Cycling performance of the PNM- and PN-based ASSBs at 60 °C and (e) 0.1C and (f) 0.5C (reproduced with permission,[3] Copyright 2020 Springer Nature).

interfacial resistance was also highly decreased. In addition, the cycling and realized rate performance showed higher capacity and longer cycling stability after the addition of MOF material.

4.2 Zn batteries

In view of its high theoretical capacity (820 mA h g^{-1}), eco-friendly nature, low redox potential (−0.76 V *vs.* SHE), abundant and available resources/low cost, metallic Zn is considered as a potential candidate for the anode material.[112,113] However, in aqueous electrolytes, the Zn metal batteries still suffer from dendrite formation and growth, resulting in poor deposition reversibility, which plague its practical applications.[114]

The Zhi group used the property of catalysis of the Fe-based MOF fabricated with an elastic polyacrylamide hydrogen-based electrolyte, and tailored the Zn electrode, as shown in Fig. 12(a–c).[8] The SSE can still maintain high elasticity in the corrosive alkaline environment. With almost no charge/discharge and output power deterioration, the obtained battery can be condensed by up to 54% strain and bent up to 90°. The MOF used in this system functioned as an oxygen catalyst. Furthermore, a novel single ion Zn^{2+} SSE was fabricated using post-synthetic modified MOF-808 ($[Zr_6O_4(OH)_4(HCOO)_6(BTC)_2]$) for a dendrite-free Zn battery.[12] After being treated by HCl, the neutral MOF-808 was charged negatively, along with a high charge density. Simultaneously, $Zn(H_2O)_6^{2+}$ took the place of the H^+ counter ions in the pores. As a result, high ionic conductivity, minor activation energy, and high Zn^{2+} transference number were realized, accompanied by stable mechanical and electrochemical performance. Because the $Zn(H_2O)_6^{2+}$ ions were caged in the nanowetted Zn/SSE interface, the uniform Zn deposition revealed excellent compatibility on the interfaces between the Zn anode and the SSE. This was consistent with the stable Zn plating/stripping performance, leading to a uniform, dense and smooth Zn deposition layer. The function of the MOF SSE was further confirmed by VS_2/Zn batteries, which exhibited a high and reversible capacity during long-term cycling without serious capacity decay.

Fig. 12(e) shows the compatibility between the crystalline single-ion water@ZnMOF-808 (WZM) SSE and the Zn metal anode.[12] Under the current density of 0.1 mA cm^{-2}, the cycle can be stable within 360 h. During this period, the voltage distribution of each cycle is relatively smooth, and the potential

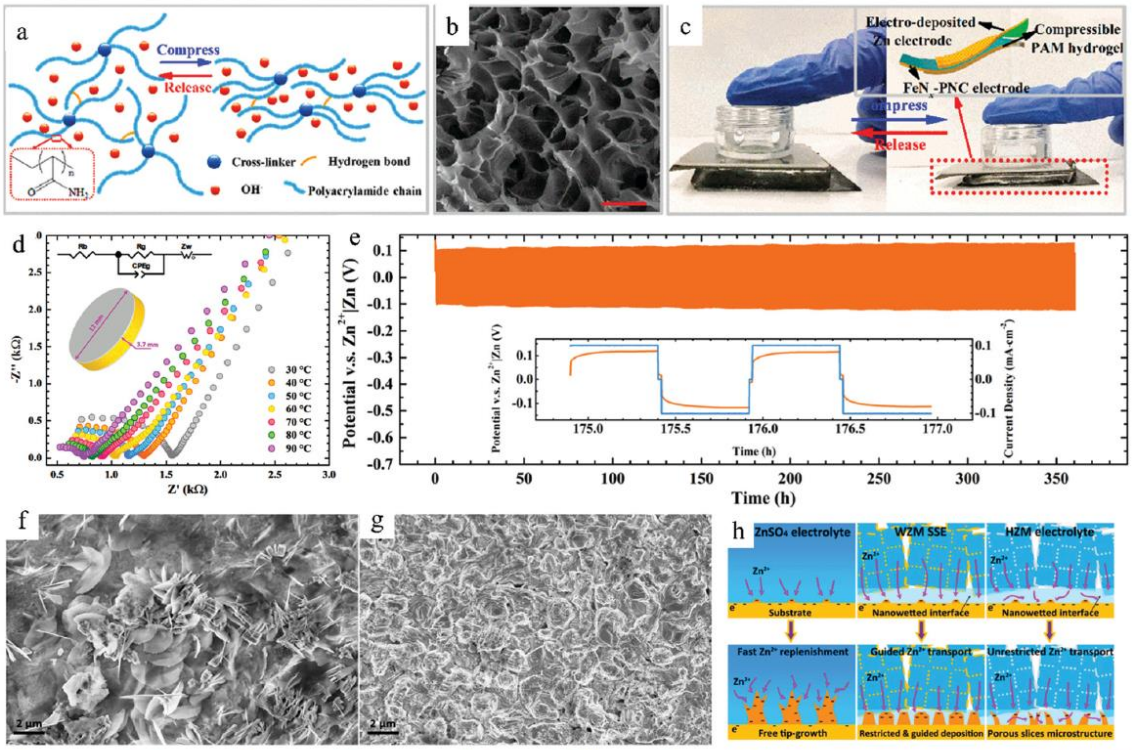

Fig. 12 (a) Schematic diagram of the origin of high compressibility for a PAM hydrogel electrolyte. The inset is the molecular formula of PAM. (b) SEM image of a freeze-dried polyacrylamide (PAM) hydrogel. (c) Compression–release process of the as-assembled compressible zinc–air battery. The inset is a schematic diagram of the construction process for the solid-state zinc–air battery (reproduced with permission,[8] copyright 2018 American Chemical Society). (d) Scheme for the post-synthetic modification chemistry, inset: size of the SSE pellet for EIS test. (e) Zn plating/stripping performance of the Zn|WZM|Zn symmetric cell under a current density of 0.1 mA cm^{-2} at room temperature. SEM images of the Zn foils after plating/stripping cycles of (f) the Zn|$ZnSO_4$|Zn cell and (g) Zn|WZM|Zn cell. (h) Proposed mechanism for the different deposition behaviors of the $ZnSO_4$ aqueous electrolyte (left column), WZM SSE (middle column) and HZM electrolyte (right column) (reproduced with permission,[12] Copyright 2018 Elsevier B.V.).

View Article Online
Materials Chemistry Frontiers Review

increases from 0.10 V to 0.12 V. Because of the slack interfacial contact between SSE and the Zn anode during the aging time, the polarization of the initial cycle is larger than other cycles. By repeating the Zn plating/stripping process, the interfacial resistance can be reduced after cycling, thus boosting the interfacial contact. The electrolyte can highly determine the deposition morphologies of the Zn metal. SEM images show the morphologies of the Zn foil with liquid and MOF-based SSE after cycling in Fig. 12(f and g). It is clear that for the batteries with MOF-based SSE, a compact and uniform Zn deposition was formed on the Zn anode without Zn dendrite. After cycling, further analysis showed that there was no impure ZnO phase generated by the unwanted $Zn(OH)_2$ deposition.

For comparison in Fig. 12h, after the charge/discharge process in the $ZnSO_4$ electrolyte, numerous micro-sized Zn flakes with sharp edges were formed on the Zn foil, which consequently formed a porous and loose Zn layer, causing large pulverization. On the contrary, the $Zn(H_2O)_6^{2+}$ ions transport into the sub-nano channels of the MOF host. The nano-wetted interface was also beneficial to the movement of Zn^{2+}, which enabled the uniform and dendrite-free Zn deposition. The results show that the MOF-fabricated SSE has better compatibility with the Zn anode than traditional liquid electrolytes, and can effectively avoid the loose deposition and dendrite Zn deposition.

4.3 Mg batteries

As a promising candidate to lithium-ion batteries, magnesium batteries have been studied because of their higher volumetric capacity of 3832 mA h cm^{-3}, low cost and abundant resource compared to Li metal.[115] In addition, Mg possesses the safety property in that Mg metal is not sensitive to dendrite.[116] However, finding the suitable electrolytes is still the challenge that blocks the application of Mg batteries.[117] For the first time, the Long group investigated a series of solid magnesium electrolytes through MOFs soaked with three different magnesium phenolates.[7] The mechanically robust transparent electrolytes exhibited unprecedentedly high room-temperature ionic conductivities of 0.25 mS cm^{-1}. As shown in Fig. 13, several MOF-based magnesium electrolytes were constructed, and their ionic conductivity were also tested and compared. It was found that the ionic conductivity values can vary by over four orders of magnitude, through changing the pore sizes and altering the anion basicity of the guest electrolyte salts. The highest values can also reach 0.25 mS cm^{-1}. Mircea Dincă's group probed the Mg^{2+} ion conductivity in the Cu-azolate MOF.[84,118] The result showed that MOF-$MgBr_2$ possessed a high ionic conductivity of 1.3×10^{-4} S cm^{-1} with relatively low active energy, which can be the good conductive media of Mg^{2+} ion SSE.[84] Although there is quite limited research on the

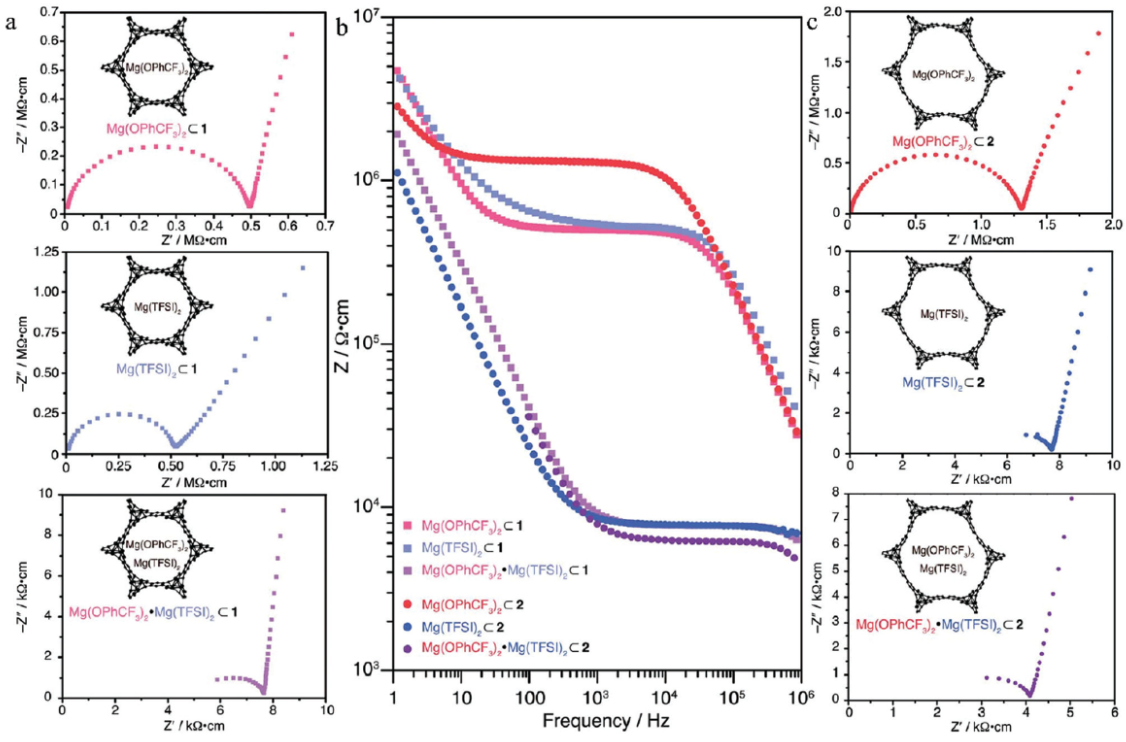

Fig. 13 AC impedance data (1 MHz to 1 Hz) at 298 K. Center: Bode plot illustrating the bulk impedance as a plateau for $Mg(OPhCF_3)_2 < 1$ (light red), $Mg(TFSI)_2 < 1$ (light blue), $Mg(OPhCF_3)_2{\cdot}Mg(TFSI)_2 < 1$ (light purple), $Mg(OPhCF_3)_2 < 2$ (dark red), $Mg(TFSI)_2 < 1$ (dark blue), and $Mg(OPhCF_3)_2{\cdot}Mg(TFSI)_2 < 1$ (dark purple). Left: Nyquist plots for the host framework 1, and right: Nyquist plots for the host framework 2; colors match those in the Bode plot. The leftmost point in the Nyquist plots corresponds to an AC frequency of 1 MHz (reproduced with permission,[7] Copyright 2014 Royal Society of Chemistry).

study of SSEs for Mg batteries, the MOF material can be the most advanced candidate for exploring new methods to construct and design Mg batteries.

5. Conclusions and perspectives

As a good choice for the solid-state electrolytes for Li metal and other metal batteries, MOF-based solid electrolytes hold the promise of achieving high performance batteries in recent years. In this paper, the current research on MOFs and their derivatives as SSE materials for Li and other metal batteries is reviewed. These MOF-based solid electrolytes can realize the flexibility and mechanical robustness, thus enhancing the performance of the Li metal batteries. Research progress has illustrated that the MOF-based SSEs serve as multifunctional SSEs with impressive performances. The unique properties of the porous MOF materials with tunable components and unsaturated sites have been widely used for high performance metal batteries. Although they have been widely studied, lithium and other metal batteries are still in the initial stages for commercial application, and the interface problem, safety issues, and lithium dendrite still hinder the advance of metal batteries. MOFs and their derived metal oxides are still facing some challenges in the following aspects.

(1) The stability of MOFs, especially the porous structure, is still the most important issue to be used in metal batteries. However, the long-term stability of MOFs in the complex electrochemical environment of batteries is still not so good, which is also the reason for the limited rate and cycle stability of the MOFs-based electrode or SSEs. Pre- or post-modification of the MOF material with different methods can be fully developed to enhance the stability, and meet the requirement of SSEs for metal batteries.

(2) The intrinsic ionic conductivity of MOFs and MOF-derivatives needs to be improved, which is very important for the capacity and rate performance of lithium and other metal batteries. New MOF materials and an effective modification method need to be deeply developed. Effects of the MOF structure, including pore size, nanoparticle morphology, crystallite size, and framework topology, on the charge transport properties are expected to be explored. In addition, the cations and anions of the guest salt, solvent polarity, and cathode material matching have an impact on the behavior of SSEs.

(3) The lack of efficient approaches to fabricate the film of MOF containing SSEs. Currently, there are two main ways to prepare the film, including doctor blading method and hot-pressing method. The Doctor blading method needs a relatively long time, and the films are sensitive to temperature. Prepared films made by hot-pressing method are too thick for the transport of Li ions, and are rigid to stabilize the interfacial contact. Moreover, the uneven distribution of each component is inevitable. Other advanced ways, like 3D printing, can be explored in terms of producing the film.

(4) A deep investigation of the electrochemical mechanism of MOFs in SSEs should be further studied. The compatibility of bulk MOF with polymers is not fully studied. One main function of fillers is to decrease the crystalline of polymers, thus boosting the metal ion transport. Through suitable regulation, such as changing the pore size or reducing the grain boundary, the crystallinity of the polymers would be highly decreased and the compatibility can also be improved.

(5) Other functions of MOF materials, including the absorption of trace gas and liquids, are not investigated and fully developed. For instance, in the process of *in situ* polymerization induced by AIBN (azodiisobutyronitrile) inside the battery, trace gas nitrogen will be produced, which poses a threat to the battery system. The existence of nanoporous MOF particles can absorb the trace gas to guarantee the safety. The metallic cation and Lewis acid can induce the ring opening polymerization, which are not explored in the system. In addition, careful research on the safety tests, like the thermal runaway, need to be carried out to extend the application of this type of SSE.

Overall, although the application of MOF-based SSEs for metal batteries have been widely studied, the full utilization of MOF materials need innovative exploration.

Conflicts of interest

There are no conflicts to declare.

Acknowledgements

We are grateful to the National Natural Science Foundation of China (Grant No. 51922099), Innovation Academy for Light-duty Gas Turbine, Chinese Academy of Sciences (Grant No. CXYJJ20-MS-05), and Natural Science Foundation of Hebei Province for Distinguished Young Scholars (E2020103052).

References

1 B. M. Wiers, *et al.*, A Solid Lithium Electrolyte *via* Addition of Lithium Isopropoxide to a Metal–Organic Framework with Open Metal Sites, *J. Am. Chem. Soc.*, 2011, **133**(37), 14522–14525.
2 Z. Wang, *et al.*, A Metal–Organic-Framework-Based Electrolyte with Nanowetted Interfaces for High-Energy-Density Solid-State Lithium Battery, *Adv. Mater.*, 2018, **30**(2), 1704436.
3 Z. Ge, J. Li and J. Liu, Enhanced electrochemical performance of all-solid-state sodium-sulfur batteries by PEO-$NaCF_3SO_3$-MIL-53(Al) solid electrolyte, *Ionics*, 2020, **26**(4), 1787–1795.
4 D.-D. Han, *et al.*, Metal–Organic-Framework-Based Gel Polymer Electrolyte with Immobilized Anions To Stabilize a Lithium Anode for a Quasi-Solid-State Lithium–Sulfur Battery, *ACS Appl. Mater. Interfaces*, 2019, **11**(20), 18427–18435.
5 S. Bai, *et al.*, High-Power Li-Metal Anode Enabled by Metal-Organic Framework Modified Electrolyte, *Joule*, 2018, **2**(10), 2117–2132.
6 L. Cao, *et al.*, A high performance O_2 selective membrane based on CAU-1-NH_2@polydopamine and the PMMA

polymer for Li–air batteries, *Chem. Commun.*, 2015, **51**(21), 4364–4367.
7 M. L. Aubrey, *et al.*, Metal–organic frameworks as solid magnesium electrolytes, *Energy Environ. Sci.*, 2014, **7**(2), 667–671.
8 L. Ma, *et al.*, Single-Site Active Iron-Based Bifunctional Oxygen Catalyst for a Compressible and Rechargeable Zinc–Air Battery, *ACS Nano*, 2018, **12**(2), 1949–1958.
9 N. Chen, *et al.*, A Li^+ conductive metal organic framework electrolyte boosts the high-temperature performance of dendrite-free lithium batteries, *J. Mater. Chem. A*, 2019, **7**(16), 9530–9536.
10 D. E. Mathew, *et al.*, Influence of MOF ligands on the electrochemical and interfacial properties of PEO-based electrolytes for all-solid-state lithium batteries, *Electrochim. Acta*, 2019, **319**, 189–200.
11 S. Suriyakumar, *et al.*, Charge–discharge studies of all-solid-state Li/$LiFePO_4$ cells with PEO-based composite electrolytes encompassing metal organic frameworks, *RSC Adv.*, 2016, **6**(99), 97180–97186.
12 Z. Wang, *et al.*, A MOF-based single-ion Zn^{2+} solid electrolyte leading to dendrite-free rechargeable Zn batteries, *Nano Energy*, 2019, **56**, 92–99.
13 J.-F. Wu and X. Guo, Nanostructured Metal–Organic Framework (MOF)-Derived Solid Electrolytes Realizing Fast Lithium Ion Transportation Kinetics in Solid-State Batteries, *Small*, 2019, **15**(5), 1804413.
14 N.-W. Li, *et al.*, Passivation of Lithium Metal Anode via Hybrid Ionic Liquid Electrolyte toward Stable Li Plating/Stripping, *Adv. Sci.*, 2017, **4**(2), 1600400.
15 D. Rehnlund, *et al.*, Lithium trapping in alloy forming electrodes and current collectors for lithium based batteries, *Energy Environ. Sci.*, 2017, **10**(6), 1350–1357.
16 D. Fang, *et al.*, ZnS quantum dots@multilayered carbon: geological-plate-movement-inspired design for high-energy Li-ion batteries, *J. Mater. Chem. A*, 2018, **6**(18), 8358–8365.
17 P. Chiochan, *et al.*, A Metal Organic Framework Derived Solid Electrolyte for Lithium–Sulfur Batteries, *Adv. Energy Mater.*, 2020, **10**(27), 2001285.
18 X. Wang, *et al.*, Supercritical fluid-assisted preparation of Si/CNTs@FG composites with hierarchical conductive networks as a high-performance anode material, *Appl. Surf. Sci.*, 2020, **522**, 146507.
19 K. Wen, *et al.*, Solid–Liquid Electrolyte as a Nanoion Modulator for Dendrite-Free Lithium Anodes, *ACS Appl. Mater. Interfaces*, 2018, **10**(24), 20412–20421.
20 Y. Chen, *et al.*, Recent progress in all-solid-state lithium batteries: the emerging strategies for advanced electrolytes and their interfaces, *Energy Storage Mater.*, 2020, **31**, 401–433.
21 W. Li, *et al.*, Nanoporous Adsorption Effect on Alteration of the Li^+ Diffusion Pathway by a Highly Ordered Porous Electrolyte Additive for High-Rate All-Solid-State Lithium Metal Batteries, *ACS Appl. Mater. Interfaces*, 2018, **10**(28), 23874–23882.
22 W. Xu, *et al.*, A Metal–Organic Framework of Organic Vertices and Polyoxometalate Linkers as a Solid-State Electrolyte, *J. Am. Chem. Soc.*, 2019, **141**(44), 17522–17526.
23 S. Yuan, *et al.*, A versatile single-ion electrolyte with a Grotthuss-like Li conduction mechanism for dendrite-free Li metal batteries, *Energy Environ. Sci.*, 2019, **12**(9), 2741–2750.
24 L. Buannic, *et al.*, Dual Substitution Strategy to Enhance Li^+ Ionic Conductivity in $Li_7La_3Zr_2O_{12}$ Solid Electrolyte, *Chem. Mater.*, 2017, **29**(4), 1769–1778.
25 N.-W. Li, *et al.*, An Artificial Solid Electrolyte Interphase Layer for Stable Lithium Metal Anodes, *Adv. Mater.*, 2016, **28**(9), 1853–1858.
26 F. Mizuno, *et al.*, New, Highly Ion-Conductive Crystals Precipitated from Li_2S–P_2S_5 Glasses, *Adv. Mater.*, 2005, **17**(7), 918–921.
27 K. Wen, *et al.*, Fast Li-ion transport and uniform Li-ion flux enabled by a double-layered polymer electrolyte for high performance Li metal battery, *Energy Storage Mater.*, 2020, **32**, 55–64.
28 F. Chu, *et al.*, Metal–Organic Frameworks as Electrolyte Additives To Enable Ultrastable Plating/Stripping of Li Anode with Dendrite Inhibition, *ACS Appl. Mater. Interfaces*, 2019, **11**(4), 3869–3879.
29 G. Hou, *et al.*, Lithium Dendrite Suppression and Enhanced Interfacial Compatibility Enabled by an *Ex Situ* SEI on Li Anode for LAGP-Based All-Solid-State Batteries, *ACS Appl. Mater. Interfaces*, 2018, **10**(22), 18610–18618.
30 X. Chen, *et al.*, Enhancing interfacial contact in all solid state batteries with a cathode-supported solid electrolyte membrane framework, *Energy Environ. Sci.*, 2019, **12**(3), 938–944.
31 K. Pan, *et al.*, A Flexible Ceramic/Polymer Hybrid Solid Electrolyte for Solid-State Lithium Metal Batteries, *Adv. Mater.*, 2020, **32**(17), 2000399.
32 S. Wang, *et al.*, Interfacial Chemistry in Solid-State Batteries: Formation of Interphase and Its Consequences, *J. Am. Chem. Soc.*, 2018, **140**(1), 250–257.
33 B. Wu, *et al.*, The role of the solid electrolyte interphase layer in preventing Li dendrite growth in solid-state batteries, *Energy Environ. Sci.*, 2018, **11**(7), 1803–1810.
34 H. Huo, *et al.*, Rational Design of Hierarchical "Ceramic-in-Polymer" and "Polymer-in-Ceramic" Electrolytes for Dendrite-Free Solid-State Batteries, *Adv. Energy Mater.*, 2019, **9**(17), 1804004.
35 L. Han, *et al.*, An ordered mesoporous silica framework based electrolyte with nanowetted interfaces for solid-state lithium batteries, *J. Mater. Chem. A*, 2018, **6**(43), 21280–21286.
36 M. Eddaoudi, *et al.*, Systematic Design of Pore Size and Functionality in Isoreticular MOFs and Their Application in Methane Storage, *Science*, 2002, **295**(5554), 469–472.
37 O. M. Yaghi, *et al.*, Reticular synthesis and the design of new materials, *Nature*, 2003, **423**(6941), 705–714.
38 Z. Wang, *et al.*, Covalently linked metal–organic framework (MOF)-polymer all-solid-state electrolyte membranes for room temperature high performance lithium batteries, *J. Mater. Chem. A*, 2018, **6**(35), 17227–17234.
39 D. Fang, *et al.*, Synergistic Regulation of Polysulfides Conversion and Deposition by MOF-Derived Hierarchically Ordered Carbonaceous Composite for High-Energy Lithium–Sulfur Batteries, *Adv. Funct. Mater.*, 2019, **29**(19), 1900875.

40 L. Wei, *et al.*, MOF-derived lithiophilic CuO nanorod arrays for stable lithium metal anodes, *Nanoscale*, 2020, **12**(17), 9416–9422.
41 D. Fang, *et al.*, Spider-Web-Inspired Nanocomposite-Modified Separator: Structural and Chemical Cooperativity Inhibiting the Shuttle Effect in Li–S Batteries, *ACS Nano*, 2019, **13**(2), 1563–1573.
42 D. Sheberla, *et al.*, Conductive MOF electrodes for stable supercapacitors with high areal capacitance, *Nat. Mater.*, 2017, **16**(2), 220–224.
43 N. Xin, *et al.*, In-situ construction of metal organic frameworks derived Co/Zn–S sandwiched graphene film as free-standing electrodes for ultra-high energy density supercapacitors, *J. Power Sources*, 2020, **451**, 227772.
44 H. Yang, *et al.*, A Single-Ion Conducting UiO-66 Metal–Organic Framework Electrolyte for All-Solid-State Lithium Batteries, *ACS Appl. Energy Mater.*, 2020, **3**(4), 4007–4013.
45 H. Huo, *et al.*, Anion-immobilized polymer electrolyte achieved by cationic metal-organic framework filler for dendrite-free solid-state batteries, *Energy Storage Mater.*, 2019, **18**, 59–67.
46 B. Y. Xia, *et al.*, A metal–organic framework-derived bifunctional oxygen electrocatalyst, *Nat. Energy*, 2016, **1**(1), 15006.
47 D. Y. Ahn, *et al.*, Novel Solid-State Solar Cell Based on Hole-Conducting MOF-Sensitizer Demonstrating Power Conversion Efficiency of 2.1%, *ACS Appl. Mater. Interfaces*, 2017, **9**(15), 12930–12935.
48 R. Ameloot, *et al.*, Ionic Conductivity in the Metal–Organic Framework UiO-66 by Dehydration and Insertion of Lithium tert-Butoxide, *Chem. – Eur. J.*, 2013, **19**(18), 5533–5536.
49 B. Gui, *et al.*, Tuning the Photoinduced Electron Transfer in a Zr-MOF: Toward Solid-State Fluorescent Molecular Switch and Turn-On Sensor, *Adv. Mater.*, 2018, **30**(34), 1802329.
50 B. M. Wiers, *et al.*, A Solid Lithium Electrolyte via Addition of Lithium Isopropoxide to a Metal–Organic Framework with Open Metal Sites, *J. Am. Chem. Soc.*, 2011, **133**(37), 14522–14525.
51 C.-E. Lin, *et al.*, Carboxylated polyimide separator with excellent lithium ion transport properties for a high-power density lithium-ion battery, *J. Mater. Chem. A*, 2018, **6**(3), 991–998.
52 E. M. Miner and M. Dincă, Metal- and covalent-organic frameworks as solid-state electrolytes for metal-ion batteries, *Philos. Trans. R. Soc., A*, 2019, **377**(2149), 20180225.
53 R. Zhao, *et al.*, Metal–organic frameworks for solid-state electrolytes, *Energy Environ. Sci.*, 2020, **13**(8), 2386–2403.
54 Q. Zhao, *et al.*, Designing solid-state electrolytes for safe, energy-dense batteries, *Nat. Rev. Mater.*, 2020, **5**(3), 229–252.
55 A. Manthiram, X. Yu and S. Wang, Lithium battery chemistries enabled by solid-state electrolytes, *Nat. Rev. Mater.*, 2017, **2**(4), 16103.
56 C. Monroe and J. Newman, The Impact of Elastic Deformation on Deposition Kinetics at Lithium/Polymer Interfaces, *J. Electrochem. Soc.*, 2005, **152**(2), A396.
57 G. M. Stone, *et al.*, Resolution of the Modulus versus Adhesion Dilemma in Solid Polymer Electrolytes for Rechargeable Lithium Metal Batteries, *J. Electrochem. Soc.*, 2012, **159**(3), A222–A227.
58 Y. Shen, *et al.*, Unlocking the Energy Capabilities of Lithium Metal Electrode with Solid-State Electrolytes, *Joule*, 2018, **2**(9), 1674–1689.
59 W. D. Richards, *et al.*, Interface Stability in Solid-State Batteries, *Chem. Mater.*, 2016, **28**(1), 266–273.
60 Y. Zhu, X. He and Y. Mo, First principles study on electrochemical and chemical stability of solid electrolyte–electrode interfaces in all-solid-state Li-ion batteries, *J. Mater. Chem. A*, 2016, **4**(9), 3253–3266.
61 C. F. N. Marchiori, *et al.*, Understanding the Electrochemical Stability Window of Polymer Electrolytes in Solid-State Batteries from Atomic-Scale Modeling: The Role of Li-Ion Salts, *Chem. Mater.*, 2020, **32**(17), 7237–7246.
62 T. Zhang, *et al.*, Designing composite solid-state electrolytes for high performance lithium ion or lithium metal batteries, *Chem. Sci.*, 2020, **11**(33), 8686–8707.
63 S. Chen, *et al.*, Progress and future prospects of high-voltage and high-safety electrolytes in advanced lithium batteries: from liquid to solid electrolytes, *J. Mater. Chem. A*, 2018, **6**(25), 11631–11663.
64 B. Liu, J.-G. Zhang and W. Xu, Advancing Lithium Metal Batteries, *Joule*, 2018, **2**(5), 833–845.
65 Z. Wu, *et al.*, Utmost limits of various solid electrolytes in all-solid-state lithium batteries: a critical review, *Renewable Sustainable Energy Rev.*, 2019, **109**, 367–385.
66 D. Lin, Y. Liu and Y. Cui, Reviving the lithium metal anode for high-energy batteries, *Nat. Nanotechnol.*, 2017, **12**(3), 194–206.
67 C.-Z. Zhao, *et al.*, Liquid phase therapy to solid electrolyte–electrode interface in solid-state Li metal batteries: a review, *Energy Storage Mater.*, 2020, **24**, 75–84.
68 N. Yanai, *et al.*, Inclusion and dynamics of a polymer–Li salt complex in coordination nanochannels, *Chem. Commun.*, 2011, **47**(6), 1722–1724.
69 K. Fujie, *et al.*, Introduction of an Ionic Liquid into the Micropores of a Metal–Organic Framework and Its Anomalous Phase Behavior, *Angew. Chem., Int. Ed.*, 2014, **53**(42), 11302–11305.
70 Y. Ban, *et al.*, Confinement of Ionic Liquids in Nanocages: Tailoring the Molecular Sieving Properties of ZIF-8 for Membrane-Based CO_2 Capture, *Angew. Chem., Int. Ed.*, 2015, **54**(51), 15483–15487.
71 Q. Zhang, *et al.*, The Optimized Interfacial Compatibility of Metal–Organic Frameworks Enables a High-Performance Quasi-Solid Metal Battery, *ACS Energy Lett.*, 2020, **5**(9), 2919–2926.
72 R. Dutta and A. Kumar, Probing the ionic transport dynamics in ionic liquid incorporated CuBTC-Metal-Organic Framework based PVdF-HFP nanocomposite membranes, *Solid State Sci.*, 2020, **100**, 106115.
73 Q. Li and H. Ardebili, Flexible thin-film battery based on solid-like ionic liquid-polymer electrolyte, *J. Power Sources*, 2016, **303**, 17–21.

74 M. Forsyth, *et al.*, Innovative Electrolytes Based on Ionic Liquids and Polymers for Next-Generation Solid-State Batteries, *Acc. Chem. Res.*, 2019, **52**(3), 686–694.
75 V. K. Singh, *et al.*, Solid polymer electrolytes based on Li^+/ionic liquid for lithium secondary batteries, *J. Solid State Electrochem.*, 2017, **21**(6), 1713–1723.
76 D. Golodnitsky, *et al.*, Review—On Order and Disorder in Polymer Electrolytes, *J. Electrochem. Soc.*, 2015, **162**(14), A2551–A2566.
77 K. Fujie, *et al.*, Lithium Ion Diffusion in a Metal–Organic Framework Mediated by an Ionic Liquid, *Chem. Mater.*, 2015, **27**(21), 7355–7361.
78 T.-S. Wang, *et al.*, High Areal Capacity Dendrite-Free Li Anode Enabled by Metal–Organic Framework-Derived Nanorod Array Modified Carbon Cloth for Solid State Li Metal Batteries, *Adv. Funct. Mater.*, 2020, 2001973.
79 J. Qian, *et al.*, Protecting lithium/sodium metal anode with metal-organic framework based compact and robust shield, *Nano Energy*, 2019, **60**, 866–874.
80 G. Wang, P. He and L.-Z. Fan, Asymmetric Polymer Electrolyte Constructed by Metal–Organic Framework for Solid-State, Dendrite-Free Lithium Metal Battery, *Adv. Funct. Mater.*, 2020, 2007198.
81 C. Gerbaldi, *et al.*, Innovative High Performing Metal Organic Framework (MOF)-Laden Composite Polymer Electrolytes for All Solid State Lithium Batteries, *J. Mater. Chem. A*, 2014, **2**(26), 9948–9954.
82 R. Senthil Kumar, *et al.*, Metal organic framework-laden composite polymer electrolytes for efficient and durable all-solid-state-lithium batteries, *RSC Adv.*, 2014, **4**(50), 26171–26175.
83 C. Yuan, *et al.*, Enhanced electrochemical performance of poly(ethylene oxide) based composite polymer electrolyte by incorporation of nano-sized metal-organic framework, *J. Power Sources*, 2013, **240**, 653–658.
84 E. M. Miner, S. S. Park and M. Dincă, High Li^+ and Mg^{2+} Conductivity in a Cu-Azolate Metal–Organic Framework, *J. Am. Chem. Soc.*, 2019, **141**(10), 4422–4427.
85 N. Angulakshmi, *et al.*, Composite Polymer Electrolytes Encompassing Metal Organic Frame Works: A New Strategy for All-Solid-State Lithium Batteries, *J. Phys. Chem. C*, 2014, **118**(42), 24240–24247.
86 Z. Zhang, *et al.*, MOF-derived ionic conductor enhancing polymer electrolytes with superior electrochemical performances for all solid lithium metal batteries, *J. Membr. Sci.*, 2020, **598**, 117800.
87 N. Angulakshmi, *et al.*, Microporous Metal–Organic Framework (MOF)-Based Composite Polymer Electrolyte (CPE) Mitigating Lithium Dendrite Formation in All-Solid-State-Lithium Batteries, *ACS Omega*, 2020, **5**(14), 7885–7894.
88 Z. Wang, *et al.*, Boosting interfacial Li^+ transport with a MOF-based ionic conductor for solid-state batteries, *Nano Energy*, 2018, **49**, 580–587.
89 J. Sun, *et al.*, Facilitating Interfacial Stability Via Bilayer Heterostructure Solid Electrolyte Toward High-energy, Safe and Adaptable Lithium Batteries, *Adv. Energy Mater.*, 2020, **10**(31), 2000709.
90 H. Wang, *et al.*, Thiol-Branched Solid Polymer Electrolyte Featuring High Strength, Toughness, and Lithium Ionic Conductivity for Lithium-Metal Batteries, *Adv. Mater.*, 2020, **32**(37), 2001259.
91 N. Li, *et al.*, From interlayer to lightweight capping layer: Rational design of mesoporous TiO_2 threaded with CNTs for advanced Li–S batteries, *Carbon*, 2019, **143**, 523–530.
92 X. Li, *et al.*, Hierarchically Porous C/Fe_3C Membranes with Fast Ion-Transporting Channels and Polysulfide-Trapping Networks for High-Areal-Capacity Li–S Batteries, *Nano Lett.*, 2020, **20**(1), 701–708.
93 Y. Li, *et al.*, Engineering stable electrode-separator interfaces with ultrathin conductive polymer layer for high-energy-density Li-S batteries, *Energy Storage Mater.*, 2019, **23**, 261–268.
94 Y. Wang, *et al.*, High-capacity lithium sulfur battery and beyond: a review of metal anode protection layers and perspective of solid-state electrolytes, *J. Mater. Sci.*, 2019, **54**(5), 3671–3693.
95 X.-B. Cheng, J.-Q. Huang and Q. Zhang, Review—Li Metal Anode in Working Lithium-Sulfur Batteries, *J. Electrochem. Soc.*, 2017, **165**(1), A6058–A6072.
96 J. Zheng, *et al.*, Lewis Acid–Base Interactions between Polysulfides and Metal Organic Framework in Lithium Sulfur Batteries, *Nano Lett.*, 2014, **14**(5), 2345–2352.
97 H. Jiang, *et al.*, Metal–Organic Frameworks for High Charge–Discharge Rates in Lithium–Sulfur Batteries, *Angew. Chem., Int. Ed.*, 2018, **57**(15), 3916–3921.
98 X. Liu, *et al.*, A new cathode material synthesized by a thiol-modified metal–organic framework (MOF) covalently connecting sulfur for superior long-cycling stability in lithium–sulfur batteries, *J. Mater. Chem. A*, 2019, **7**(42), 24515–24523.
99 S. Bai, *et al.*, Metal–organic framework-based separator for lithium–sulfur batteries, *Nat. Energy*, 2016, **1**(7), 16094.
100 Q.-C. Liu, *et al.*, Artificial Protection Film on Lithium Metal Anode toward Long-Cycle-Life Lithium–Oxygen Batteries, *Adv. Mater.*, 2015, **27**(35), 5241–5247.
101 Y.-C. Lu, *et al.*, Lithium–oxygen batteries: bridging mechanistic understanding and battery performance, *Energy Environ. Sci.*, 2013, **6**(3), 750–768.
102 L. Feng, *et al.*, Heterostructured CoO–Co_3O_4 nanoparticles anchored on nitrogen-doped hollow carbon spheres as cathode catalysts for Li–O_2 batteries, *Nanoscale*, 2019, **11**(31), 14769–14776.
103 C. Shu, *et al.*, Understanding the Reaction Chemistry during Charging in Aprotic Lithium–Oxygen Batteries: Existing Problems and Solutions, *Adv. Mater.*, 2019, **31**(15), 1804587.
104 J. Zhang, *et al.*, A versatile functionalized ionic liquid to boost the solution-mediated performances of lithium-oxygen batteries, *Nat. Commun.*, 2019, **10**(1), 602.
105 R. Bi, *et al.*, 3D Hollow α-MnO_2 Framework as an Efficient Electrocatalyst for Lithium–Oxygen Batteries, *Small*, 2019, **15**(10), 1804958.
106 A. Hu, *et al.*, Improved Cyclability of Lithium–Oxygen Batteries by Synergistic Catalytic Effects of Two-Dimensional MoS_2

Nanosheets Anchored on Hollow Carbon Spheres, *ACS Sustainable Chem. Eng.*, 2019, **7**(7), 6929–6938.

107 B. Lee, *et al.*, Sodium Metal Anodes: Emerging Solutions to Dendrite Growth, *Chem. Rev.*, 2019, **119**(8), 5416–5460.

108 Y. Lu, *et al.*, Electrolyte and Interface Engineering for Solid-State Sodium Batteries, *Joule*, 2018, **2**(9), 1747–1770.

109 T. Chen, *et al.*, Electrospun carbon nanofibers as anode materials for sodium ion batteries with excellent cycle performance, *J. Mater. Chem. A*, 2014, **2**(12), 4117–4121.

110 X. Ge, Z. Li and L. Yin, Metal-organic frameworks derived porous core/shell CoP@C polyhedrons anchored on 3D reduced graphene oxide networks as anode for sodium-ion battery, *Nano Energy*, 2017, **32**, 117–124.

111 Z. Li, *et al.*, Core-shell structured CoP/FeP porous microcubes interconnected by reduced graphene oxide as high performance anodes for sodium ion batteries, *Nano Energy*, 2017, **32**, 494–502.

112 Y. Tian, *et al.*, Flexible and Free-Standing $Ti_3C_2T_x$ MXene@Zn Paper for Dendrite-Free Aqueous Zinc Metal Batteries and Nonaqueous Lithium Metal Batteries, *ACS Nano*, 2019, **13**(10), 11676–11685.

113 Z. Hong, Z. Ahmad and V. Viswanathan, Design Principles for Dendrite Suppression with Porous Polymer/Aqueous Solution Hybrid Electrolyte for Zn Metal Anodes, *ACS Energy Lett.*, 2020, **5**(8), 2466–2474.

114 S. Deng, *et al.*, Electrochemically Induced MOF-Derived Amorphous V_2O_5 for Superior Rate Aqueous Zn-Ion Batteries, *Angew. Chem., Int. Ed.*, 2020, **132**(49), 22186–22190.

115 P. W. Jaschin, *et al.*, A materials perspective on magnesium-ion-based solid-state electrolytes, *J. Mater. Chem. A*, 2020, **8**(6), 2875–2897.

116 J. Song, *et al.*, Mapping the Challenges of Magnesium Battery, *J. Phys. Chem. Lett.*, 2016, **7**(9), 1736–1749.

117 J. Muldoon, *et al.*, Electrolyte roadblocks to a magnesium rechargeable battery, *Energy Environ. Sci.*, 2012, **5**(3), 5941–5950.

118 S. S. Park, Y. Tulchinsky and M. Dincă, Single-Ion Li^+, Na^+, and Mg^{2+} Solid Electrolytes Supported by a Mesoporous Anionic Cu–Azolate Metal–Organic Framework, *J. Am. Chem. Soc.*, 2017, **139**(38), 13260–13263.

2.9 Reference

1. Zubi, G., et al., The lithium-ion battery: State of the art and future perspectives. *Renewable and Sustainable Energy Reviews*, 2018. **89**: p. 292-308.

2. Li, J., et al., From Materials to Cell: State-of-the-Art and Prospective Technologies for Lithium-Ion Battery Electrode Processing. *Chemical Reviews*, 2022. **122**(1): p. 903-956.

3. Yang, Y., et al., On the sustainability of lithium ion battery industry – A review and perspective. *Energy Storage Mater.*, 2021. **36**: p. 186-212.

4. Li, Q., et al., Progress in electrolytes for rechargeable Li-based batteries and beyond. *Green Energy & Environment*, 2016. **1**(1): p. 18-42.

5. Wang, Q., et al., Progress of enhancing the safety of lithium ion battery from the electrolyte aspect. *Nano Energy*, 2019. **55**: p. 93-114.

6. Feng, X., et al., Thermal runaway mechanism of lithium ion battery for electric vehicles: A review. *Energy Storage Mater.*, 2018. **10**: p. 246-267.

7. Chen, J., et al., Research progress and application prospect of solid-state electrolytes in commercial lithium-ion power batteries. *Energy Storage Mater.*, 2021. **35**: p. 70-87.

8. Lv, F., et al., Challenges and development of composite solid-state electrolytes for high-performance lithium ion batteries. *Journal of Power Sources*, 2019. **441**: p. 227175.

9. Zheng, Y., et al., A review of composite solid-state electrolytes for lithium batteries: fundamentals, key materials and advanced structures. *Chemical Society Reviews*, 2020. **49**(23): p. 8790-8839.

10. Wang, Z., et al., 10 μm-Thick High-Strength Solid Polymer Electrolytes with Excellent

Interface Compatibility for Flexible All-Solid-State Lithium-Metal Batteries. *Adv. Mater.*, 2021. **33**(25): p. 2100353.

11. Wu, J., et al., Ultrathin, Flexible Polymer Electrolyte for Cost-Effective Fabrication of All-Solid-State Lithium Metal Batteries. *Adv. Energy Mater.*, 2019. **9**(46): p. 1902767.

12. Jiang, T., et al., Solvent-Free Synthesis of Thin, Flexible, Nonflammable Garnet-Based Composite Solid Electrolyte for All-Solid-State Lithium Batteries. *Adv. Energy Mater.*, 2020. **10**(12): p. 1903376.

13. Wu, J., et al., Reducing the thickness of solid-state electrolyte membranes for high-energy lithium batteries. *Energy Environ. Sci.*, 2021. **14**(1): p. 12-36.

14. Balaish, M., et al., Processing thin but robust electrolytes for solid-state batteries. *Nature Energy*, 2021. **6**(3): p. 227-239.

15. Zhang, Z., et al., New horizons for inorganic solid state ion conductors. *Energy Environ. Sci.*, 2018. **11**(8): p. 1945-1976.

16. Li, W., B. Song, and A. Manthiram, High-voltage positive electrode materials for lithium-ion batteries. *Chemical Society Reviews*, 2017. **46**(10): p. 3006-3059.

17. Li, M., et al., 30 Years of Lithium-Ion Batteries. *Adv. Mater.*, 2018. **30**(33): p. 1800561.

18. Niu, H., et al., Recent Advances in Application of Ionic Liquids in Electrolyte of Lithium Ion Batteries. *Journal of Energy Storage*, 2021. **40**: p. 102659.

19. Han, D.D., et al., Metal-Organic-Framework-Based Gel Polymer Electrolyte with Immobilized Anions To Stabilize a Lithium Anode for a Quasi-Solid-State Lithium-Sulfur Battery. *ACS Appl Mater Interfaces*, 2019. **11**(20): p. 18427-18435.

20. Liu, K., et al., Ionic liquids for high performance lithium metal batteries. *Journal of Energy Chemistry*, 2021. **59**: p. 320-333.

21. Liu, M., et al., Improving Li-ion interfacial transport in hybrid solid electrolytes. *Nature Nanotechnology*, 2022. **17**(9): p. 959-967.

22. Yang, M.Y., et al., Characterization of the Solid Electrolyte Interphase at the Li Metal–Ionic Liquid Interface. *Advanced Energy Materials*, 2023. **13**(3): p. 2202949.

23. Huang, G., et al., Tuning a Solvation Structure of Lithium Ions Coordinated with Nitrate Anions through Ionic Liquid-Based Solvent for Highly Stable Lithium Metal Batteries. *Advanced Functional Materials*, 2023. **33**(6): p. 2211364.

24. Yang, Y., et al., Ionic liquid enhanced composite solid electrolyte for high-temperature/long-life/dendrite-free lithium metal batteries. *Journal of Membrane Science*, 2020. **612**: p. 118424.

25. Wang, Z., et al., A Metal–Organic-Framework-Based Electrolyte with Nanowetted Interfaces for High-Energy-Density Solid-State Lithium Battery. *Advanced Materials*, 2018. **30**(2): p. 1704436.

26. Karuppasamy, K., et al., Ionic Liquid-Based Electrolytes for Energy Storage Devices: A Brief Review on Their Limits and Applications. *Polymers*, 2020. **12**(4): p. 918.

27. Nam, Y.J., et al., Toward practical all-solid-state lithium-ion batteries with high energy density and safety: Comparative study for electrodes fabricated by dry- and slurry-mixing processes. *Journal of Power Sources*, 2018. **375**: p. 93-101.

28. Shen, Y., et al., Unlocking the Energy Capabilities of Lithium Metal Electrode with Solid-State Electrolytes. *Joule*, 2018. **2**(9): p. 1674-1689.

29. McOwen, D.W., et al., 3D-Printing Electrolytes for Solid-State Batteries. *Adv. Mater.*, 2018. **30**(18): p. 1707132.

30. Cheng, M., et al., Elevated-Temperature 3D Printing of Hybrid Solid-State Electrolyte for Li-Ion Batteries. *Adv. Mater.*, 2018. **30**(39): p. 1800615.

31. Chen, A., et al., Manufacturing Strategies for Solid Electrolyte in Batteries. *Frontiers in Energy Research*, 2020. **8**.

32. Chen, D., et al., In Situ Preparation of Thin and Rigid COF Film on Li Anode as Artificial Solid Electrolyte Interphase Layer Resisting Li Dendrite Puncture. *Adv. Funct. Mater.*, 2020. **30**(7): p. 1907717.

33. Xu, S., et al., Homogeneous and Fast Ion Conduction of PEO-Based Solid-State Electrolyte at Low Temperature. *Adv. Funct. Mater.*, 2020. **30**(51): p. 2007172.

34. Walden, P., Molecular weights and electrical conductivity of several fused salts. *Bull. Acad. Imper. Sci.(St. Petersburg)*, 1914. **1800**.

35. Wilkes, J.S. and M.J. Zaworotko, Air and water stable 1-ethyl-3-methylimidazolium based ionic liquids. *J. Chem. Soc., Chem. Commun.*, 1992(13): p. 965-967.

36. Bonhôte, P., et al., Hydrophobic, Highly Conductive Ambient-Temperature Molten Salts. *Inorg. Chem.*, 1996. **35**(5): p. 1168-1178.

37. Welton, T., Ionic liquids: a brief history. *Biophysical Reviews*, 2018. **10**(3): p. 691-706.

38. Ren, F., et al., Applications of ionic liquids in starch chemistry: a review. *Green Chemistry*, 2020. **22**(7): p. 2162-2183.

39. Chatterjee, K., et al., Synthesis, characterization and application of a non-flammable

dicationic ionic liquid in lithium-ion battery as electrolyte additive. *Scientific Reports*, 2020. **10**(1): p. 9606.

40. Li, N.-W., et al., Passivation of Lithium Metal Anode via Hybrid Ionic Liquid Electrolyte toward Stable Li Plating/Stripping. *Advanced Science*, 2017. **4**(2): p. 1600400.

41. Hagiwara, R. and J.S. Lee, Ionic Liquids for Electrochemical Devices. *Electrochemistry*, 2007. **75**(1): p. 23-34.

42. Liu, X., et al., Locally Concentrated Ionic Liquid Electrolytes for Lithium-Metal Batteries. *Angewandte Chemie International Edition*. **n/a**(n/a): p. e202219318.

43. Wang, Z., et al., Covalently linked metal–organic framework (MOF)-polymer all-solid-state electrolyte membranes for room temperature high performance lithium batteries. *Journal of Materials Chemistry A*, 2018. **6**(35): p. 17227-17234.

44. Li, Y., et al., A single-ion conducting and shear-thinning polymer electrolyte based on ionic liquid-decorated PMMA nanoparticles for lithium-metal batteries. *Journal of Materials Chemistry A*, 2016. **4**(47): p. 18543-18550.

45. Guo, Q., et al., Flame Retardant and Stable Li1.5Al0.5Ge1.5(PO4)3-Supported Ionic Liquid Gel Polymer Electrolytes for High Safety Rechargeable Solid-State Lithium Metal Batteries. *The Journal of Physical Chemistry C*, 2018. **122**(19): p. 10334-10342.

46. Chen, T., et al., Metal-organic frameworks containing solid-state electrolytes for lithium metal batteries and beyond. *Materials Chemistry Frontiers*, 2021. **5**(4): p. 1771-1794.

CHAPTER 3:

Incorporating Metal-Organic Framework with Ionic Liquid as Ion Diffusion Booster for Flexible Solid-State Lithium Metal Batteries

1 Statement of Authorship

Statement of Authorship

Title of Paper	Incorporating Metal-Organic Framework with Ionic Liquid as Ion Diffusion Booster for Flexible Solid-State Lithium Metal Batteries
Publication Status	☐ Published ☐ Accepted for Publication ☐ Submitted for Publication ☑ Unpublished and Unsubmitted work written in manuscript style
Publication Details	Tianhua Chen, Jian Wang, Simeng Wang, Jin Lib, Dusan Losic, Shimou Chen, Incorporating Metal-Organic Framework with Ionic Liquid as Ion Diffusion Booster for Flexible Solid-State Lithium Metal Batteries

Principal Author

Name of Principal Author (Candidate)	Tianhua Chen		
Contribution to the Paper	Prepared, edited and revised the manuscript.		
Overall percentage (%)	85%		
Certification:	This paper reports on original research I conducted during the period of my Higher Degree by Research candidature and is not subject to any obligations or contractual agreements with a third party that would constrain its inclusion in this thesis. I am the primary author of this paper.		
Signature		Date	20/04/2023

Co-Author Contributions

By signing the Statement of Authorship, each author certifies that:

i. the candidate's stated contribution to the publication is accurate (as detailed above);
ii. permission is granted for the candidate in include the publication in the thesis; and
iii. the sum of all co-author contributions is equal to 100% less the candidate's stated contribution.

Name of Co-Author	Jian Wang		
Contribution to the Paper	Edited, revised manuscript, and acted as the corresponding author.		
Signature		Date	20/04/2023

Name of Co-Author	Simeng Wang		
Contribution to the Paper	Edited and revised the manuscript.		
Signature		Date	20/04/2023

Please cut and paste additional co-author panels here as required.

2

Name of Co-Author	Jin Li		
Contribution to the Paper	Edited and revised the manuscript.		
Signature		Date	20/04/2023

Name of Co-Author	Dusan Losic		
Contribution to the Paper	Supervised the development of work, edited and revised the manuscript, and acted as the corresponding author.		
Signature		Date	24 April 2023

Name of Co-Author	Shimou Chen		
Contribution to the Paper	Co-supervised and revised manuscript, and acted as the corresponding author.		
Signature		Date	20/04/2023

1

Interfacial Diffusion Booster Enabled by MOF sieve and Ionic Liquid wettability for Stabilizing Flexible Solid-State Lithium Metal Batteries

Tianhua Chen[a,b], Jian Wang[b]*, Simeng Wang[b], Jin Li[b], Dusan Losic[a]*, Shimou Chen[d]*

[a]*School of Chemical Engineering and Advanced Materials, The University of Adelaide, Adelaide, SA 5005, Australia*

[b]*Helmholtz Institute Ulm (HIU), Ulm D89081, Germany*

[c]*Institute of Process Engineering, Chinese Academy of Sciences, 100190, Beijing, China*

[d]*State Key Laboratory of Chemical Resource Engineering, Beijing University of Chemical Technology, Beijing, 100029, China*

Corresponding author email: Jian Wang, Jian.wang@kit.edu (J. Wang), Dusan Losic, dusan.losic@adelaide.edu.au (D. Losic), Shimou Chen, chensm@mail.buct.edu.cn (S. Chen)

Abstract

Solid-state batteries (SSBs) are a promising technology for safe energy storage, but they have been limited by poor Li^+ transport kinetics and the growth of lithium dendrites, leading to large interfacial impedance and low energy density. This is mainly caused by the barrier created by free anions in solid polymer electrolytes. To address these issues and improve energy density, this work proposed a nano-wetted IL@MOF based electrolyte PEO-IL@MOF (PIM). The PIM electrolyte has excellent electrochemical properties, including a high ionic conductivity of 3.0×10^{-4} S cm^{-1} at 60 °C, an improved Li^+ transference number of 0.65, and good compatibility with both Li metal and cathode electrodes. By taking advantage of the confinement effect of TFSI anions by the metal atoms present in the MOF, the electrolyte exhibits exceptional electrochemical characteristics. This enables Li/Li cells to run steadily for over 1000 hours at 60 °C, with minor overpotential changes. In summary, the PIM electrolyte is a promising solution to improve the energy density and performance of Li metal battery. Its excellent electrochemical properties, low interfacial resistances, and high compatibility with both Li metal anode and cathode electrodes make it a promising candidate for future solid-state battery technology.

Key words: **PIM electrolyte, Li^+ transference number, Confinement effect, Interfacial resistances**

1. Introduction

Solid-state lithium metal batteries are considered the next most promising generation among various batteries for reaching ever-increasing demands.[1] Compared with liquid carbonate or ether electrolyte, the solid-state electrolytes (SSEs) show the superiorities in safety, board working window and enhanced electrochemical stability, attracting the researchers' pursuit for higher energy density. Different from the sulfide-based or garnet-based SSE, the solid state polymer electrolytes i.e., Poly(ethylene oxide) (PEO), has been extensively studied due to its compatibility and robustness with various lithium salts or metallic Li surface. [2, 3] Despite their potential benefits, all-solid-state polymer electrolyte/lithium salt complexes are often constrained by their low ionic conductivity, low Li+ transference number, huge interfacial resistance and potential formation lithium dendrites, thereby limiting their applicability in high-rate solid-state lithium batteries, thereby limiting their applicability in solid-state lithium batteries.[4, 5]

To overcome this limitation, numerous efforts have been dedicated to enhancing the ionic conductivity of PEO-based solid electrolytes. Investigations have indicated that nano-sized particles endowed with Lewis acidic surface properties or decorating functional groups into the polymer skeleton hold significant promise in enhancing the ionic conductivity of electrolytes.[6, 7] However, researches related to PEO-based SSE still have insufficient contact with the metallic Li, which would shorten the lifespan and broaden the overpotentials with low Li ion transfer kinetics. To address the issue of mobility, ionic liquids (IL) are often introduced into the solid

polymer electrolyte, enhancing the wettability and ionic conductivity. Actually, in the mixed IL-decorated polymer electrolyte, there are two dual ion promotors and the ionic conductivity is governed by the free ions and anions. This would form a gradual concentrations of Li ion distribution and causing uneven dendrite formation. Therefore, it is much urgent to confine the anion species to uniformize ion diffusion, so that to improve the lithium-ion conductivity.

Metal-organic frameworks (MOFs), as a porous material family, exhibit the merits in adjustable pore size, abundant coordination ligands, desirable high conductivity, excellent chemical, and thermal stability. Recently, researchers have found that introducing MOF into the polymer solution could form a new type SSE and possesses several advantages in providing a unique pathway for the transport of lithium ions by confining the larger anions.[8, 9] For example, by integrating the metal sites and transmission channels, Long et al. produced the first MOF-based SSE with high ionic conductivity (3.1 × 10-4 S cm-1).[8] Additionally, the decreasing the MOF particles into nanosize, the surface tension and area are significantly enhanced, then the contact between the SSE and electrode interface is more intimate, promoting ion transport kinetics. In combination with the ILs, Wang prepared a new type of solid state electrolyte in the with the introduction of nano porous UIO-66, by introducing ionic liquid (IL), realizedachieving fast lithium ion transportation in the solid-state lithium batteries.[10] By integrating the metal sites and transmission channels, Long et al. produced the first MOF-based SSE with high ionic conductivity (3.1×10^{-4} S cm^{-1}).[8] In combination with the ILs, Wang prepared a new type of solid state electrolyte with the introduction of nanoporous UIO-66, achieving fast lithium ion transportation in the solid-state lithium batteries.[11] Briefly, all these works demonstrated the

enhanced ionic transportation kinetics at the interfaces, making MOF-derived nanostructured electrolyte more promising candidate in solid-state batteries. However, issues and the properties of MOF-derived nanostructure electrolyte in solid-state batteries, such as chemical and electrochemical stabilities, electrodes and electrolyte interfacial contact, and their ability to maintain stable Li deposition have not been adequately studied and lack of deep understanding.

In this study, the ionic liquid decorated MOF-5 nanoparticles is incorporated into a PEO/lithium bis(trifluoromethylsulfonyl)imide (LiTFSI) matrix, forming a composite electrolyte (named as PIM electrolyte). In this design, the IL is capable of wetting the Li anode with the high contact angle from 88.92 to 121.34°, shrinking the interfacial resistance. The MOF serves as the sieving mesh to filter the large anion species. Benefiting from above merits, the optimized electrolyte results in ten times higher improvement of conductivity (3.1×10^{-3} S cm^{-1}) than PEO electrolyte at 60 °C. Meanwhile, the TFSI anion group has been confined in the MOF-5 structure, highly improving Li^+ transference number above 0.40 and preventing dendrite formation on Li anodes for stabilizing 1000 hours. The study suggests that the anion-immobilized electrolytes have great potential to develop lithium metal batteries with high performance.

2. Experimental section

2.1 Chemical Materials

1-ethyl-3-methylimidazoliumbis(trifluoromethylsulfonyl)imide (EMIMTFSI, 99.99%, Lanzhou Institute of Chemical Physics, China), Zinc nitrate ($Zn(NO_3)_2 \cdot 6H_2O$, 99.9%, Aladdin),

1,4-benzenedicarboxylate acid (H_2BDC, 99%, Aladdin), anhydrous acetonitrile (AN, 99.6%, Fisher), N,N-dimethylformamide (DMF, 99.9%, Aladdin), triethylamine (TEA, Aladdin), methylene chloride (CH_2Cl_2, 99.9%, Aladdin), polyethylene oxide (PEO, MW=600000~1000000, Sigma-Aldrich), lithium bis(trifluoromethanesulfonyl)imide (LiTFSI, 99.99%, Sigma-Aldrich). All the regents are used without any purification.

2.2 Synthesis of MOF-5 and IL-decorated MOF

A solvothermal method was used to prepare nano-sized MOF-5 according to the similar work.[12] Specifically, 1.35 g $Zn(NO_3)_2 \cdot 6H_2O$ and 0.25 g H_2BDC were dissolved in 150 ml DMF in a 250 ml two-neck flask. The mixture was treated with ultrasound and then the flask was equipped with a spherical condenser tube and tee coupling. The sealed apparatus was degassed using argon, and then 1 ml of TEA was injected into the reactor under argon protection without stirring. The mixture was allowed to react for 7 hours at 25 °C, resulting in a solution containing white precipitation. The precipitation was soaked in 100 ml DMF for 12 hours with 3 times to remove unreacted $Zn(NO_3)_2 \cdot 6H_2O$, and then soaked in 100 ml of CH_2Cl_2 for 12 hours. The sample was dried in an evacuated oven at 150 °C for 12 hours. Then the MOF-5 and ionic liquid EMIMTFSI were homogenized in a certain molar ratio by grinding in a mortar, followed by drying at 150°C for 12 hours to facilitate the infiltration of the ionic liquid into the pores of the MOF. The obtained IL@MOF-5 nanoparticles were prepared.

2.3 Preparation of PEO-MOF-IL (PIM) composite solid electrolytes

Fixed EO:Li^+ at molar ratio of 16:1, PEO, LiTFSI, and different mass ratios of IL@MOF-5 nanofillers were dissolved in AN solution and dispersed by ultrasound for 2 h. The contents of

nano-sized IL@MOF-5 in PEO is 10 wt%. To create a homogenous emulsion, the suspension was continually swirled for 24 hours. Then resultant emulsion was applied on the PTFE plate. By vacuum drying at 50 °C for 12 h to remove the remaining solvent, the composite solid-state electrolytes film with thickness of 80-100 micrometers was eventually produced. Also, PEO, and PEO-IL@Mof-5 (PEM) electrolytes were also prepared in the same way.

2.4 Characterization

The FT-IR spectra were obtained using a Nicolet Avatar 360 infrared spectrometer with a thermal detector, in the wavenumber range of 4000-500 cm^{-1}. The surface morphology and cross-sections of the samples were analyzed using scanning electron microscopy (SEM, Haitich SU8020, Japan). To examine the changes in the proportion of elements in the samples, an element distribution diagram (EDS) was employed. The crystallinity of the samples was determined using a Bruker D8 Focus X-ray diffractometer with Cu-Kα (λ= 0.15406 nm). To investigate the changes in the surface composition of cycled lithium metal, X-ray photoelectron spectroscopy (XPS) was performed using the Thermo Fisher Scientific ESCALAB 250 Xi instrument. AFM was used to assess the Young's modulus (Bruker Fastscabio). The Zeta potential of the MOF-5 nanoparticle samples in acetonitrile solution was measured using a DelsaNano C instrument, and the ^{1}H solid-state NMR measurements were conducted on a JNM-ECZ600R with a resonance frequency of 233MHz. By thermogravimetric (Setaram Labsys), differential scanning calorimetry (DSC) was performed using a heating rate of 5 °C min^{-1}.

2.5 Electrochemical characterization

A The samples were placed between two stainless steel disc electrodes and the ionic conductivity was determined by measuring the electrochemical impedance spectroscopy (EIS) curves, including a frequency range of 0.01 Hz to 100 kHz, an amplitude of 10 mV, and an applied DC voltage of 0 V. The electrochemical stability window of the electrolyte was assessed at 60 °C using linear sweep voltammetry (LSV) with a scanning rate of 0.1 mV/s over a range of 2.0 V to 6.0 V. The ionic conductivity can be determined using the following equation: $\sigma = L/(D * R)$, where R ($\Omega \cdot cm^2$) represents the bulk resistance of the electrolyte, L represents the thickness of the electrolyte, and D represents the effective area. The transference number (t_{Li^+}) of the battery was determined via chronoamperometry using a constant polarization potential of 10 mV at 60 °C. The calculating equation of t_{Li^+} is: $t_{Li^+} = [I_S(\Delta V - R_0 I_0)]/[I_0(\Delta V - R_S I_S)]$, where I_o and I_s correspond to the initial and steady-state currents, R_o and R_s represent the interface resistances before and after polarization. A symmetrical lithium metal battery with a Li||PIM||Li configuration was assembled to investigate the compatibility of the electrolyte with a lithium metal anode at different current densities. Galvanostatic cycling tests were performed at a temperature of 60°C. The as-prepared LFP and NCM622 active cathode materials had a mass loading about 3 mg cm^{-2}. The working voltage of LFP||PIM||Li batteries was from 2.5 to 4.0 V, and the NCM622||PIM||Li batteries was 2.8 to 4.3 V. The electrochemical floating analysis experiment was conducted by performing constant current and constant voltage tests on the NCM622||PIM||Li battery to further . The battery was charged with a constant current of 0.05mA to 4.0 V initially, then charged with 4.0 V for 10 hours, and continuously charged with a constant current 0.05 mA to 4.1 V and held for 10 hours. This process was repeated until the voltage

reached to 5.0V. All the Li battery cycles and battery cycling performance were conducted on a Xinwei or LAND battery cycler.

3. Results and discussion

3.1 Characterization of prepared materials

The simple processing method of PEO-IL@MOF-5 (PIM) is illustrated in the Fig 1(a), demonstrating the effective dispersion of IL@MOF-5 nanoparticles in the PEO matrix. The SEM image Fig 1b shows that the average particle size of MOF-5 crystals is 20-30 nm. Fig. S1 depicts the X-ray diffraction (XRD) pattern of the MOF-5 sample, which demonstrates a remarkable agreement between its characteristic peaks and the theoretical pattern generated by the lattice parameters of MOF-5.[13, 14] This congruence provides compelling evidence for the high degree of crystallinity and structural fidelity of the sample. Furthermore, a minor bifurcation in the left shoulder of the 9.7 ° peak can be ascribed to the presence of residual solvents, such as dimethylformamide (DMF) or water, which may have permeated into the interstices of the crystal.[15] Such solvent molecules may induce a perturbation in the crystal lattice, resulting in a localized deviation from perfect symmetry. Despite subjecting MOF-5 to a drying procedure at a temperature of 150 °C, which corresponds to the boiling point of DMF, residual amounts of DMF were still present within the material. Nevertheless, the pronounced adsorption capacity of MOF-5 towards solvents can be regarded as a beneficial attribute, as it can impede the diffusion of trace solvents towards the electrode interface, thus promoting the stability of the battery interphase. The formation of MOF-5 is also confirmed by the following FTIR result.

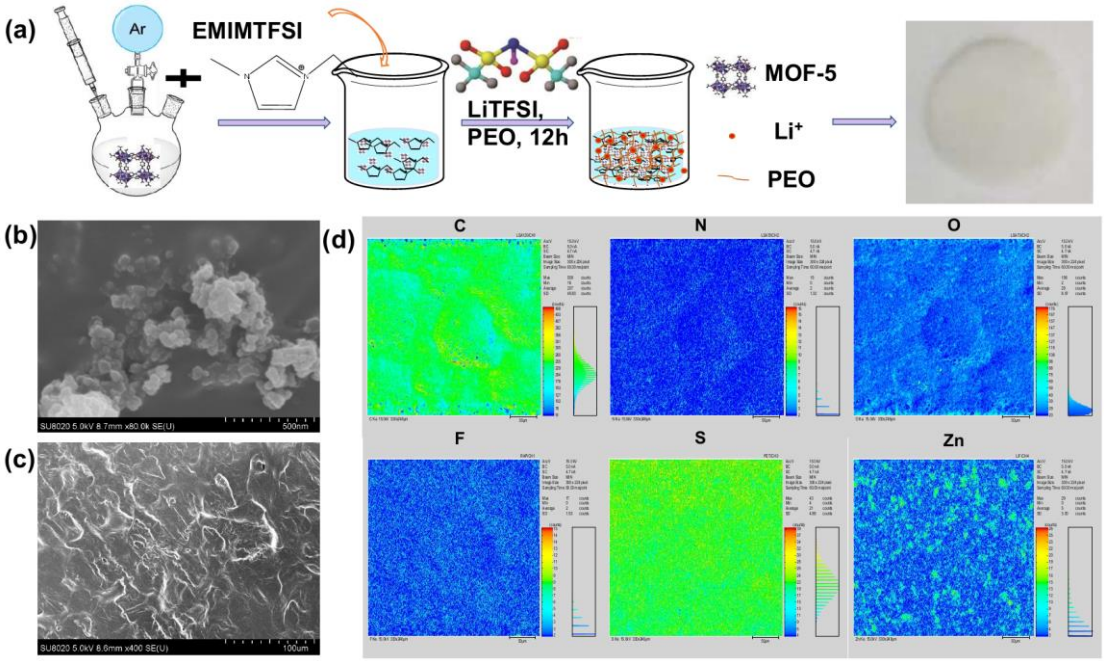

Figure 1 a) Schematic of fabrication PIM film, SEM image of b) MOF-5, and c) PIM film, d) EMPA images of corresponding Zn, C, N, S elements in PIM film

Fig. 1c and Fig. S2 show the surface of PEO, PEO-MOF(PEM), and PEO-IL@MOF-5 electrolyte (PIM). When the EO/LO ratio was set to 16:1, the electrolyte exhibited the highest mechanical strength and conductivity. Additionally, MOF-5 nanoparticles were uniformly distributed throughout the electrolyte. It can be observed that the addition of MOF-5 and IL@MOF-5 nano-wetted particles significantly decrease the crystallinity and porosity of PEO. Among them, the distribution of nanoparticles in PIM was more uniform, which can be attributed to the addition of IL that reduces the electrostatic interactions between MOF-5 particles, thus improving their dispersibility. Furthermore, the introduction of ionic liquids exerts a diluting effect on poly(ethylene oxide) (PEO), thereby reducing the intermolecular forces between polymer chains, diminishing the proclivity for polymer crystallization, and ultimately decreasing

the degree of crystallinity. It is widely accepted that a decrease in the degree of crystallinity is beneficial for enhancing the ionic conductivity of polymer matrices. This phenomenon can be attributed to the promotion of chain segment mobility and increased interfacial contact, which facilitate the migration of lithium ions. The analysis of the element distribution in PIM using EMPA indicates that each component is uniformly distributed in PIM, as shown in Fig. 1d. Furthermore, the element distribution diagram obtained by EDS mapping can also confirms this point (Fig. 3S).

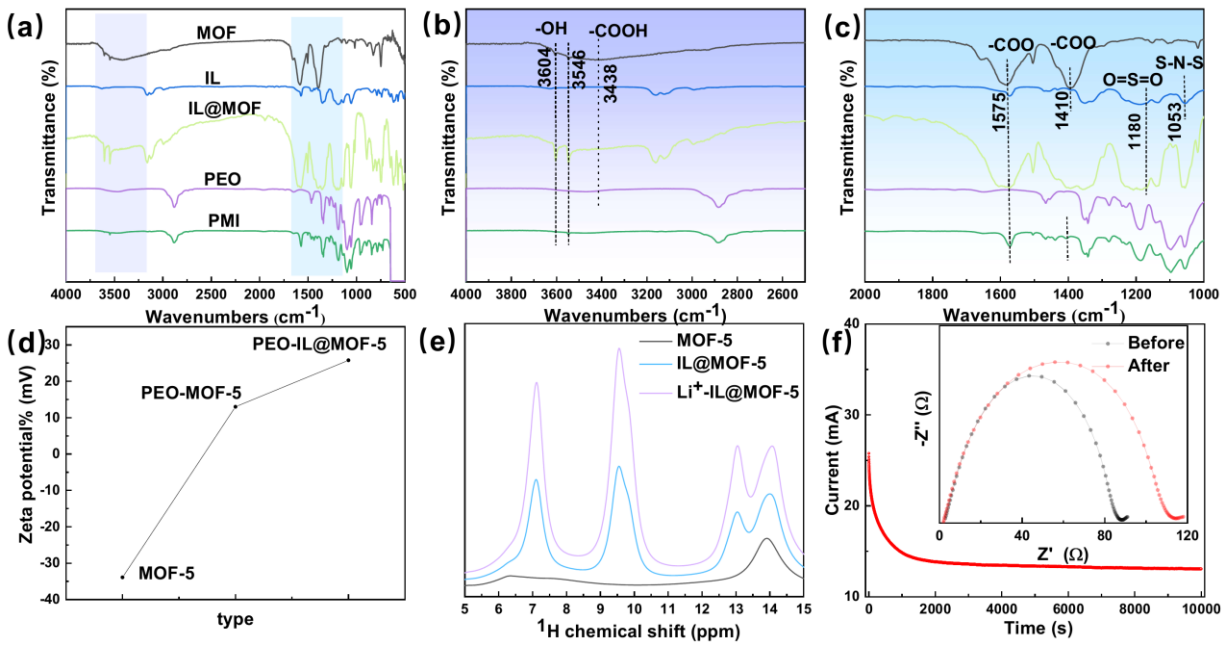

Fig. 2. (a-c) FTIR spectra comparison of MOF, IL, IL@MOF, PEO, and PIM, (d) Zeta potential of MOF-5, IL@MOF-5, and Li^+-IL@MOF-5 nanoparticles in acetonitrile suspension, (e) ^1H NMR of MOF, PEM and PIM, (f) Current-time curve following DC polarization curves of the PIM electrolyte at 60 °C (inset: EIS variation at initial and steady states).

The nanoconfinement effect of MOF-5 and IL@MOF-5 in PIM is characterized by Fourier

transform infrared (FTIR) spectra, as shown in Fig. 2(a-c). Analysis shows that there are three distinct vibrational regions in the MOF-5 and IL@MOF spectrum.[16, 17] The first major vibrational region ranges from 1390 to 1690 cm^{-1}, where four clear infrared absorption peaks can be observed. According to comparison with standard infrared spectroscopy spectra, the curve fluctuations in this region are caused by the O-C=O vibrations in the carboxyl functional group. The more prominent peak at 1585 and 1656 cm^{-1} is caused by the asymmetric stretching vibration of the carboxyl O-C=O bond, while the peak at 1393 cm^{-1} shows the symmetric stretching motion of the -COO bond. The second distinct vibrational region ranges from 660 to 1200 cm^{-1}, where the absorption peaks at 748 and 825 cm^{-1} are caused by different types of C-H bonds in the benzene ring, indicating the formation of the MOF-5 framework and the presence of terephthalate. The third region is at 544 cm^{-1}, where the peak corresponds to the Zn-O bond absorption peak in the Zn_4O tetrahedral metal cluster. The absorption peak around 3400 cm^{-1} is the stretching vibration absorption peak of the -OH group on the carboxyl group. However, in PIM, the absorption peak at this position disappears due to the reaction between Li^+ and the -OH group, which causes the hydroxyl peak to disappear almost. The peaks around 1575 and 1410 cm^{-1} are the asymmetric and symmetric stretching vibration peaks of the monodentate coordinating carboxyl group(C=O), respectively. The peak at 1510 cm^{-1} is the stretching vibration peak of the bidentate chelating carboxyl group. The differences in peak shape in the range of 1510~1610 cm^{-1} can also reflect the effect of Li^+ coordination on the stretching vibration of carboxyl groups. The characteristic peaks of the MOF become more pronounced after the addition of the ionic liquid. Peaks at 1053 and 1180 cm^{-1}, which correspond to the vibrations of

S-N-S and O=S=O, respectively, of the $TFSI^-$, were observed in the EMIMTFSI. Upon the incorporating of the IL in the MOF-5 framework, the peaks experienced a slight blue shift, implying robust interactions between the N and S atoms in the $TFSI^-$ and the Zn atoms of the MOF, which resulted in a reduced coordination environment of the Li ion.[18] The identical of MOF-5 and IL@MOF-5 displays that the IL are well combined with MOF-5 and didn't change its structure. PIM FTIR shows that Li^+ coordinated with carboxyl groups, enhancing the potential of the adsorption site, and improving the interaction between the site and Li^+, thereby improving the transportation of Li-ions. The coordination effect between lithium ions and the O-C=O & -OH groups can disrupt the solvation structure around Li^+ leading to the dissociation of solvating molecules and an increase in the number of migrating lithium ions t_{Li^+} from 0.14 for PEO and 0.2 for PEM electrolyte (Fig. S4) to 0.65 for PIM shown in Fig.2f. This low value can be attributed to the following factors. It is suspected that the mobility of $EMIM^+$ (7.9 Å) and $TFSI^-$ (7.6 Å) ions was constrained within the MOF-5 lattice, whereas the smaller size of Li^+ ions (0.76 Å) allowed for less impedance to their movement, resulting in a greater t_{Li^+} value of 0.65 for PIM electrolyte. We can summarize that the concentration of free ions from EMIMTFSI has a significant impact on the overall ionic conductivity of PIM electrolyte. As a result, the increase in ionic conductivity (Fig. 3c) is believed to be due to the interaction between $TFSI^-$ and unsaturated Zn atoms in MOF-5, which leads to an increase in the number of available Li^+.[19, 20]

In Figure 2d, the zeta potential of MOF-5, PEO-MOF-5, and PEO-IL@MOF-5 was measured in acetonitrile solution. The significance of Zeta potential lies in its numerical association with the stability of colloidal dispersions, serving as a metric for the intensity of inter-

particle repulsion or attraction. A smaller molecule or dispersed particle corresponds to a higher absolute value (either positive or negative) of Zeta potential, and therefore, a more stable system. Conversely, a lower Zeta potential (either positive or negative) indicates a higher tendency of colloidal particles to aggregate or coalesce, reflecting a dominance of attractive forces over repulsive forces. The observed change in zeta potential from -33.89 mV to 25.77 mV signifies a shift from negative to positive, implying that IL@MOF-5 particles exhibit a robust adsorption capacity for lithium ions. This phenomenon is attributed to the promotion of the dissociation of the solvation structure of lithium ions, which occurs as a result of the strong adsorption affinity of IL@MOF-5 particles towards the Li-ions. In Fig. 3e, compared with MOF-5, the increase in hydrogen bonds in the IL@MOF-5 ^{1}H NMR indicates that the IL is well integrated into the MOF-5 and can form better hydrogen bonds with PEO, thereby reducing the crystallinity of PEO, as Fig. S2 shows.

3.2 Electrochemical tests of batteries

The transport mechanism of lithium ions in the MOF nanomaterial is shown in the Fig 3a. The figure depicts the transport mechanism of lithium ions in nanomaterial MOF-5, which involves their movement through its pores and transfer between the crystals via framework interconnectivity. Notably, the smooth transportation of lithium ions is facilitated by the complexation of $TFSI^-$ anions with the MOF's unsaturated [Zn_4O] sites.[21] The compact arrangement of highly porous MOF-5 nanocrystals, characterized by a substantial concentration of encapsulated lithium ionic liquid (Li-IL), represents a potential pathway towards achieving

high ionic conductivity.[22] The ionic conductivity of solid-state electrolytes is an important factor for high performance. Figure 3b illustrates the electrochemical impedance spectroscopy (EIS) measurements of PIM electrolyte at temperatures ranging from 0 to 80 °C. Figure 3c depicts the corresponding Arrhenius plot of the ionic conductivity. Remarkably high ionic conductivities of 3.7×10^{-5}, 3.3×10^{-4}, 3.1×10^{-3}, and 2.8×10^{-2} S cm^{-1} were observed at 0, 25 (room temperature), 60 and 80 °C, respectively, which was much higher than the pure PEO electrolytes. These results demonstrate that the battery maintains stable electrochemical performance over a wide range of temperatures. The mechanism of Li-ion transport was analyzed using the traditional Arrhenius equation, which states that $\sigma\,(\mathrm{T}) = A \exp\,(-\frac{\mathrm{Ea}}{RT})$, where σ represents conductivity, E_a is the activation energy, R is the universal gas constant with a value of 8.314 J mol^{-1}, and A is the pre-exponential factor. [23] The lower the activation energy, the faster migration of Li ions. The activation energy of the conductor was estimated to be about 0.30 eV based on the Arrhenius equation, which is much lower than that of PEO-based electrolytes (about 1.66 eV), displaying a solid-state conduction behavior. Acting as a wetting agent, the IL in this system enhanced interface diffusivity. This is due to the low miscibility of EMIM-TFSI in PEO, which results in its placement at the phase boundaries.[24] As a result, the IL here acts as a bridge for Li-ion transport, facilitating the movement of ions between the phases.

The electrochemical window of the PIM electrolyte was determined by linear sweep voltammetry (LSV) profiles, measured from Li||PEO||SS, Li||PEM||SS, and Li||PIM||SS asymmetric cell at 60 °C, as illustrated in Figure 3d. The PIM electrolyte demonstrated a stable electrochemical window between 2 and 4.2 V higher than the PEO and PEM electrolytes. This

result can be attributed to the stability of the MOF-5 host against Li metal over a wide potential range, which allows the PIM electrolyte to maintain its electrochemical stability. The comparation between the electrochemical floating analysis in Figures 3e and 3f indicate that the highest withstand voltage for PIM electrolyte is 4.5V, and when the voltage exceeds 4.5V, the leakage current increases significantly. But the highest voltage for PEO is only 4.2V. In practical environments, however, PIM electrolyte may not necessarily operate at 4.5V due to the influence of other factors such as the lack of matched positive electrode materials and temperature.

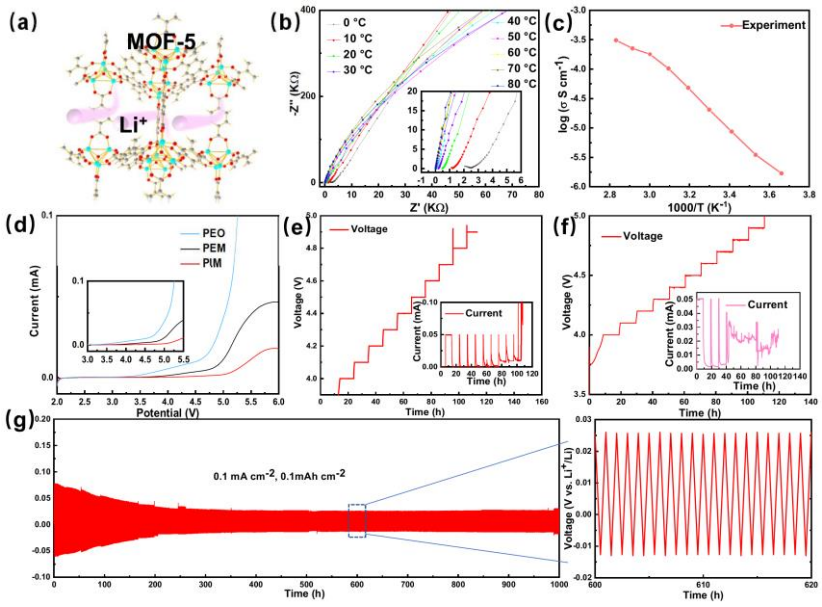

Figure 3 (a) Schematic illustration of Li^+ transportation pathways in the nano-wetted IL@MOF-5 particles, (b) electrochemical impedance spectroscopy plots of SS||PIM||SS batteries ranging from 0 - 80 °C, (c) corresponding Arrhenius plot of the ionic conductivity, (d) LSV curve of Li||PEO||SS, Li||PEM||SS, Li||PIM||SS at 60°C. Electrochemical floating analysis of (e) NCM622||PIM||Li battery, (f) NCM622||PEO||Li battery, (g) voltage profiles for the Li||PIM||Li symmetric battery at current densities of 0.1 mA cm^{-2} at 60 °C.

To evaluate the stability of the interface between the electrolyte and lithium electrodes and Li^+ transportation ability under cycling conditions, Li||Li symmetrical lithium metal batteries with PEO, PEM, and PIM electrolytes were assembled and tested under 60 °C. The results in Fig. 3g shows that the Li||PIM||Li symmetrical battery can maintain superior cycling stability for up to 1000 hours at 0.1 mA cm^{-2} with an area capacity of 0.1mAh cm^{-2}. The battery showed an initial overpotential of 140 mV and slowly minored and a remaining at around 38 mV after 200 h. Additionally, the voltage profile exhibited a consistently smooth pattern, indicating a stable interface between the PIM solid electrolyte and the Li metal throughout 1000 hours of cycling. When the current density increased to 0.2mA cm^{-2}, the polarization voltage of a symmetrical lithium battery increased and fluctuated around 60 mV, and can maintain stable cycling for about 840 h. In contrast, the PEO system can only maintain for less than 250 h with a much high polarization voltage of 160 mV, shown in Fig. S6. Then the overpotential dropped sharply to less than 0.05mV, which was considered as short circuit. This process corresponds to the growth of dendritic crystals in the Li||PEO||Li battery, which prevented the Li deposition, eventually the electrodes at both ends are short-circuited due to lithium dendrites penetrating the PEO membrane. The stable stripping/plating voltages observed in the Li||PIM||Li cell indicate that the PIM electrolyte has great potential as a high-performance material for lithium metal batteries.

Figure S7 presents a comparison of the EIS Nyquist plots obtained from the Li||PIM||Li cell before and after the Li plating/stripping cycling process. The total cell resistance was measured to be approximately 86 before cycling, and it decreased to 75 Ω after cycling. The slight increase means the battery possess a steady cycling condition but not ‘fake stable’

phenomenon. We hypothesis that the uniform deposition of Li is attributed to the influence of nano-wetted interfaces and the superior mechanical stability of the PIM electrolyte film. This suggests that the utilization of stable PIM films and nano-wetted interfaces could potentially serve as a viable approach to attain uniform Li deposition in a variety of applications. Therefore, the excellent compatibility between the PIM electrolyte and Li metal, as well as the low interfacial resistance between them, can be effectively elucidated. The contact angles between the electrolyte slurry and the positive and negative electrodes can be employed as a tool to probe the microscopic interfacial phenomena in the battery, as shown in Fig. S8. With the addition of ionic liquid, the contact angles between the electrolyte with both the positive and negative electrodes are significantly reduced, indicating that the IL@MOF nanostructure can increase the interfacial contact area between the electrolyte and electrode materials, promoting multipoint deposition of lithium, effectively suppressing the formation of lithium dendrites.

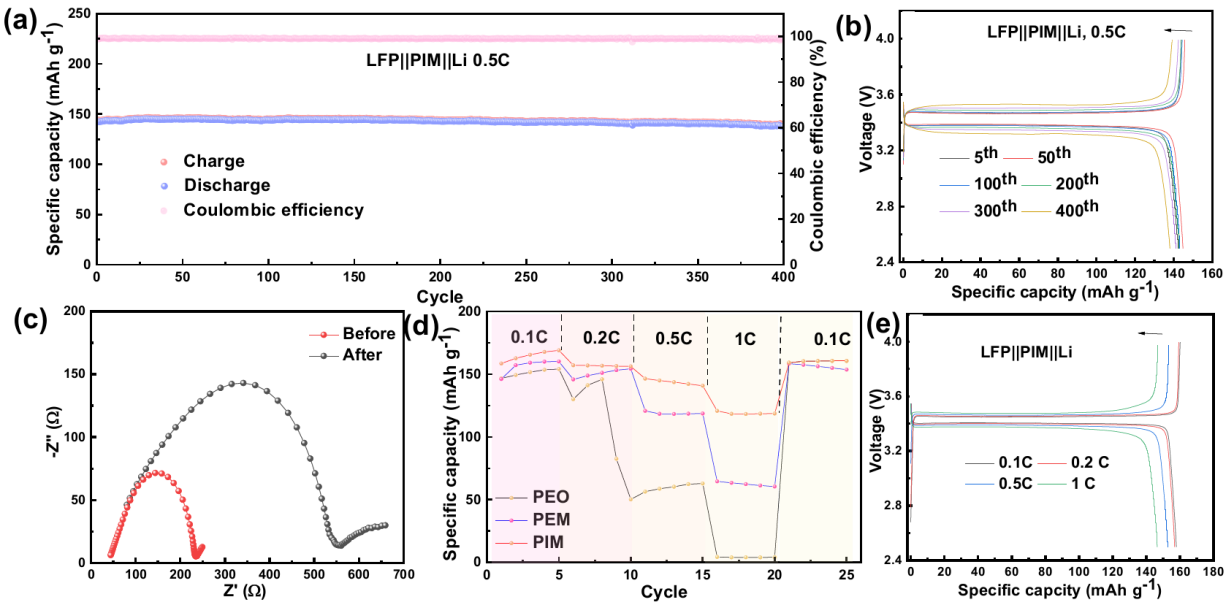

Figure 4 (a) Cycle performance of the LFP||PIM||Li cell at 0.5 C, (b) Galvanostatic

charge/discharge curve of the LFP||PIM||Li cell at 0.5 C. (c) Evolution of the impedance response of a LFP||PIM||Li cell before and after cycling, (d) Rate performance of LFP||PIM||Li, LFP||PEM||Li and LFP||PEO||Li cell, (e) Galvanostatic charge/discharge curve of the LFP||PIM||Li cell at different rates. All the batteries were tested at 60 °C.

The LFP||PIM||Li (Fig. 4), NCM622||PIM||Li (Fig. 6) cells were packed with 250mm thick Li foil to evaluate the performance of lithium metal batteries at 60 °C. As depicted, the LFP||PIM||Li battery had a slight decline of specific discharge capacity from 142 to 138 mAh g^{-1} after 500 cycles with a rate of 0.8 ‰ $cycle^{-1}$(Fig. 4a). Fig. 4c shows the overpotential increased slightly with the cycle and rate growing. In Fig. 4c, the initial resistance was only about 235 Ω before cycling due to the nano wetted IL@MOF-5 structure in PIM electrolyte, which offers a capable interfacial contact. Thus, the interfacial contact facilitates Li-ion transport across the interface of PIM electrolyte and electrodes. Fig. 4b shows the galvanostatic charge/discharge curve of the LFP||PIM||Li cell at 0.5 C. The total resistance of the LFP||PIM||Li battery increased more than 300 Ω after 500 cycles. And Fig 4d compared the rate performance of PEO. PEM, and PIM electrolyte. The high discharge capacity of PIM-based battery confirms the possibility of this kind of electrolyte for high performance application. Combined the conductivity and the galvanostatic charge/discharge curve of the LFP||PIM||Li cell at different rates in Fig. 4d, it is suspected that the battery would performance excellent at other temperatures. Fig S9 displays the stable cycling performance of LFP||PIM||Li battery at 0.2 C lasting for about 300 cycles with a subtle decline.

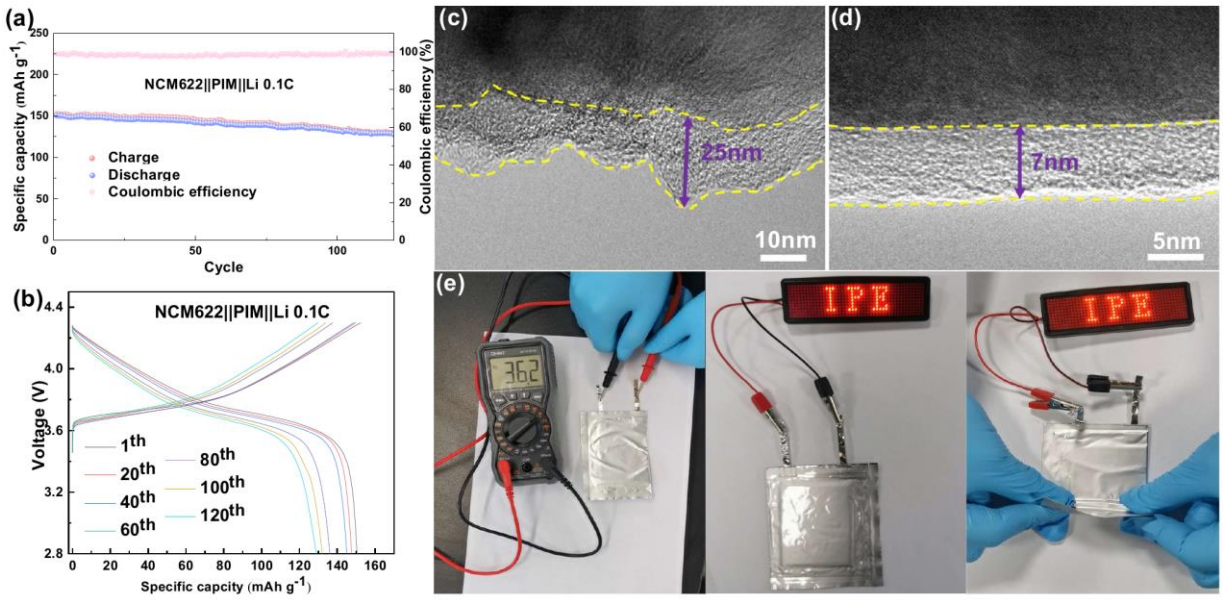

Figure 5 (a) Cycling performance of NCM622||PIM||Li cell at 0.1C at 60 °C, (b) Charge and discharge profiles of NCM622||PIM||Li battery at 0.1 C at different cycles at 60 °C. TEM images of the NCM622 cathode at 60 °C of (c) PEO electrolyte, (d) PIM electrolyte. (e) Pouch cell of LFP||PIM||Li battery with electrolyte PIM electrolyte at room temperature.

NCM622||PIM||Li batteries were assembled to evaluate their compatibility (Fig. 5a-b). The 2025-coin cell exhibited a discharge capacity of 150.4 mAh g^{-1} at a 0.1 C rate within the voltage range of 2.8 - 4.3V at 60 °C. With a discharge capacity of 127.5 mAh g^{-1} after 120 cycles, the battery shows an acceptable stability. This further indicates that the PMI electrolyte has excellent contact performance with the negative electrode. Moreover, the MOF@IL system can enhance the voltage tolerance of PEO. The surface of NCM622 cathodes after 20 cycles at were observed by TEM, as shown in Fig. 5c-d. the NCM622 CEI layer for PEO electrolyte was uneven and has sharp edges reached to 25 nm maximum, which may cause poor interfacial contact and thereby has adverse effect on the battery performance. With a uniformly thick film about nanometers, the CEI layer of NCM622 reflects good interfacial contact between the PIM electrolyte and the

cathode. LFP||PIM||Li pouch cell was packed and tested in room temperature (Fig. 5e). As can be seen from the figure, the open circuit voltage of the pouch battery is 3.62V and can illuminate the LED light after being charged. Moreover, the LED remains lit even after the battery was bent, indicating that this electrolyte has the potential to be used in practical applications.

3.3 Characterization of electrolyte-electrodes interface

The surface of lithium anode was observed after 50 cycles by SEM and TEM in Fig. 6. For the battery using PEO, large patches of moss-like lithium dendrites have appeared on the surface, and severely impacts the lithium deposition. Moreover, the thickness of the lithium deposition layer reached to 45 μm, which has a negative impact on the long-term cycling performance. For the PIM, the surface of lithium anode was flat, even and with a thickness of 17 μm, proposing a consistent interface may be attributed to the even intercalation/deintercalation of Li metal, which is facilitated by the anion confined effect by MOF-5. The absence of free anions prevents any interference and enables Li ions to diffuse through the electrolyte membrane rapidly and uniformly before uniformly depositing on the Li metal surface. By maintaining a consistent environment throughout the PIM electrolyte and Li metal surface, the formation of a strong electric field is prevented, resulting in the deposition of dendrite-free Li.[25]

The TEM images compare the CEI layer of LFP cathode after cycling 20 times at 0.5 C with PEO and PIM, respectively. As depicted in Fig. 6g, the PEO-LFP CEI layer is quite uneven and with a maximum thickness of 26 nm, superior to that 8 nm for the PIM-LFP. XPS was used to explain the difference between the above CEI layers (Fig. 6i, j). The CO_3^{2-} on C spectrum

around 298 eV disappeared, and the peak at 531.8 eV decreased on the O spectrum in Fig. 6j compared to 6i proved that the formation of unexpected component Li_2CO_3 in CEI has been reduced. And the peak at 685 eV represents LiF on the F spectrum. The increased LiF is beneficial for CEI, indicating that the PIM electrolyte is helpful for the battery stability.[26]

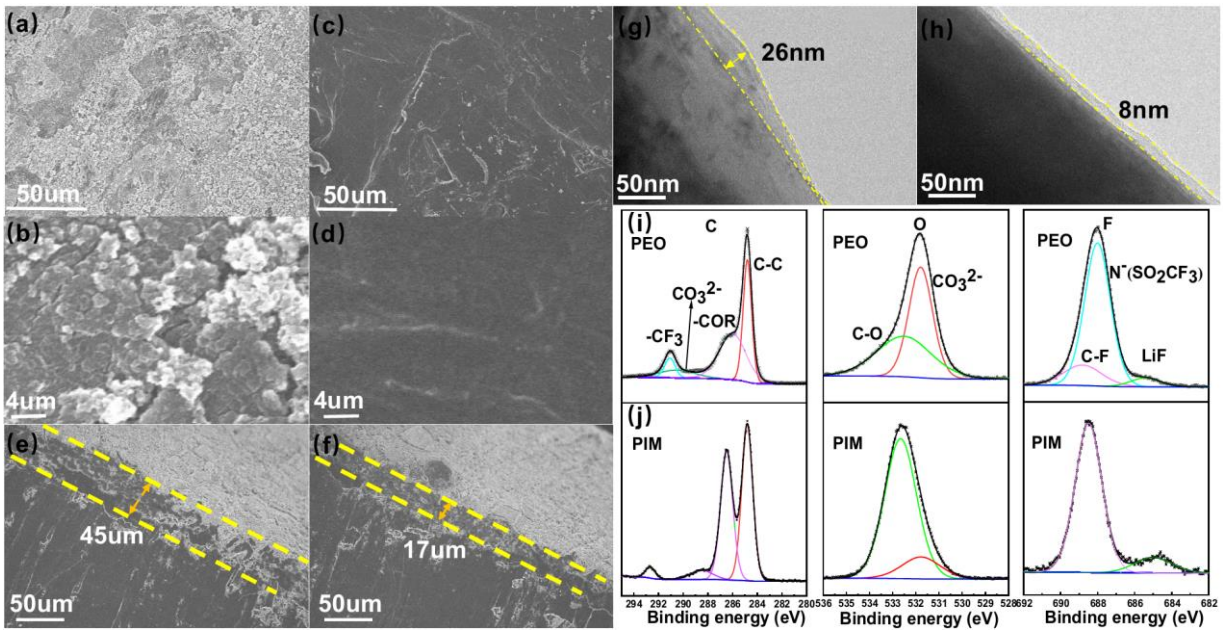

Figure 6 The surface SEM images of lithium deposition of (a, b) PEO electrolyte, (c, d) PIM electrolyte. SEM image of cross section of lithium deposition with (e) PEO electrolyte, (f) PIM electrolyte after 100 cycles. TEM images of LFP cathode after 20 cycling of (g) PEO electrolyte, (h) PIM electrolyte. (C, O, F) XPS spectra of LFP cathode of (i) PEO electrolyte, (j) PIM electrolyte. The batteries are LFP||PEO||Li, LFP||PIM||Li, respectively. All the batteries were cycled at 60 °C.

4. Conclusion

This work demonstrated a nano-wetted solid-state PIM electrolyte composed of an ionic liquid(IL) infused into metal–organic framework(MOF-5). By chemical bonding, the IL and

MOF was well incorporated with Li^+ in the system. The PIM electrolyte enables a close and nano-wetted interfacial contact and high ionic conductivity, leading to an improved lithium ion transference number of 0.65. The PIM electrolyte also has good compatibility with both the LFP/NCM622 cathode and Li metal anode due to uniform Li deposition and excellent interfacial contact stability. Additionally, the PIM electrolyte exhibits high electrochemical activity and good capacity retention over a long cycling in the LFP||PIM||Li cell at different rates. Due to the anions confined in the MOF host network, the Li metal deposit uniformly and the cathode also exhibit thick and homogenous CEI layer. This work suggests that the IL@MOF based electrolyte has significant potential for enabling high-performance Li-based batteries and other energy storage devices by changing the kind of ionic liquid or host material.

Acknowledgements

The authors thank the Australian Government for providing Tianhua Chen with Beacon of Enlightenment PhD Scholarship to undertake PhD at the University of Adelaide and Institute of Process Engineering, Chinese Academy of Sciences. This work was partly supported by Australian Research Cuncil (ARC), Research Hub for Graphene Enabled Industry Transformation (IH IH150100003), and National Natural Science Foundation of China (52171198, 51922099).

Declaration of Competing Interest

The authors declare that they have no known competing financial interests or personal relationships that could have appeared to influence the work reported in this paper.

Reference

1. Liang, J., et al., Recent progress on solid-state hybrid electrolytes for solid-state lithium batteries. *Energy Storage Materials*, 2019. **21**: p. 308-334.

2. Zhang, H., et al., Single lithium-ion conducting solid polymer electrolytes: advances and perspectives. *Chemical Society Reviews*, 2017. **46**(3): p. 797-815.

3. Sun, Z. and S. Ding, PEO-based polymer electrolytes in lithium ion batteries. *Chinese Science Bulletin*, 2018. **63**(22): p. 2280-2295.

4. Xu, H., et al., Safe solid-state PEO/TPU/LLZO nano network polymer composite gel electrolyte for solid state lithium batteries. *Colloids and Surfaces A: Physicochemical and Engineering Aspects*, 2022. **653**: p. 130040.

5. Wang, X., et al., Constructing Interfacial Nanolayer Stabilizes 4.3 V High-Voltage All-Solid-State Lithium Batteries with PEO-Based Solid-State Electrolyte. *Adv. Funct. Mater.*, 2022. **32**(23): p. 2113068.

6. Wang, T.-S., et al., High Areal Capacity Dendrite-Free Li Anode Enabled by Metal–Organic Framework-Derived Nanorod Array Modified Carbon Cloth for Solid State Li Metal Batteries. *Adv. Funct. Mater.*, 2020. **n/a**(n/a): p. 2001973.

7. Zhu, F., et al., High-Performance Metal–Organic Framework-Based Single Ion Conducting Solid-State Electrolytes for Low-Temperature Lithium Metal Batteries. *ACS Appl. Mater. Interfaces*, 2019. **11**(46): p. 43206-43213.

8. Wiers, B.M., et al., A Solid Lithium Electrolyte via Addition of Lithium Isopropoxide to a Metal–Organic Framework with Open Metal Sites. *Journal of the American Chemical Society*, 2011. **133**(37): p. 14522-14525.

9. Shen, L., et al., Anchoring anions with metal–organic framework-functionalized separators for advanced lithium batteries. *Nanoscale Horizons*, 2019. **4**(3): p. 705-711.

10. Chen, T., et al., Metal-organic frameworks containing solid-state electrolytes for lithium metal batteries and beyond. *Materials Chemistry Frontiers*, 2021. **5**(4): p. 1771-1794.

11. Wang, Z., et al., A Metal–Organic-Framework-Based Electrolyte with Nanowetted Interfaces for High-Energy-Density Solid-State Lithium Battery. *Advanced Materials*, 2018. **30**(2): p. 1704436.

12. Yuan, C., et al., Enhanced electrochemical performance of poly(ethylene oxide) based composite polymer electrolyte by incorporation of nano-sized metal-organic framework. *Jounal of Power source*, 2013. **240**: p. 653-658.

13. Kim, J., et al., Assembly of Metal−Organic Frameworks from Large Organic and Inorganic Secondary Building Units: New Examples and Simplifying Principles for Complex Structures. *Journal of the American Chemical Society*, 2001. **123**(34): p. 8239-8247.

14. Tranchemontagne, D.J., J.R. Hunt, and O.M. Yaghi, Room temperature synthesis of metal-organic frameworks: MOF-5, MOF-74, MOF-177, MOF-199, and IRMOF-0. *Tetrahedron*, 2008. **64**(36): p. 8553-8557.

15. Li, Y. and R.T. Yang, Hydrogen Storage in Metal−Organic Frameworks by Bridged Hydrogen Spillover. *Journal of the American Chemical Society*, 2006. **128**(25): p. 8136-8137.

16. Horcajada, P., et al., Flexible Porous Metal-Organic Frameworks for a Controlled Drug Delivery. *Journal of the American Chemical Society*, 2008. **130**(21): p. 6774-6780.

17. Hermes, S., et al., Loading of porous metal–organic open frameworks with organometallic CVD precursors: inclusion compounds of the type [LnM]a@MOF-5. *J. Mater. Chem.*, 2006. **16**(25): p. 2464-2472.

18. Chen, N., et al., A Li^+ conductive metal organic framework electrolyte boosts the high-temperature performance of dendrite-free lithium batteries. *Journal of Materials Chemistry A*, 2019. **7**(16): p. 9530-9536.

19. Fujie, K., et al., Lithium Ion Diffusion in a Metal–Organic Framework Mediated by an Ionic Liquid. *Chemistry of Materials*, 2015. **27**(21): p. 7355-7361.

20. Fujie, K., et al., Low temperature ionic conductor: ionic liquid incorporated within a metal–organic framework. *Chemical Science*, 2015. **6**(7): p. 4306-4310.

21. Wiers, B.M., et al., A Solid Lithium Electrolyte via Addition of Lithium Isopropoxide to a Metal-Organic Framework with Open Metal Sites. *Journal of the American Chemical Society*, 2011. **133**(37): p. 14522-14525.

22. Han, X., et al., Negating interfacial impedance in garnet-based solid-state Li metal batteries. *Nature Materials*, 2017. **16**(5): p. 572-579.

23. Jensen, F., Activation energies and the arrhenius equation. *Quality and Reliability Engineering International*, 1985. **1**(1): p. 13-17.

24. Liu, M., et al., Improving Li-ion interfacial transport in hybrid solid electrolytes. *Nature Nanotechnology*, 2022. **17**(9): p. 959-967.

25. Li, C., et al., Heteroatomic interface engineering in MOF-derived carbon heterostructures with built-in electric-field effects for high performance Al-ion batteries. *Energy & Environmental Science*, 2018. **11**(11): p. 3201-3211.

26. Zhu, F., et al., High-Performance Metal-Organic Framework-Based Single Ion Conducting Solid-State Electrolytes for Low-Temperature Lithium Metal Batteries. *ACS Appl Mater Interfaces*, 2019. **11**(46): p. 43206-43213.

Supporting Information

Incorporating Metal-Organic Framework with Ionic Liquid as Ion diffusion booster for flexible Solid-State Lithium Metal Batteries

Tianhua Chen[a,b], Jian Wang[b]*, Simeng Wang[b], Jin Li[b], Dusan Losic[a]*, Shimou Chen[d]*, , Suojiang Zhang [b]*

[a]*School of Chemical Engineering and Advanced Materials, The University of Adelaide, Adelaide, SA 5005, Australia*

[b]*Helmholtz Institute Ulm (HIU), Ulm D89081, Germany*

[c]*Institute of Process Engineering, Chinese Academy of Sciences, 100190, Beijing, China*

[d]*State Key Laboratory of Chemical Resource Engineering, Beijing University of Chemical Technology, Beijing, 100029, China*

Corresponding author email: Jian Wang, Jian.wang@kit.edu (J. Wang), Dusan Losic, dusan.losic@adelaide.edu.au (D. Losic), Shimou Chen, chensm@mail.buct.edu.cn (S. Chen)

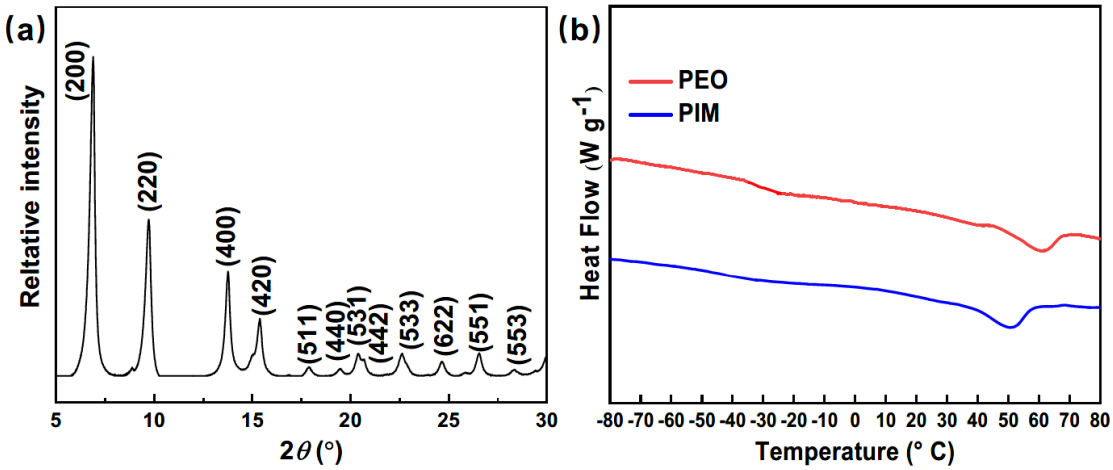

Figure S1 (a) XRD pattern of the MOF-5 sample, (b) DSC curve of PEO and PIM electrolyte.

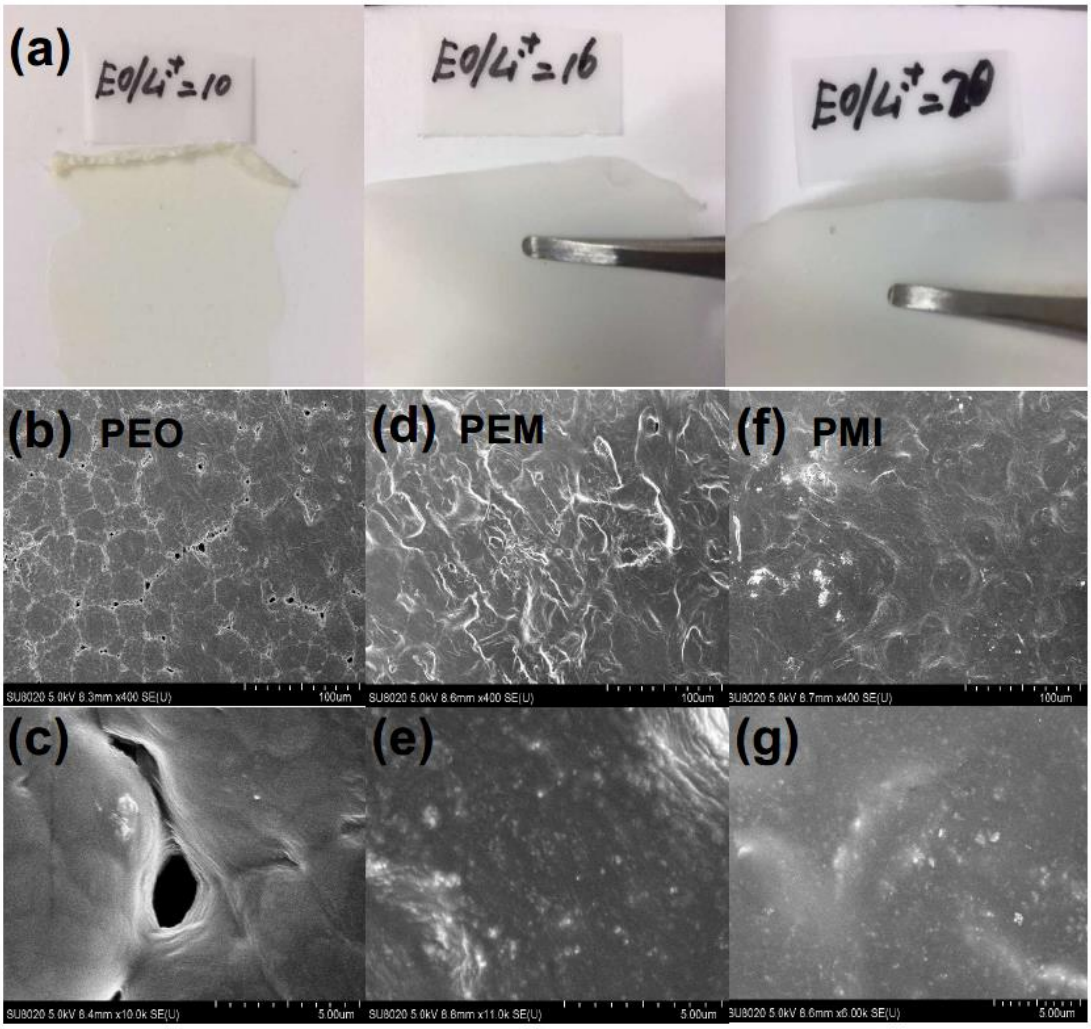

Figure S2 (a) Pictures of PIM films with different molar EO/Li^+ ratio SEM images of (b-c) PEO, (d-e) PEM, and (f-g) PIM electrolyte

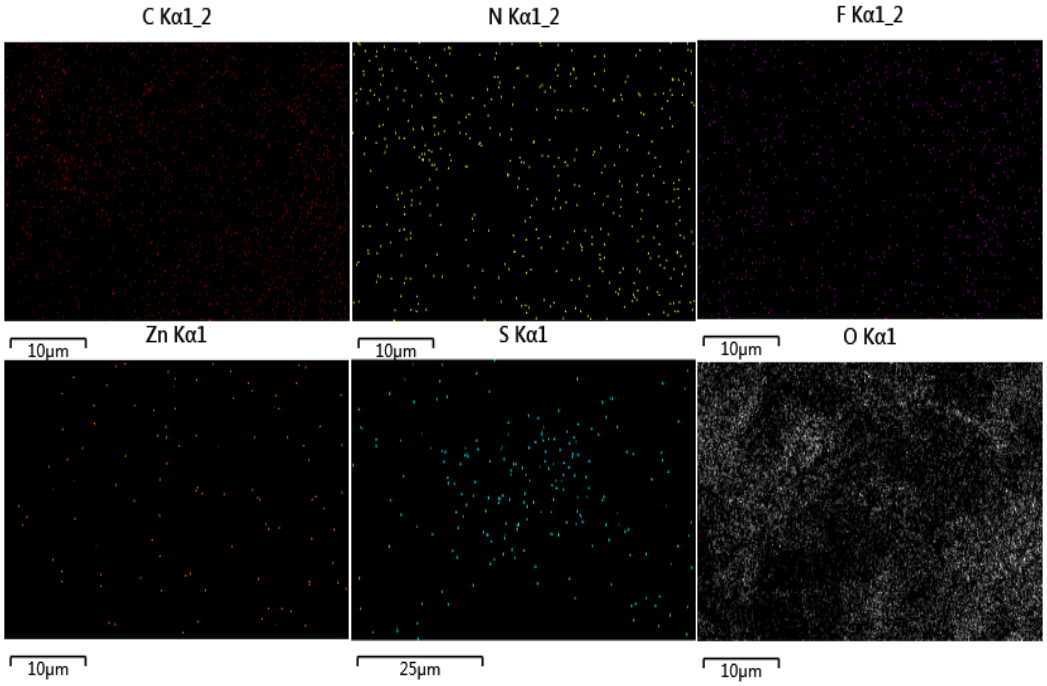

Figure S3 EDS mapping of distribution of different elements in the PIM membrane

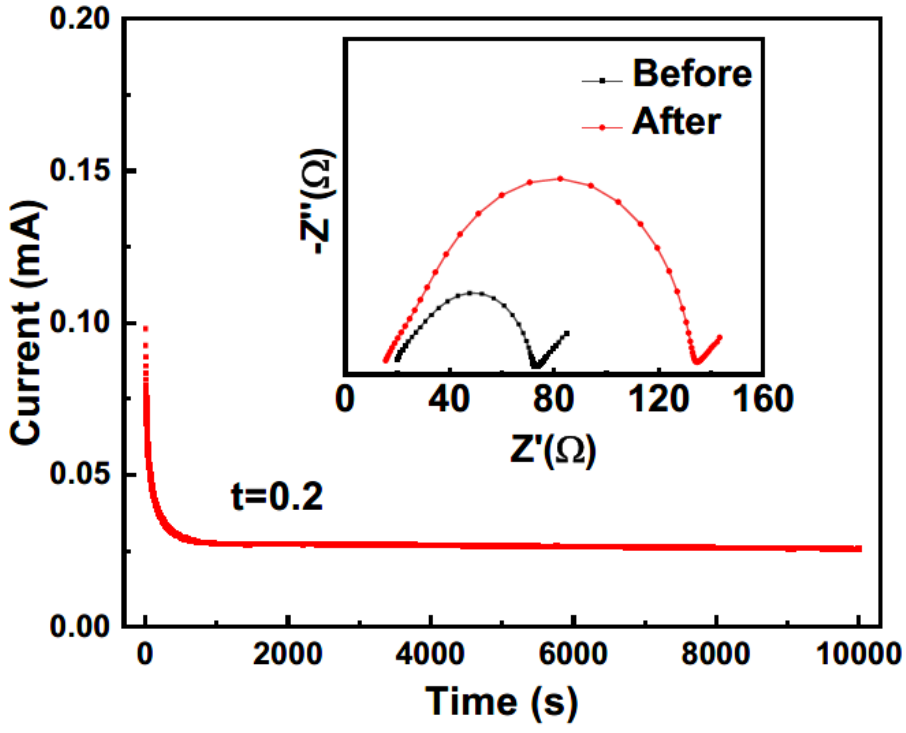

Figure S4 Current-time curve following DC polarization curves of the PEO electrolyte at 60 °C (inset: EIS variation at initial and steady states).

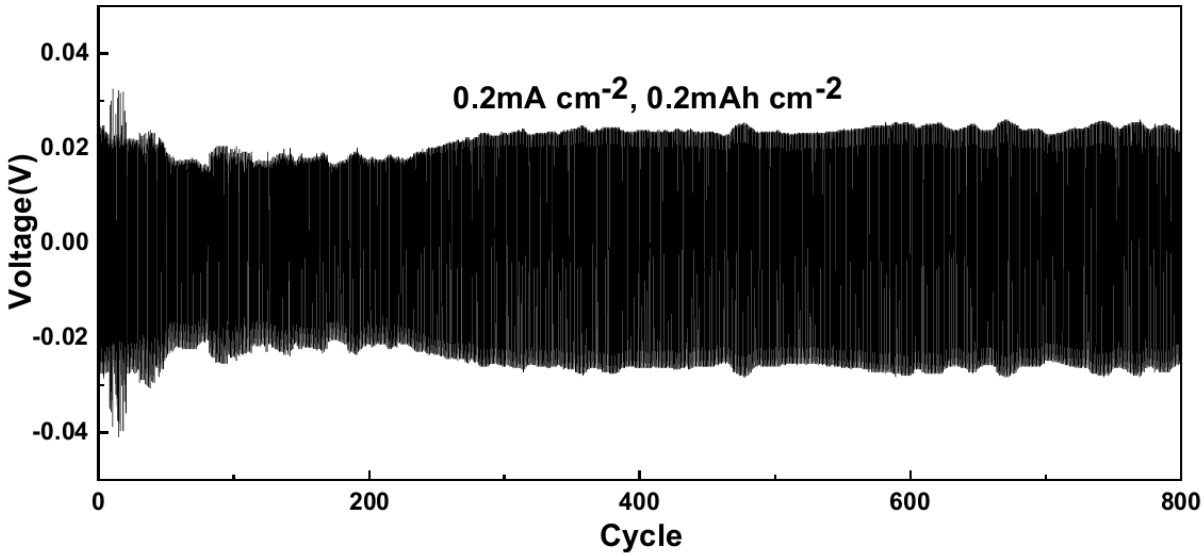

Figure S5 Voltage profiles for the Li||PIM||Li symmetric battery at current densities of 0.2 mA cm^{-2} at 60 °C.

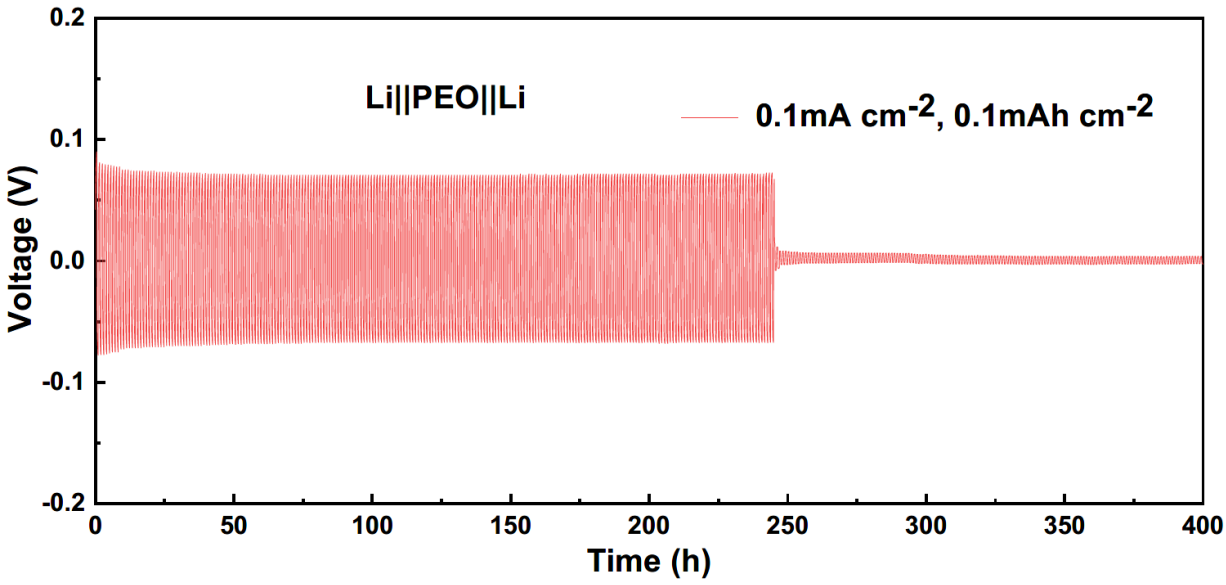

Figure S6 Voltage profiles for the Li||PEO||Li symmetric battery at current densities of 0.1 mA cm^{-2} at 60 °C.

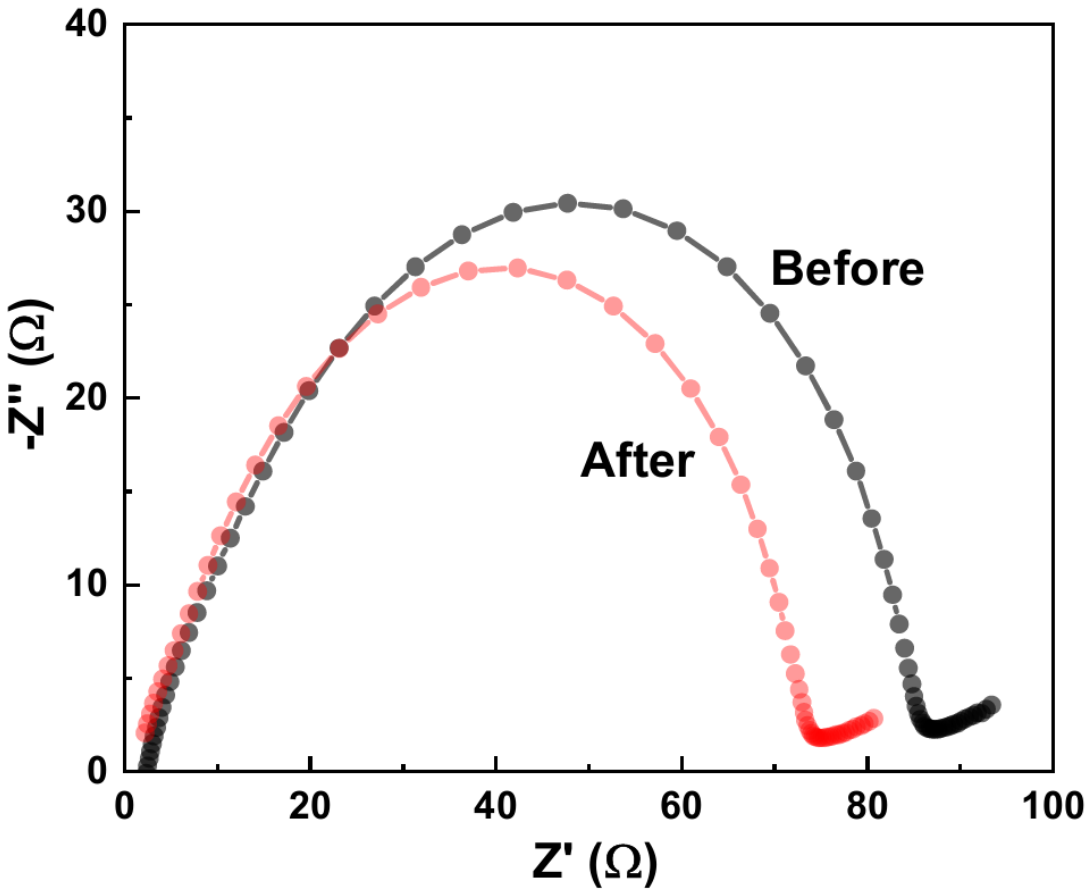

Figure S7 EIS before and after Li plating/stripping cycling for the Li||PIM||Li symmetric battery at current densities of 0.1 mA cm^{-2} at 60 °C.

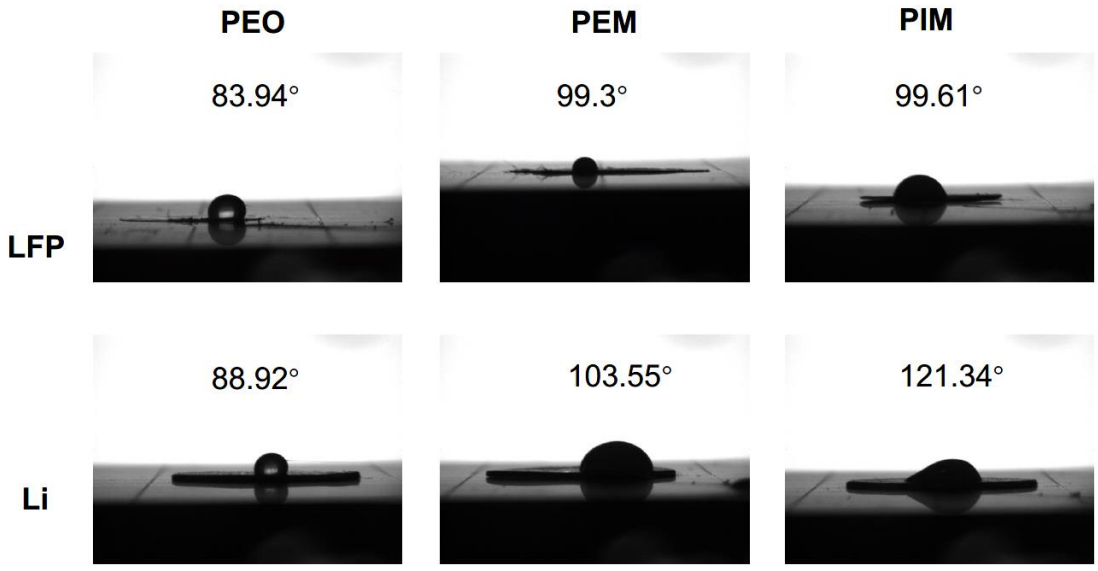

Figure S8 Contact angles of three electrolytes on the surface of LFP and Li anode

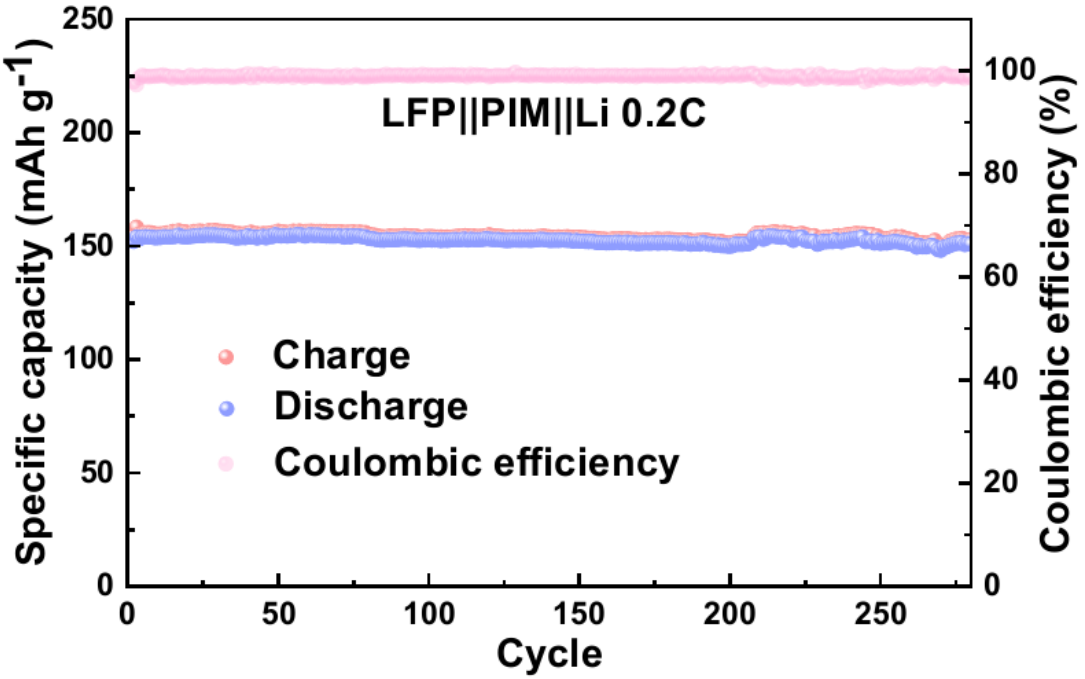

Figure S9 Galvanostatic charge/discharge curve of the LFP||PIM||Li cell at 0.2 C and 60 °C

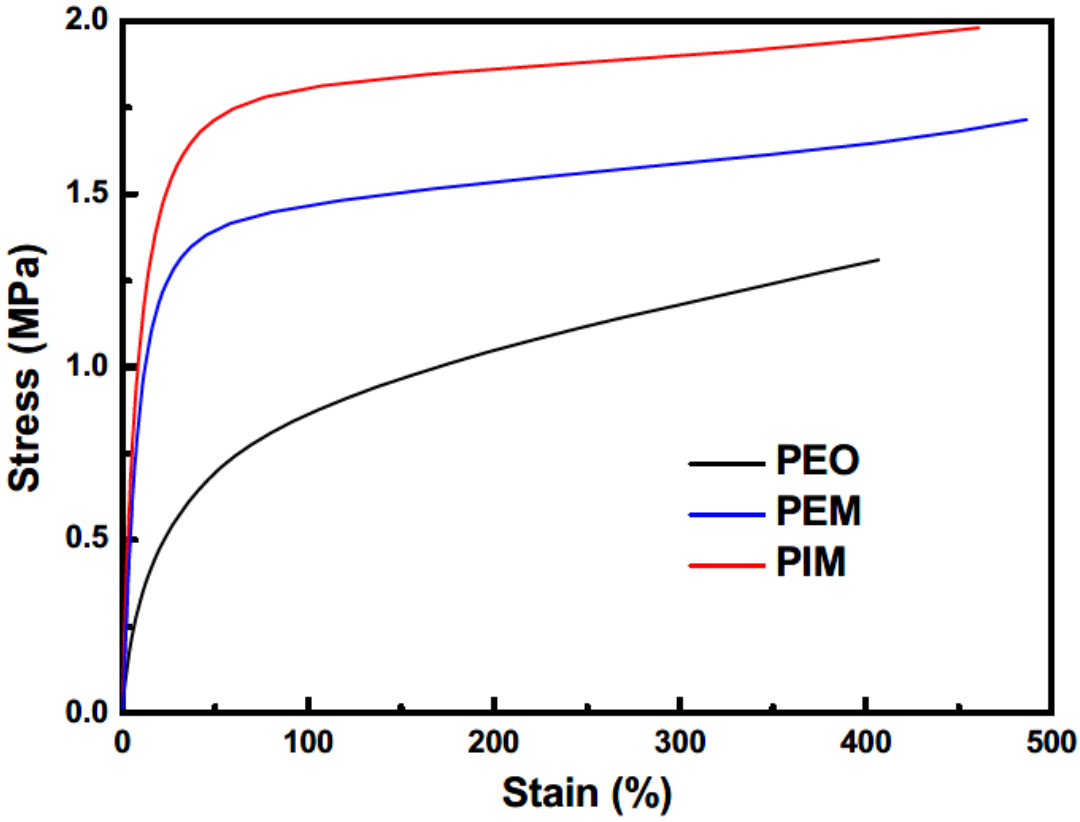

Figure S10 Stress-strain curves of PEO, PEM, and PIM films

CHAPTER 4:

Ionic Liquid Participated In-situ Electrolytes Enabling Stable Cycling of Wide-Temperature Li Metal Batteries

Statement of Authorship

Statement of Authorship

Title of Paper	Ionic Liquid Participated In-situ Electrolytes Enabling Stable Cycling of Wide-Temperature Li Metal Batteries
Publication Status	☐ Published ☐ Accepted for Publication ☐ Submitted for Publication ☑ Unpublished and Unsubmitted work written in manuscript style
Publication Details	Tianhua Chen, Jin Li, Dusan Losic, Jian Wang, Haitao Zhang

Principal Author

Name of Principal Author (Candidate)	Tianhua Chen		
Contribution to the Paper	Prepared, edited and revised the manuscript.		
Overall percentage (%)	85%		
Certification:	This paper reports on original research I conducted during the period of my Higher Degree by Research candidature and is not subject to any obligations or contractual agreements with a third party that would constrain its inclusion in this thesis. I am the primary author of this paper.		
Signature		Date	23/04/2023

Co-Author Contributions

By signing the Statement of Authorship, each author certifies that:

i. the candidate's stated contribution to the publication is accurate (as detailed above);

ii. permission is granted for the candidate in include the publication in the thesis; and

iii. the sum of all co-author contributions is equal to 100% less the candidate's stated contribution.

Name of Co-Author	Jin Li		
Contribution to the Paper	Edited and revised the manuscript.		
Signature		Date	23/04/2023

Name of Co-Author	Dusan Losic		
Contribution to the Paper	Supervised the development of work, edited and revised the manuscript, and acted as the corresponding author.		
Signature		Date	23/04/2023

Please cut and paste additional co-author panels here as required.

Name of Co-Author	Jian Wang		
Contribution to the Paper	Edited and revised the manuscript, and acted as the corresponding author.		
Signature		Date	23/04/2023

Name of Co-Author	Haitao Zhang		
Contribution to the Paper	Co-supervised and revised manuscript, and acted as the corresponding author.		
Signature		Date	23/04/2023

Ionic Liquid Participated In-situ Electrolytes Enabling Stable Cycling of Wide-Temperature Li Metal Batteries

Tianhua Chen[a,b], Jin Li[b], Dusan Losic[a]*, Jian Wang[c]*, Haitao Zhang[b]*

[a]*School of Chemical Engineering and Advanced Materials, The University of Adelaide, Adelaide, SA 5005, Australia*

[b]*Institute of Process Engineering, Chinese Academy of Sciences, 100190, Beijing, China*

[c]*Helmholtz Institute Ulm (HIU), Ulm D89081, Germany*

Corresponding author email: Dusan Losic, dusan.losic@adelaide.edu.au (D. Losic), Jian Wang, Jian.wang@kit.edu (J. Wang), Haitao Zhang, htzhang@ ipe.ac.cn (H. Zhang)

Abstract

Solid-state batteries (SSBs) are a promising technology to meet safe and high-capacity energy application. Nevertheless, the utilization of SSBs is still limited due to inadequate ionic conductivity and sluggish interfacial transportation at subzero temperatures, which slow their widespread application. To address this problem, a stable and highly conductive gel polymer electrolyte is developed by infusing ionic liquid into in situ polymerized electrolyte using electrospinning polyacrylonitrile (PAN) separator. The electrolyte possesses high conductivity (7.08×10^{-3} S cm^{-1} at room temperature), high Li ion transference number of 0.63, and excellent compatibility with the Li metal. $LiFePO_4$||pDOL-py||Li and $LiNi_{0.6}Mn_{0.2}Co_{0.2}O_2$||pDOL-py||Li batteries displayed long cycling ability at high rate and widened working temperature range, such as 2000 cycles at 2 C at room temperature. The excellent performance of this gel electrolyte is credited to its distinctive property which facilitates rapid transportation of Li^+ and ensures remarkable interfacial stability. Therefore, the newly developed electrolyte can realize practical low temperature is a very promising solution for long-term cycling solid-state Li batteries.

Key words: **highly conductive gel polymer electrolyte, low temperature, compatibility, long-term cycling**

1. Introduction

As the booming demand for consumer electronics, electric vehicles, and grid storage continues to increase, there is an urgent requirement for electrochemical storage systems that have high energy density.[1] Unfortunately, current battery systems fall short of the necessary energy density for many practical uses. Li metal has emerged as a potential solution to this problem due to its high theoretical specific capacity of 3860 mAh g^{-1} and low negative electrochemical potential (-3.04 V vs Li^+/Li).[2] Despite its potential, rechargeable Li metal batteries have not been commonly used commercially due to a number of obstacles, such as low Coulombic efficiency, unregulated growth of Li dendrites, and the accumulation of 'dead Li' or corrosion of the Li metal anode.[3] When exposed to many organic electrolyte solvents and Li salts, Li metal naturally creates a solid electrolyte interphase (SEI) layer that is electrically insulating but ionically conductive.[4] Nonetheless, the SEI layer is fragile and unable to withstand the physical deformation caused by the Li plating and stripping procedures, especially at subzero temperature.[5] As a result, the SEI layer breaks and repairs continuously during cycling, resulting in the development of Li dendrites in areas where the current density is particularly high.[6]

Efforts have been suggested to address these issues. Recently, the in situ polymerization technique has been employed to produce efficient interfacial transportation of Li^+ ions in polymer electrolytes, which can be directly implemented in battery related fields.[7] Through the in situ polymerization, the battery is built with integrated structure that enables the electrolyte to

encompass the whole battery, resulting in a stabilized electrochemical reaction interface between the electrolyte and electrodes.[8]

To address this problem in this paper we proposed new concept to convert a typical ether-based electrolyte, which contained 1 M of lithium bis(tri-fluoromethanesulfonyl)imide (LiTFSI, 1M) in DOL and 1,2-dimethoxyethane (DME), into gel polymer electrolyte. This was achieved by carrying out an in situ cationic ring-opening polymerization process using commercial lithium hexafluorophosphate ($LiPF_6$, 1 M) and DOL, incorporating with N-propyl-N-methylpyrrolidinium bis(trifluoromethanesulfonyl)amide ($Py_{13}TFSI$) ionic liquid and electrospun PAN used as the separator. The addition of $Py_{13}TFSI$ is specifically used to significantly improve the reversibility of Li plating/stripping as well as lowering the impedance of the battery. The stability of SEI layer is proposed to be improved by the in situ process. In addition, the growth of Li dendrites and the corrosion of the Li metal anode can be effectively inhibited during the cycling process. The properties of prepared gel-polymer electrolyte are evaluated by series structural, chemical and electrochemical characterized methods to confirm their structure, composition and proposed performance.

2. Experimental section

2.1 Materials

1-Methyl-1-propylpyrrolidinium bis(trifluoromethylsulfonyl)imide ($Py_{13}TFSI$, 99.99%, Lanzhou Institute of Chemical Physics Co., Ltd.). 1,3-dioxolane (DOL, 99.99%, Sigma-Aldrich), N,N-Dimethylformamide (DMF, Aladdin, AR), polyacrylonitrile (PAN, Aladdin, AR), 1,2-

Dimethoxyethane (DME, 99.99%, Sigma-Aldrich), lithium bis(trifluoromethanesulfonyl)imide (LiTFSI, 99.99%, Sigma-Aldrich), Lithium hexafluorophosphate ($LiPF_6$, 99.99%, Sigma-Aldrich), $LiNi_{0.6}Co_{0.2}Mn_{0.2}O_2$ (NCM622) and $LiFePO_4$ (LFP) materials were purchased from Guangdong Canrd New Energy Technology Co. Ltd. Super P powder, N-methylpyrrolidone (NMP), polyvinylidene fluoride (PVDF, MW = 1,000,000) was provided by Aladdin and used as received. All of the chemicals mentioned were purchased commercially and were used as-is without any additional purification steps.

2.2 Materials synthesis

The PAN electrospinning separator was made by electrospinning technology. To create a homogeneous spinning solution, 2.0 g of PAN particles were dissolved in 18 g DMF solution. The solution was then magnetically stirred for 8 hours at 60°C to ensure transparency and uniform. The above solution was then moved into a 20mL syringe with a stainless-steel spinning needle with a No. 16 size, and the aluminum foil as receiver. The electrospinning process was conducted with the following specific parameters: a 15 cm gap between the roller and needle, a voltage of approximately 20 kV, and a roller speed of 500 revolutions per minute. The solution was dispensed at a rate of 1.5 ml/h, with a total volume of 18 ml. After the process was complete, the resulting PAN electrospinning membrane had a thickness of 200 μm and was dried in a vacuum oven for 24 hours at 80°C. Finally, the electrospinning membrane was pressed into 20 μm by a sealing machine.

The polymeric electrolyte was synthesized by mixing and in-situ polymerization of DOL

monomer, 1M/L LiTFSI salt, DME solvent, PP separator or PAN separator, and 1M/L $LiPF_6$ initiator at room temperature. The electrolyte used PE separator without the addition of ionic liquids was named polyDOL electrolyte. The electrolyte with the addition of Py_{13}TFSI ionic liquids was named pDOL-py electrolyte, and the content of Py_{13}TFSI will be indicated as a percentage in front of it.

To prepare the cathode, a slurry was made by mixing 80 wt% of LFP or NCM622, 10 wt% of Super P carbon, and 10 wt% of PVDF. This slurry was then spread onto aluminum foil and dried in a vacuum oven at 80 °C for 24 hours. The aluminum foil was then cut into circular discs with a diameter of 14 mm, which were used as cathodes. Li metal foils were used as anodes. The cathodes were loaded with LFP or NCM622 in the range of 3 mg cm^{-2} to 5 mg cm^{-2}. The solid-state lithium metal batteries were assembled by placing the SPE between the cathode and Li anode in CR2025 coin cells inside a glove box.

2.3 Characterizations

The Fourier transform infrared spectroscopy (FT-IR) spectra were obtained using the Nicolet Avatar 360 Spectrometer in the range of 4000-500 cm-1. The surface morphology of the samples was examined using the Haitich SU8020 scanning electron microscope (SEM) and Transmission electron microscopy (TEM, JEM-2100HR, Japan). To analyze changes in the composition of both the surface and underlying structure of the recycled lithium metal and cathode, X-ray photoelectron spectroscopy (XPS) was performed using the Thermo Fisher Scientific ESCALAB 250 Xi apparatus with Al Ka radiation (hv=1486.6 eV) as the X-ray source.

The thermal properties of the samples were measured using differential scanning calorimetry (DSC) with a heating rate of 5 °C min^{-1} and thermogravimetric analysis, ^{13}C and ^{7}Li NMR measurements were conducted on a JNM-ECZ600R with a resonance frequency of 233MHz.

2.4 Electrochemical measurements

The performance of Li||PPE||LFP/NCM622 half cells was tested using a LAND test system (CT2001A, China) with a working voltage range of 2.5 - 4.0 V, and 2.8 - 4.3V. The Li||PPE||LFP rate test of charge-discharge current was conducted with current densities from 0.1 C to 10 C, without using a constant-voltage mode. Li||PEE||Li symmetric cells were tested with Land setting for galvanostatic cycling at current densities of 0.2, 0.5, and 1 mA cm^{-2}. An Li||PPE||stainless steel (ss) asymmetrical cell was used for linear scanning voltammetry (LSV) in the Autolab (PGSTAT302N) electrochemical workstation at a scanning rate of 1 mV s^{-1}, with the working electrode consisting of a stainless-steel sheet as the working electrode and Li foil as the counter electrode and reference electrode. Electrochemical impedance spectroscopy (EIS) was carried out in the Autolab (PGSTAT302N) with a frequency range of 10^5 - 10^{-2} Hz and an amplitude of 5 mV. Constant current and constant voltage tests were performed on the NCM622||pDOL-py||Li battery to conduct the electrochemical floating analysis experiment. The ionic conductivity of polymer electrolyte membranes was measured using the formula σ=L/(D*R), where R ($\Omega \cdot cm^2$) represents the bulk resistance of the electrolyte, L represents the thickness of the electrolyte, and D represents the effective area. The transference number (t_{Li^+}) of the battery was calculated using chronoamperometry by maintaining a constant polarization potential of 10 mV at ambient

temperature. The formula used to calculate the transference number of the battery is $t_{Li^+} = [I_S(\Delta V - R_0 I_0)]/[I_0(\Delta V - R_S I_S)]$. Here, I_o and I_s refer to the initial and steady-state currents, respectively, while R_o and R_s denote the interface resistances before and after polarization.

3. Result and discussion

3.1 Characterization of in situ polymerization of gel electrolyte

The critical process in creating an artificial SEI layer is the ring-opening polymerization. This process was confirmed through the Fourier transform infrared spectroscopy (FTIR) test and is presented in Figure 1a. As shown in the spectrum, the feather peaks of DOL between 900 and 1100 cm^{-1} were notably missing after the completion of the polymerization procedure. On the contrary, it was noted that there was wide and distinct peak at approximately 833 cm^{-1} for the long chains of O–C–O bond present in polyDOL, which signifies the accomplishment of the polymerization process and a negligible retention of DOL monomer.[9] In addition, the long chain structure can enhance its ability to withstand high voltage.[10] At 1060 cm^{-1}, relating to the C-O-C bond, strongly suggests that the components of the SEI layer were determined as reported.[11]

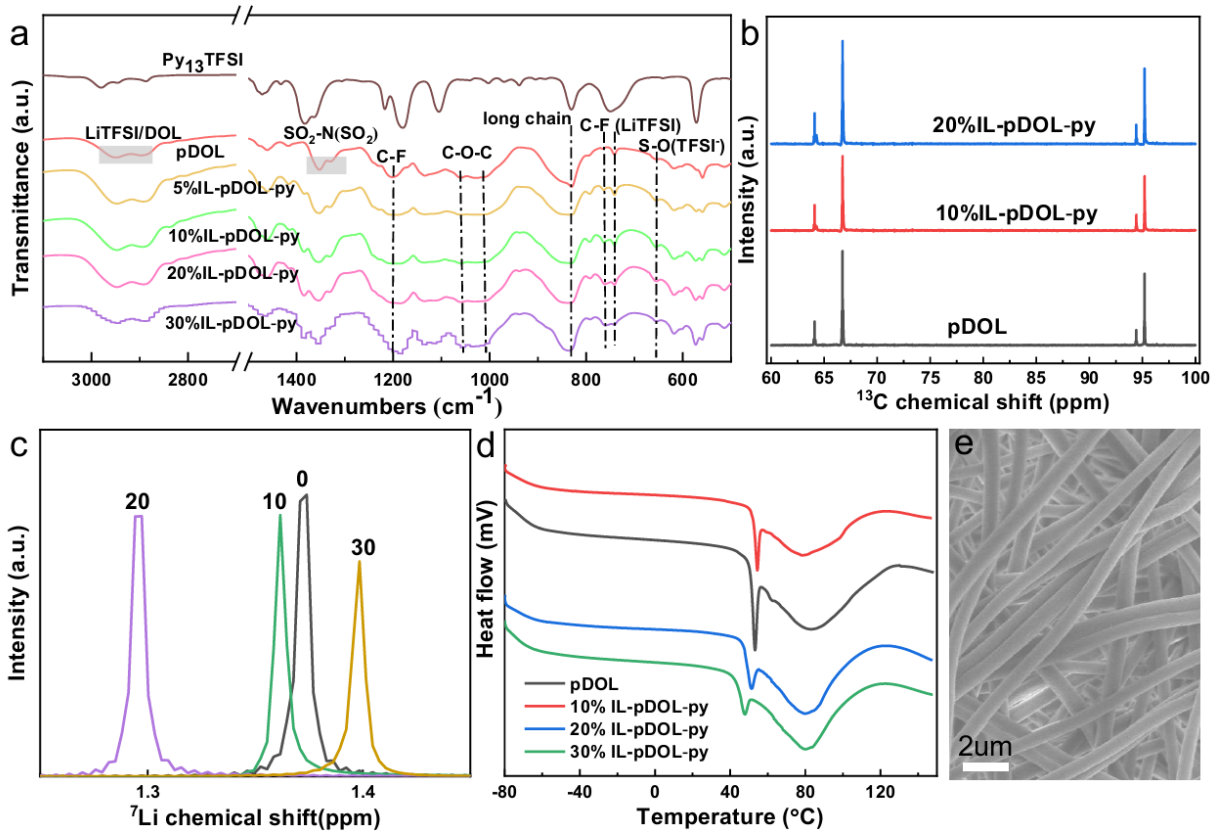

Figure 1 (a) ARI-FTIR spectra of $Py_{13}TFSI$, pDOL electrolyte, and pDOL-py electrolytes with different concentration of $Py_{13}TFSI$, (b) ^{13}C spectra of in-situ polymerization (pDOL, pDOL-py electrolytes) samples, (c) ^{7}Li spectra of in-situ polymerization (pDOL, pDOL-py electrolytes) samples, (d) DSC curves of pDOL and pDOL-py samples, (e) SEM image of electrospinning PAN separator.

Figure 1b further supports the structure and composition of electrolytes through ^{13}C NMR. The peaks of C 1s at 66.7 and 95.3 cm^{-1} in the electrolyte samples, corresponding to the -C-O-C- and -O-C-C-O- bond, respectively.[12] These two typical peaks did not shift, implying that DOL ring-opening polymerization was the only process taking place without the involvement of any other solvents. The ^{7}Li NMR in Fig. 3c displays the shift after the addition of ionic liquid.

The left shift represents the enhanced transportation of Li^+, while the right shift means the weakened mobility of Li ions. This is due to the imidazole groups in $Py_{13}TFSI$ have the ability to vie with lithium salts for hydrogen bonding with the carbonyl group from polyDOL. Moreover, the $TFSI^-$ of $Py_{13}TFSI$ can act in coordination with Li^+ and the polymerized carbonyl group.[13] These result in the weakened Li^+ transfer barrier, which in turn enable the electrolyte to have a greater ionic conductivity and enhanced lithium transference number. Within the range of 0 to 20 wt% of the $Py_{13}TFSI$ content in the pDOL-py electrolyte, as the amount of ionic liquid increases, the affinity for lithium continuously increased. However, after exceeding 20 wt%, the affinity for lithium sharply decreased. As a consequence, it can be concluded that adding 10 ~ 20 wt% $Py_{13}TFSI$ to the electrolyte system results in the best lithiophilicity for the electrolyte. According to the above FTIR and NMR analyses, there was no evidence of the participation of $Py_{13}TFSI$ during the in -situ polymerization process of DOL. In addition to its wetting effect, $Py_{13}TFSI$ ionic liquids can also reduce the crystallinity of the polymer, as shown in Fig. 1d of the DSC curves, further facilitating the transport of lithium ions and improving the free segments for Li^+ transport. The SEM image of electrospinning PAN separator in Fig. 1e shows the fibers was rough and uniform, providing attachment sites for the electrolyte.

3.2 Electrochemical properties

Due to its limited oxidative stability beyond 4.0 V (versus Li^+/Li), the use of pure polyDOL electrolyte is not widespread in Li metal batteries. Tests using linear sweep voltammetry (LSV) were performed to investigate how the oxidation limitation of the in situ-formed electrolytes is

influenced by $Py_{13}TFSI$, illustrated in Figure 2a. There were no notable alterations observed in the oxidation current prior to reaching 4.2 V (vs Li^+/Li). The results indicate that pDOL-py electrolytes exhibit enhanced anti-oxidation potential resistance to oxidation reached to 5.2 V. On the other hand, the pure polyDOL electrolyte undergoes oxidative decomposition at approximately 4.2 V. Hence, the addition of $Py_{13}TFSI$ ionic liquid process of polymerization has been identified as a potentially effective approach to increase the oxidative stability at high voltages. To further confirm the practical electrochemical stability of the solid-state electrolyte, an electrochemical floating experiment using the $LiNi_{0.6}Co_{0.2}Mn_{0.2}O_2$ (NCM622) battery is conducted. The oxidation stability of the electrolyte is assessed by recording the leakage current during the constant voltage charging. The results are presented in Fig. 2 b - c. At the voltage between 4.0 to 4.5 V, the current in pDOL-py electrolyte decreased slightly, which exhibits excellent oxidation stability at 4.5 V, and it decreased sharply at 4.6 V, from 41 to 13 μA. As a contrast, the operating window of the battery with polyDOL electrolyte was 4.2 V. The current of the pDOL-py battery shows a significant decrease at 4.5V, while the pDOL battery cannot maintain stability at 4.3V. In this situation, continuing to charge with an overpotential exceeding the operating window leads to dendritic growth and “dead Li” on the anode and collapse of the cathode material.

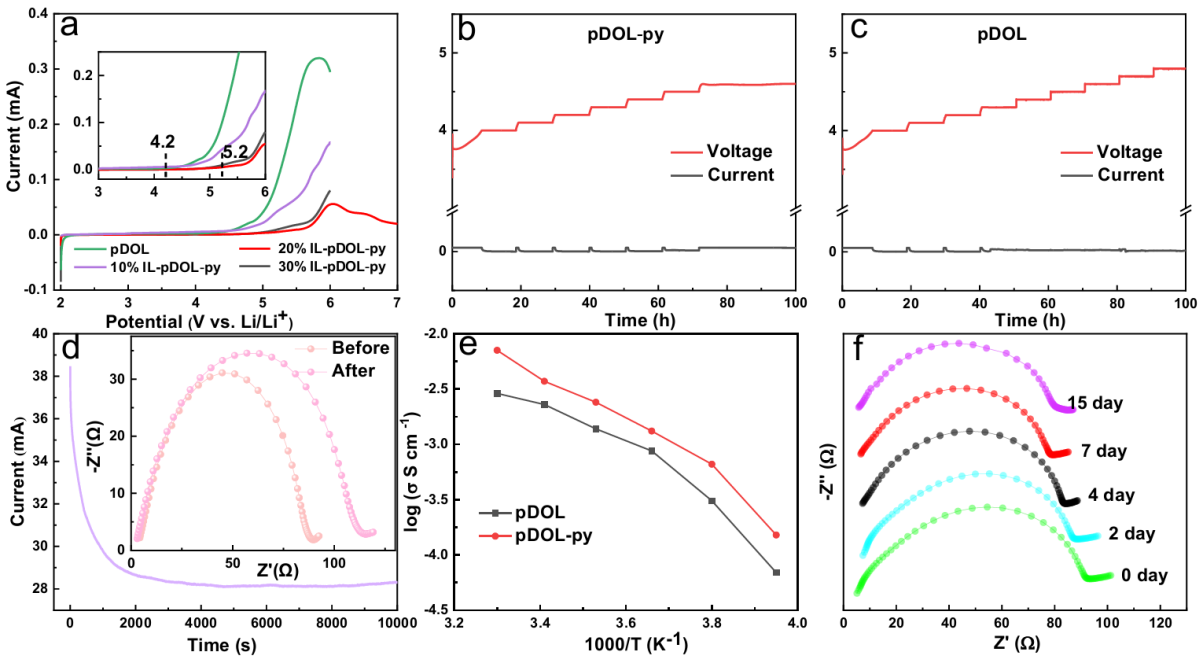

Figure 2 (a) Linear sweep voltammetry (LSV) measurements of pDOL and diffent IL concerntation of pDOL-py electrolytes, (b) electrochemical floating analysis of NCM622|| pDOL-py ||Li battery, (c) electrochemical floating analysis of NCM622||pDOL||Li battery, (d) current-time curve following DC polarization curves of the pDOL-py electrolyte at room temperature (the insets are the EIS plot before and after polarization), (e) Arrhenius plot of the ionic conductivity of polyDOL and pDOL-py electrolyte, (f) Time evolution of the EIS plots of a symmetrical Li|| pDOL-py ||Li cell at room temperature.

The current values of the lithium symmetric batteries assembled by pDOL and pDOL-py electrolyte were measured at a constant bias voltage. The Bruce-Vincent-Evans equation was used in combination with the impedance values measured before and after polarization to calculate the Li^+ transference number t_{Li^+} of the electrolytes. Fig. 2d shows that at a bias voltage of 10 mV, the current decreased from 3.85×10^{-4} to 2.81×10^{-4} A, and the impedance

value increased from 90 to 115 Ω. By using the previously mentioned calculation, it was calculated that the participation of $Py_{13}TFSI$ ionic liquid highly increased the Li^+ transference number of solid electrolytes to 0.63, compared with the pDOL electrolyte of 0.42.[14] The presence of high t_{Li+} can effectively minimize the concentration polarization of Li^+ ions, impede the development of lithium dendrites, and achieve higher charging/discharging rates.

The ionic conductivity of the electrolytes was measured using electrochemical impedance spectroscopy (EIS) at different temperatures, as shown in Figure S1 and the corresponding Arrhenius plot of the ionic conductivity in Fig. 2e. As depicted, the ionic conductivity of pDOL-py electrolyte increased with temperature, and was one order of magnitude higher than that of pDOL electrolyte on average. With the Arrhenius equation, the conductivities of pDOL and pDOL-py were 0.98×10^{-3} and 7.08×10^{-3} S cm^{-1} at RM, respectively. Moreover, the activation energy (Ea) for Li ion transport were 0.0258 and 0.0324 eV, separately. The pDOL-py electrolyte showed the lower Li^+ migration barrier. The lower Ea value of pDOL-py electrolyte was in agreement with the higher ionic conductivity. Thus, the enhanced ionic conductivity, Ea and t_{Li+} were ascribed to the abundance of free Li^+ ions, which was brought about by the participation of $Py_{13}TFSI$ and the use of PAN separator. The variation of the impedance of Li symmetric cell over statistic time at room temperature can also be used to measure the interface stability of the battery. During the first 4 days, the impedance of the battery gradually decreased until it reached a stable state, which was due to the gradual polymerization of the electrolyte, resulting in a stable interface.

3.3 Characterization of electrolyte-Li anode interface

Li symmetrical cell testing was carried out to examine the performance of interfacial stability and deposition behavior of Li^+, as shown in Fig. 3 a and Fig. S2. When operating at a current density of 1 mA cm^{-2}, the overpotential of Li||polyDOL||Li cell suffered a larger fluctuation and increased gradually after 160 h (up to 400 mA at maximum), which was caused by the formation of Li dendrites and accumulation of dead Li during cycling process as reported.[15] While for the Li||pDOL-py||Li cell, the overpotential remained consistent and lower at about 80 mA, which did not show significant increments after 240 h. Furthermore, the Li||pDOL-py||Li cell demonstrated a lower polarization at varying current densities, which suggests that it has improved compatibility and stability with lithium metal. Therefore, as depicted in Fig. S2, the Li||pDOL-py||Li cell operated steadily with an overpotential about 56 mA for 800 h under 0.1 mA cm^{-2}, indicating outstanding ability of inhibiting the lithium dendrites, except for the initial potential increase due to battery activation and SEI formation.

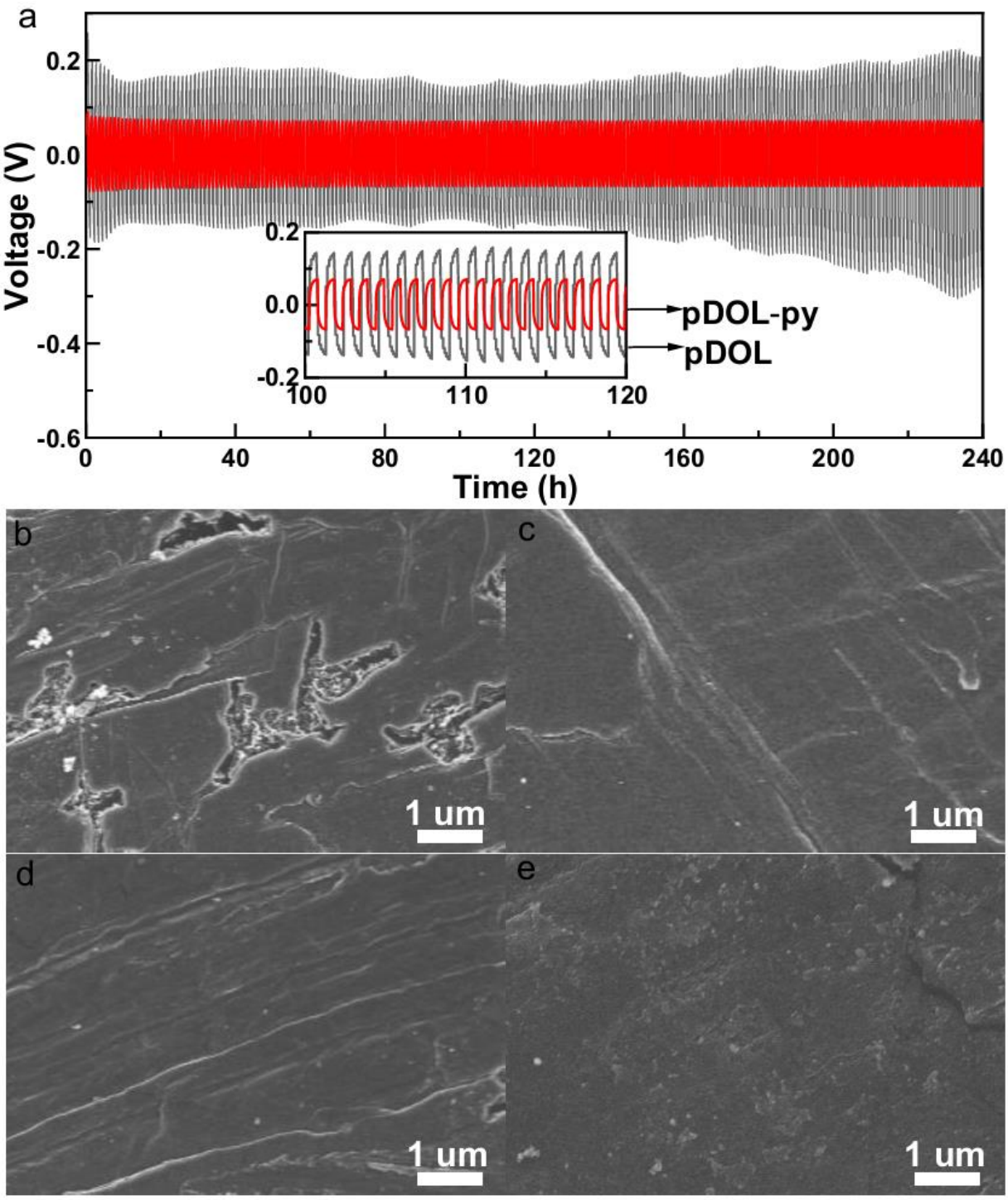

Figure 3 (a) Comparison of voltage profiles of of Li||Li symmetric cells at 1 mA cm^{-2} at room temperature. SEM images of the Li metal surface from the cycled Li||Li symmetric cells after 10 cycles at 0.1 mA cm^{-2} (0.1 mA h cm^{-2}) with (b) pDOL electrolyte, (c) pDOL-py electrolye, and pDOL-py electrolyte at (d) 0.5 mA cm^{-2}, (e) 1 mA cm^{-2}.

In order to study lithium dendrites, the surface morphology of the lithium anode after ten cycles was examined using SEM. As shown in Fig. 3b, the Li metal anode immersed in polyDOL showed dendrite. Therefore, the acceleration of the formation of Li dendrites and “dead Li” will be intensified. In contrast, the pDOL-py electrolyte and PAN separator lead to a smooth Li surface without any dendrite, as depicted in Figure 3c. A smooth surface on the Li metal anode can reduce the likelihood of side reactions between the deposited Li and pDOL-py electrolyte, thereby leading to the enhanced reversibility of Li insertion and extraction. In Fig. 3d-e, the effectiveness of the pDOL-py electrolyte in suppressing the growth of Li dendrites was assessed through different current densities of 0.1, 0.5, 1 mA cm^{-2}, respectively. Even when the current density is as high as 0.5 mA cm^{-2}, the Li metal anode still shows a smooth surface, while at the current density of 1 mA cm^{-2}, it appears to have a speckled structure, but the dendrite formation was still effectively inhibited. The results demonstrate that the pDOL-py electrolyte has strong interfacial stability with Li anode and is capable of suppressing the formation of lithium dendrites.

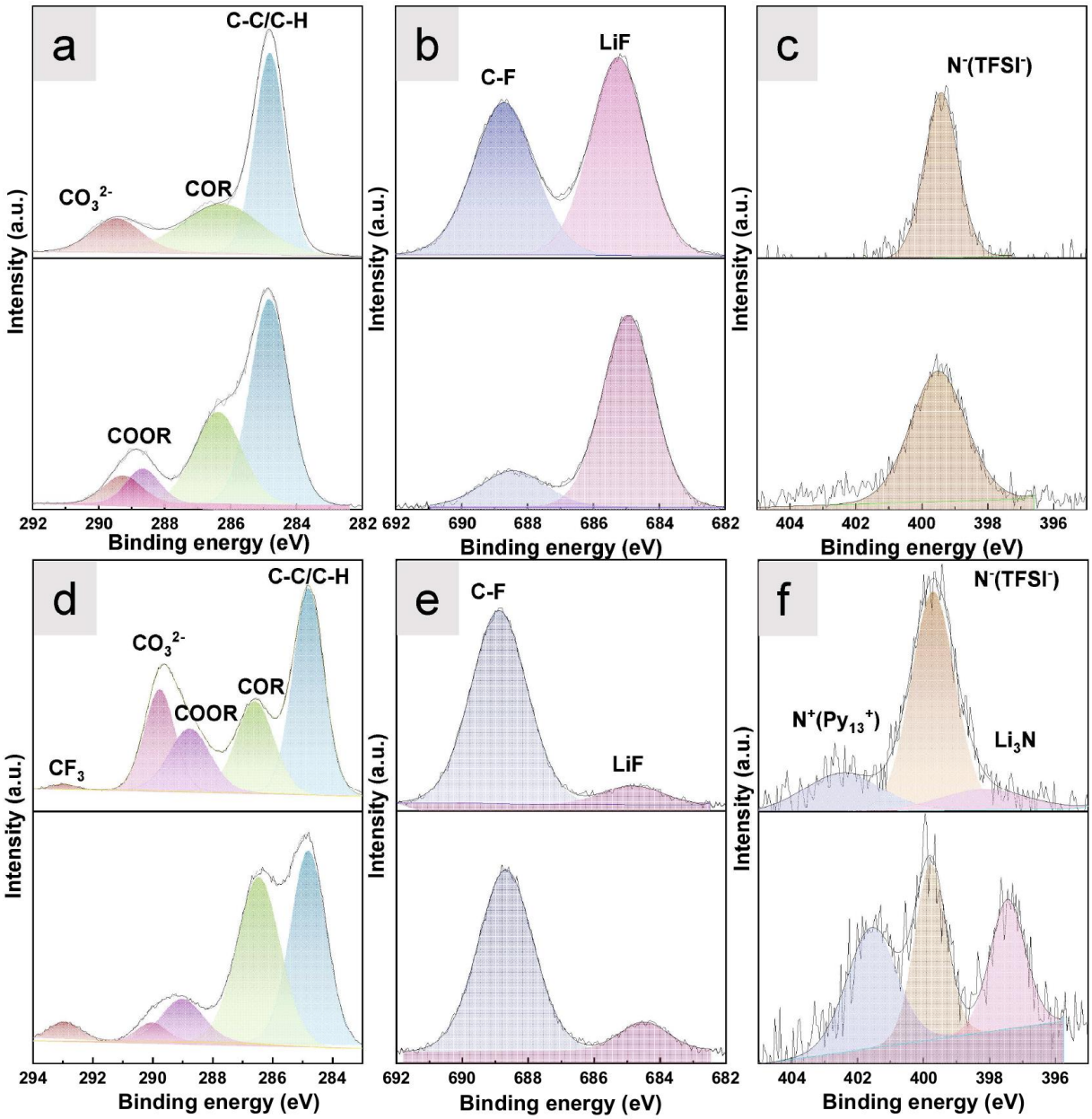

Figure 4 XPS spectra (C 1s, F 1s, N 1s) of the Li metal surface from the cycled Li||Li symmetric cells after 3 and 50 cycles at 0.2 mA cm^{-2} (0.2 mA h cm^{-2}) with (a, b, c) pDOL electrolye, and (d, e, f) pDOL-py electrolyte at romm temperature.

Fig. 4 and Fig. S3 displays the application of XPS to investigate the chemical composition of the solid electrolyte interphase (SEI) formed on Li metal obtained from Li||Li batteries after 3 and 50 cycles at 0.2 mA cm^{-2}, respectively. The spectra of the F 1s showed two distinct peaks

located at approximately 688.9 and 684.9 eV. These peaks were identified as the C-F bond and LiF, separately. The analysis of F 1s spectra indicates a notable increase in LiF content on the surface of Li metal anode, along with a sharp decline in the C-F functional group after 50 cycles in the Li||pDOL||Li battery. In contrast, the LiF concentration shows a slight increase, and there is a slight decrease in the C-F functional group after 50 cycles in the Li||pDOL-py||Li battery. it has been reported that an adequate amount of LiF content has the ability to reinforce and make the SEI layer more stable, but excessive LiF can cause an increase in battery impedance and polarization.[16] The electrochemical reactivity and lithophilicity of the electrolyte are significantly enhanced by the semi-ionic bonding features of the C-F bond.

The N 1s spectra demonstrate a peak at approximately 399.8 eV, which corresponds to $TFSI^-$ identified in LiTFSI salt or $Py_{13}TFSI$, as shown in Figure 3c and f. Furthermore, two additional peaks are observed at 397.4 and 401.5 eV, respectively, due to the existence of N^- in Li_3N and N^+ in Py_{13}^+. When $Py_{13}TFSI$ ionic liquid is used in the pDOL-py electrolyte system, it alters the SEI layers on the Li metal surface, resulting in a protective interface that remains stable during cycling and reduces undesirable reactions between the electrolyte and Li metal. Furthermore, the pDOL-py electrolyte promotes the generation of Li_3N while cycling, which inhibits the expansion of Li dendrites. Moreover, it is evident that the $Py_{13}TFSI$ ionic liquid has the capacity to moisten the boundary, broaden the electrochemical range, and decrease the crystallinity of the PDOL in this configuration. In addition, the O1s spectra (shown in Fig. S3) revealed the presence of peaks at 531.9 eV for Li_2CO_3 and LiOH, as well as 533.2 eV for Li_2O, which resulted from the breakdown of lithium salts. This occurred when Li_2O reacted with the

surrounding air, resulting in the formation of Li_2CO_3 and LiOH. In comparison to the PDOL sample, the pDOL-py cell exhibited greater Li_2O peaks, enhancing Li^+ conductivity and SEI stability. On the other hand, PDOL battery showed a higher LiOH peak, leading to an unstable SEI.

After analyzing the results, it was found that the main components of the SEI layers are LiF, C-C, LiCOOR, COR, Li_xSO_y, and Li_2CO_3. As the of Li||pDOL||Li battery cycling continuously, the amount of side reaction products increased significantly due to the ongoing process of breaking and repairing the SEI layers, as well as the continuous growth of Li dendrites. With the gradual growth of lithium dendrites, a speckled structure with a high specific surface area is formed on the surface of the lithium anode, causing the acceleration of the irreversible reaction between the Li anode and the electrolyte. Therefore, because of the uneven Li plating and stripping, a certain amount of Li dendrites become electrically isolated or rendered inactive, commonly referred to as 'dead Li', which can cause significant corrosion of the Li anode and a detectable amount of dead Li accumulation. For the pDOL-py electrolyte, Py_{13}TFSI modified the SEI layers on the surface of the Li metal, creating a passivation interphase that efficiently reduces side reactions between the Li anode and electrolyte and promoted uniform plating and stripping of the Li metal. Consequently, this leads to a compact and flat Li metal surface.

3.4 Long-term cycling and rate performance of the batteries

The aforementioned results suggest that pDOL-py electrolyte is capable of enduring Li metal and can be beneficial for the electrochemical deposition and stripping of Li metal. The

study was therefore expanded to LMBs which employed $LiFePO_4$ (LFP) and $LiNi_{0.6}Co_{0.2}Mn_{0.2}O_2$ (NCM622) as cathode electrodes, as depicted in Fig. 5, and Fig. S4. The impressive electrochemical properties served as a basis for the long cycling and rate performance. To gain a deeper comprehension of the performance at a high rate, the testing was conducted at 2 C and 1 C rate. The LFP||pDOL-py||Li battery displayed long-term reversible charge/discharge cycling performance with an average Coulumbic efficiency of 99.96 % at 2 C, as displayed in Fig. 5a and Fig. S4. The battery decreased slightly from initial discharge capacity 143.04 mA h g^{-1} to 134.61 mA h g^{-1} with a capacity retention of 94.1 % after 1000 cycles. The galvanostatic charge/discharge curve of 2 C is shown in Fig. 5b, the overpotential increased from 0.19 V to 0.56 V with the cycle and rate growing. Fig. S4 compares the charge and discharge curves of LFP||pDOL-py||Li and LFP||pDOL||Li batteries at 1C. The pDOL-py battery system remained stable for 500 cycles with capacity retention above 96.4 % (from 141.6 to 136.6 mA h g^{-1}). By contrast, the LFP||pDOL||Li declined sharply at the first 50 cycles. The LFP||pDOL-py||Li battery was able to perform well even in temperatures as low as -20 °C due to the exceptional ionic conductivity and great compatibility of with the electrodes, as shown in Fig. 5c, the battery maintained a high reversible capacity of 86 mA h g^{-1} at -20 °C (0.1 C). The discharge capacity of LFP||pDOL-py||Li battery were 165, 140, 115, 103 mA h g^{-1} at 20, 10, 0, and -10 °C, respectively. Fig. 5d-e illustrate the performance of LFP||pDOL-py||Li battery at different rates from 0.1 to 10 C, the polarization gap increased with the increasing of rate, which can be attributed to the rise in interfacial resistance when operating at long-term cycling and high rates. As shown in Fig. 5e, the NCM622||pDOL-py||Li battery were assembled and tested from 3.0 to

4.3 V at room temperature. The capacity fluctuated with the changing temperature, with initial capacity of 163.2 mA h g^{-1}.

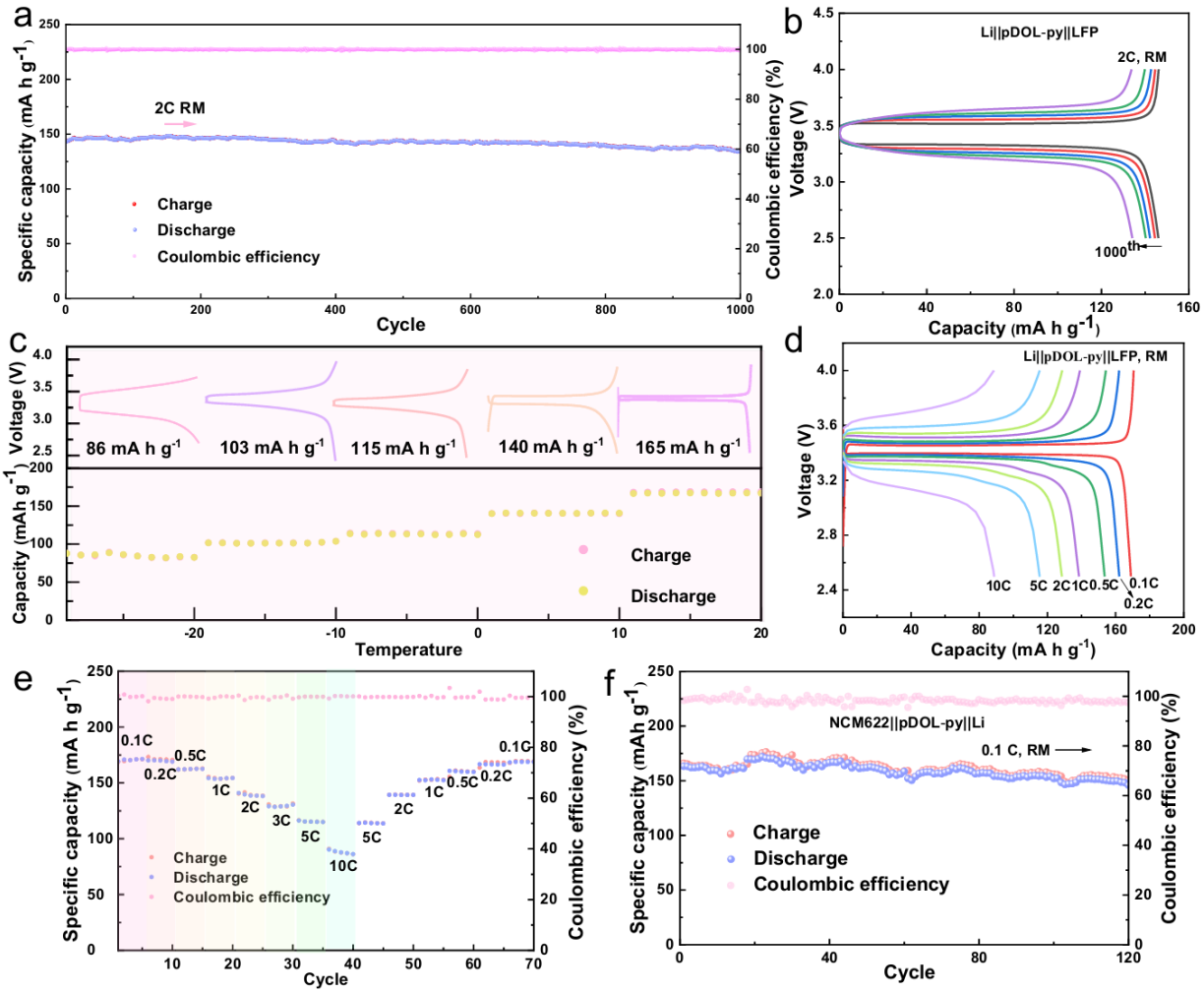

Figure 5 (a) Cycling performance of the LFP||pDOL-py||Li cell at 2 C at room temperature, galvanostatic charge/discharge curve of (b) the LFP||pDOL-py||Li cell at 2 C at room temperature, (c) the LFP||pDOL-py||Li cell at 0.1 C at different temperatures, (d) the LFP||pDOL-py||Li cell at room temperature, (e) rate performance of the LFP||pDOL-py||Li cell at room temperature, (f) charge/discharge performance of NCM622||pDOL-py||Li cell at 0.1 C at room temperature.

The morphology of the LFP and NCM622 CEI layer was examined using transmission

electron microscopy (TEM). It was observed that a much thinner layer of the CEI, 5 nm for LFP and 10 nm for NCM622 as shown in Fig. S5a and S6a, was uniformly formed on the cycled LFP in the pDOL-py-based batteries compared to the 14 nm and 29 nm in the polyDOL-based batteries (Fig. S5b and S6b). The thinner and stronger CEI layer has the ability to suppress unwanted side reactions between the electrolyte and cathode, as well as reduce the energy required for Li^+ surface diffusion. The pDOL-py-based solid-state lithium batteries exhibit significant capacities and exceptional retention owing to the electrolyte, which facilitate stable Li plating/stripping, rapid lithium-ion transportation within the electrolyte and at the electrode/electrolyte interfaces. Notably, the outstanding retention at different rates makes it possible to produce safe and durable lithium batteries.

4. Conclusion

In summary, a gel electrolyte pDOL-py is successfully developed and demonstrated by in-situ polymerization infused with the ionic liquid $Py_{13}TFSI$ on the electrospinning PAN separator, aiming to enhance high ionic conductivity, improve Li^+ transport, an expanded operating temperature range, enhance oxidative stability and long-term cycling stability. Presented results showed this electrolyte significantly improves the performance of LMBs in several aspects. Firstly, the interfacial wettability was high improved by the ionic liquid. Secondly, the electrolyte has improved the compatibility with Li anode, inhibiting the Li dendrites and improving the long cycling stability with LFP cathode. Thirdly, widened temperature range for application. The participation of $Py_{13}TFSI$ improved Li^+ transference number significantly, and decreased the

interface resistance, which makes it possible to operate the battery at low temperatures and improves its ability to transmit Li-ion in the electrolyte. It is shown the electrolyte can be applied in a wide temperature range from -20 °C to 20 °C that is significant performance not achievable by many other electrolytes. Additionally, the Li symmetrical cells demonstrated stable cycling for a duration of more than 800 hours, while only experiencing a slight overpotential of 56 mV at a current density of 0.1 mA cm^{-2}. After 1000 cycles at 2 C, the LFP||pDOL-py||Li cell exhibited a specific capacity, Coulombic efficiency, and capacity retention of 143.04 mA h g^{-1}, 99.96 %, and 94.1 %, respectively. In conclusion this development offers a promising and convenient way to provide wide temperature application for solid-state Li batteries that is problem waiting for solution.

Declaration of Competing Interest

The authors declare that they have no known competing financial interests or personal relationships that could have appeared to influence the work reported in this paper.

Acknowledgements

The authors thank the Australian Government for providing Tianhua Chen with Beacon of Enlightenment PhD Scholarship to undertake PhD at the University of Adelaide and Institute of Process Engineering, Chinese Academy of Sciences. This work was partly supported by Australian Research Cuncil (ARC), Research Hub for Graphene Enabled Industry Transformation (IH IH150100003), ZhongKe-YuNeng Joint R&D center (No. ZKYN2022006), and the International Cooperative Project of CAS (No.122111KYSB20210012).

Reference

[1] aY.-Y. Sun, F. Li, P.-Y. Hou, *Journal of Materials Chemistry A* **2021**, *9*, 9481-9505; bH. Niu, L. Wang, P. Guan, N. Zhang, C. Yan, M. Ding, X. Guo, T. Huang, X. Hu, *Journal of Energy Storage* **2021**, *40*, 102659.

[2] W. Xu, J. Wang, F. Ding, X. Chen, E. Nasybulin, Y. Zhang, J.-G. Zhang, *Energy & Environmental Science* **2014**, *7*, 513-537.

[3] X. Zhang, Y. Yang, Z. Zhou, *Chemical Society Reviews* **2020**, *49*, 3040-3071.

[4] P. Shi, X.-Q. Zhang, X. Shen, R. Zhang, H. Liu, Q. Zhang, *Advanced Materials Technologies* **2020**, *5*, 1900806.

[5] Q. Zhao, X. Liu, J. Zheng, Y. Deng, A. Warren, Q. Zhang, L. Archer, *Proc Natl Acad Sci U S A* **2020**, *117*, 26053-26060.

[6] Y. Liu, R. Hu, D. Zhang, J. Liu, F. Liu, J. Cui, Z. Lin, J. Wu, M. Zhu, *Adv Mater* **2021**, *33*, e2004711.

[7] aY.-C. Jung, M.-S. Park, D.-H. Kim, M. Ue, A. Eftekhari, D.-W. Kim, *Scientific Reports* **2017**, *7*, 17482; bQ. Zhao, X. Liu, S. Stalin, K. Khan, L. A. Archer, *Nature Energy* **2019**, *4*, 365-373.

[8] D. Chen, M. Zhu, P. Kang, T. Zhu, H. Yuan, J. Lan, X. Yang, G. Sui, *Advanced Science* **2022**, *9*, 2103663.

[9] Q. Liu, B. Cai, S. Li, Q. Yu, F. Lv, F. Kang, Q. Wang, B. Li, *Journal of Materials Chemistry A* **2020**, *8*, 7197-7204.

[10] R. Miao, J. Yang, Z. Xu, J. Wang, Y. Nuli, L. Sun, *Scientific Reports* **2016**, *6*, 21771.

[11] aW. Kam, C.-W. Liew, J. Y. Lim, S. Ramesh, *Ionics* **2014**, *20*, 665-674; bQ. Zhao, X. Liu, S. Stalin, L. Archer, *Cell Reports Physical Science* **2020**, *1*, 100146.

[12]Z. Geng, Y. Huang, G. Sun, R. Chen, W. Cao, J. Zheng, H. Li, *Nano Energy* **2022**, *91*, 106679.

[13]Z. Tian, L. Hou, D. Feng, Y. Jiao, P. Wu, *ACS Nano* **2023**, *17*, 3786-3796.

[14]H. Yang, B. Zhang, M. Jing, X. Shen, L. Wang, H. Xu, X. Yan, X. He, *Advanced Energy Materials* **2022**, *12*, 2201762.

[15]D. Lin, J. Zhao, J. Sun, H. Yao, Y. Liu, K. Yan, Y. Cui, *Proceedings of the National Academy of Sciences* **2017**, *114*, 4613-4618.

[16]Z. Li, L. Kong, C. Peng, W. Feng, *Carbon Energy*, *n/a*, e354.

Supporting information

Ionic Liquid Participated In-situ Electrolytes Enabling Stable Cycling of Wide-Temperature Li Metal Batteries

Tianhua Chen[a,b], Jin Li[b], Dusan Losic[a]*, Jian Wang[c]*,Haitao Zhang[b]*

[a]*School of Chemical Engineering and Advanced Materials, The University of Adelaide, Adelaide, SA 5005, Australia*

[b]*Institute of Process Engineering, Chinese Academy of Sciences, 100190, Beijing, China*

[c]*Helmholtz Institute Ulm (HIU), Ulm D89081, Germany*

Corresponding author email: Dusan Losic, dusan.losic@adelaide.edu.au (D. Losic), Jian Wang, Jian.wang@kit.edu (J. Wang), Haitao Zhang, htzhang@ipe.ac.cn (H. Zhang)

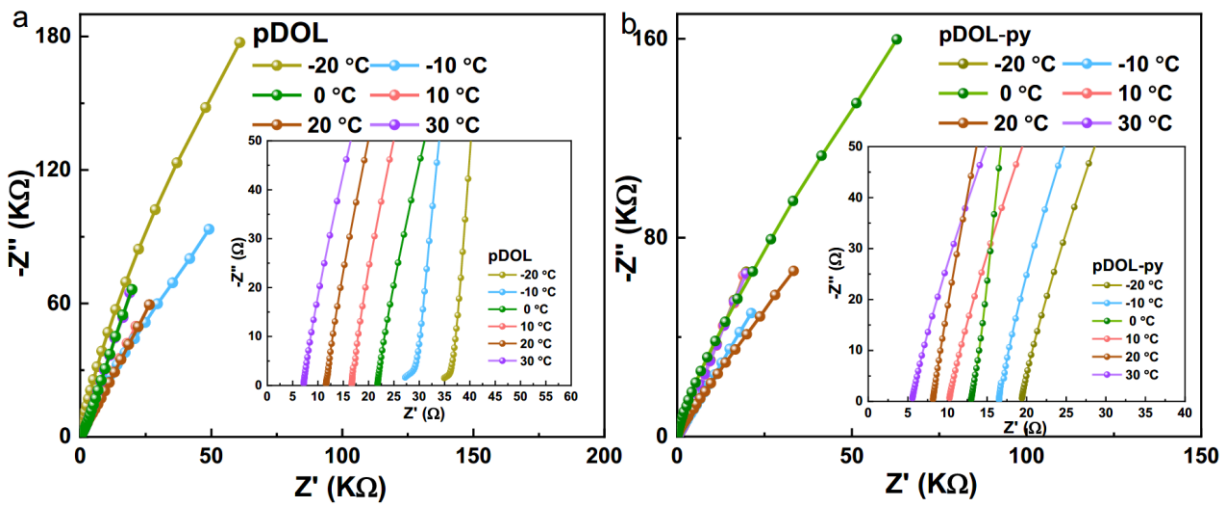

Figure S1 Nyquist plots of the electrochemical impedance spectroscopy (EIS) test of ss||pDOL||ss and ss||pDOL-py||ss battery at different temperatures

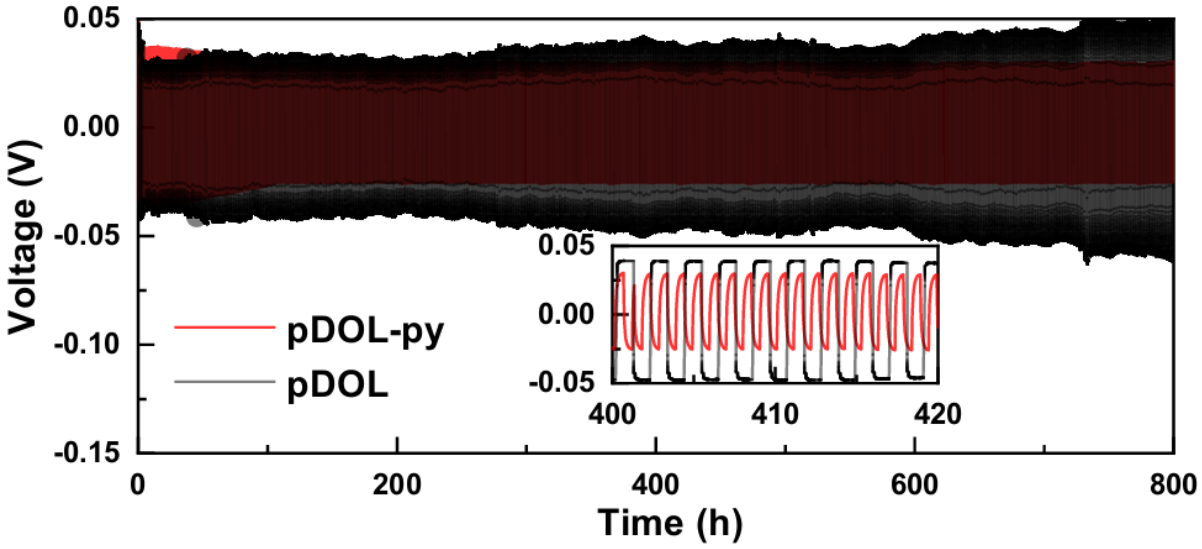

Figure S2 Comparison of voltage profiles of cycling performance of Li||Li symmetric cells at 0.1 mA cm^{-2} at room temperature.

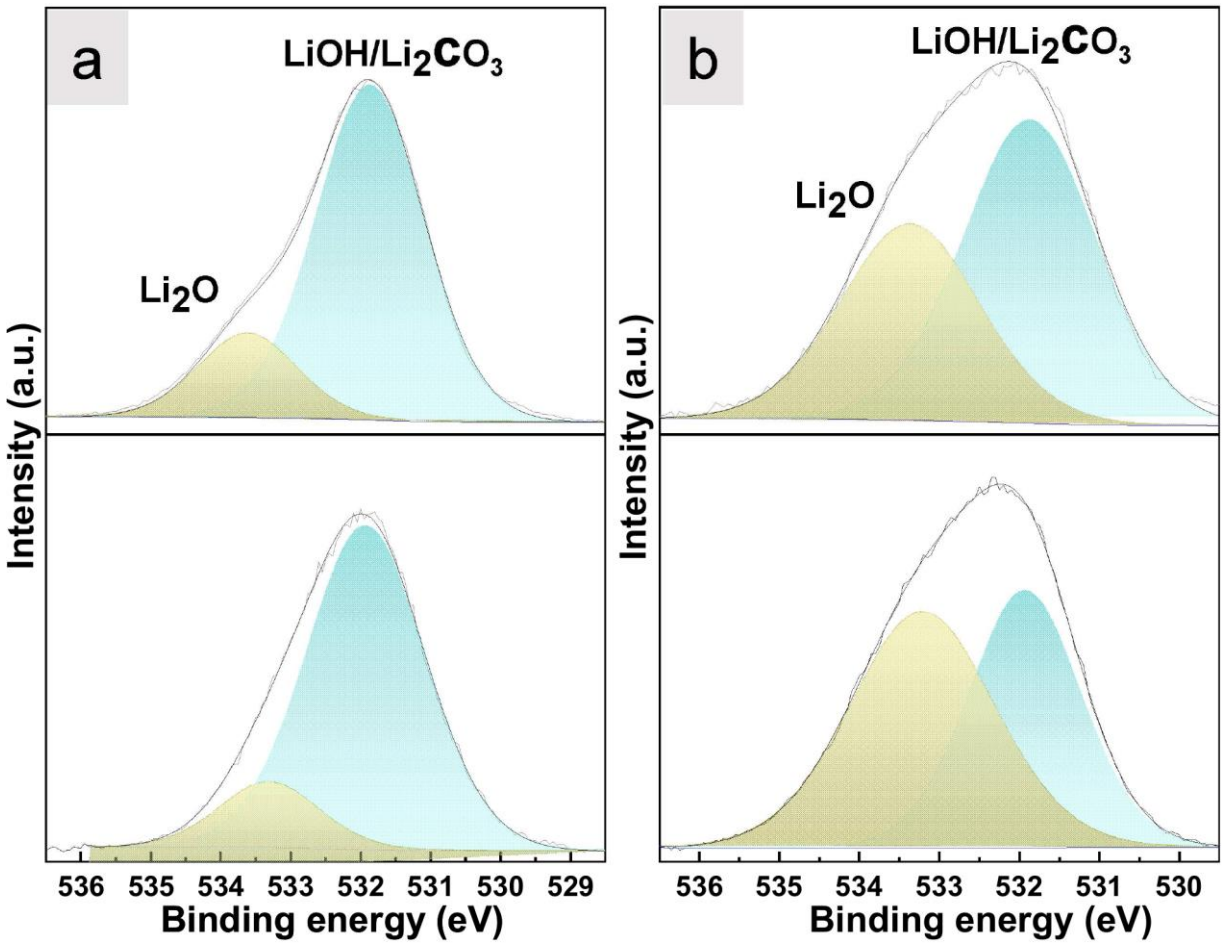

Figure S3 XPS spectra (O 1s) of the Li metal surface from the cycled Li||Li symmetric cells after 3 and 50 cycles at 0.2 mA cm^{-2} with a) PDOL electrolyte, and b) pDOL-py electrolyte.

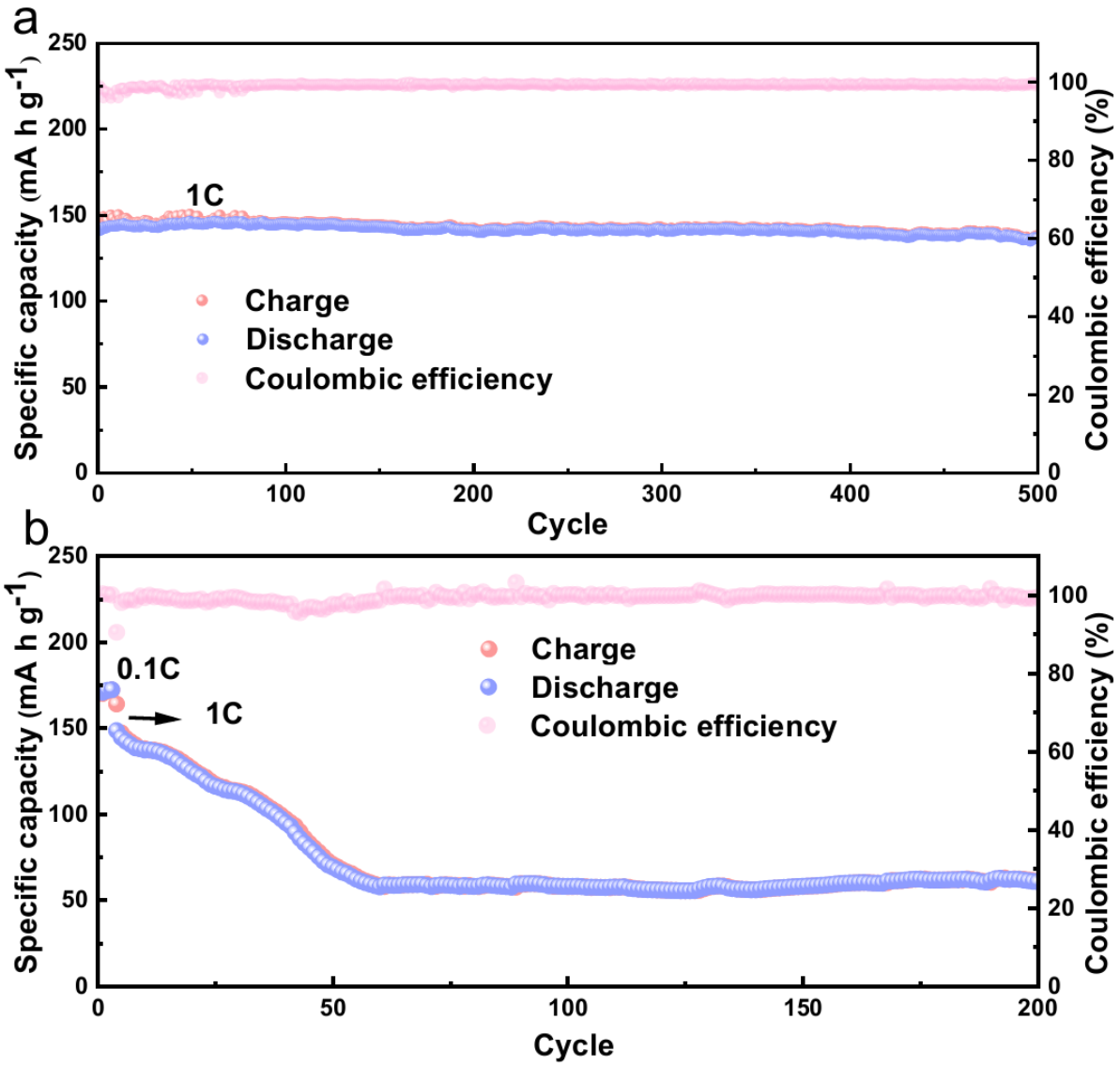

Figure S4 Cycling performance of (a) LFP||pDOL-py||Li and (b) LFP||pDOL-py||Li batteries at 1 C and room temperature

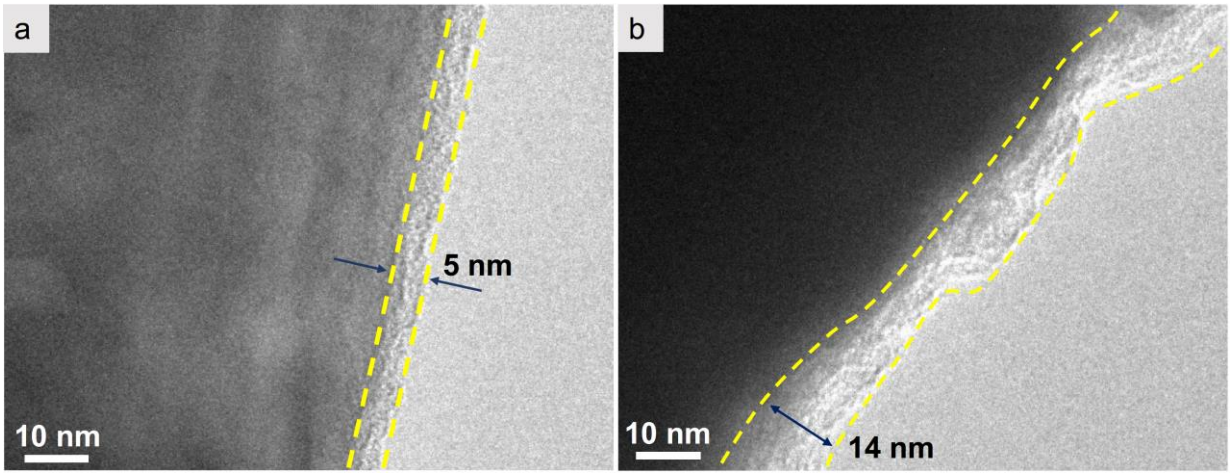

Figure S5 TEM images of LFP cathode at 0.5 C after 20 cycles at room temperature

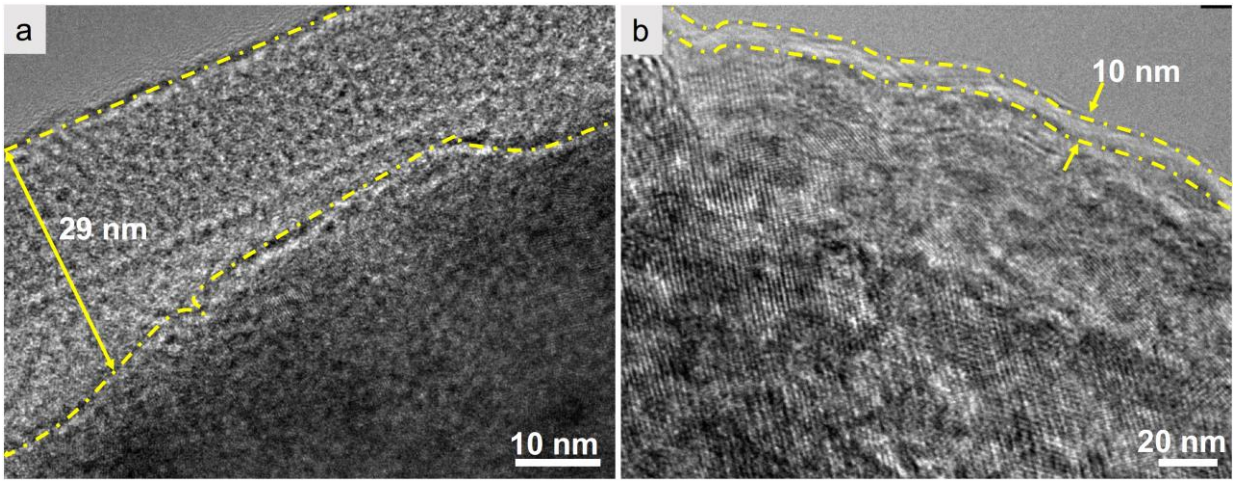

Figure S6 TEM images of NCM622 cathode at 0.1 C after 20 cycles at room temperature

CHAPTER 5:

Ionic Liquid Boosting the Electrochemical Stability of a Poly(1,3-dioxolane) Solid Electrolyte for High-voltage Solid-state Lithium Batteries

1 Statement of Authorship

Statement of Authorship

Title of Paper	Ionic liquid boosting the electrochemical stability of a poly(1,3-dioxolane) solid electrolyte for high-voltage solid-state lithium batteries
Publication Status	☐ Published ☐ Accepted for Publication ☐ Submitted for Publication ☑ Unpublished and Unsubmitted work written in manuscript style
Publication Details	Tianhua Chen, Jiaxin Liu, Dusan Losic, Jian Wang Haitao Zhang

Principal Author

Name of Principal Author (Candidate)	Tianhua Chen		
Contribution to the Paper	Prepared, edited and revised the manuscript.		
Overall percentage (%)	85%		
Certification:	This paper reports on original research I conducted during the period of my Higher Degree by Research candidature and is not subject to any obligations or contractual agreements with a third party that would constrain its inclusion in this thesis. I am the primary author of this paper.		
Signature		Date	23/04/2023

Co-Author Contributions

By signing the Statement of Authorship, each author certifies that:

i. the candidate's stated contribution to the publication is accurate (as detailed above);
ii. permission is granted for the candidate in include the publication in the thesis; and
iii. the sum of all co-author contributions is equal to 100% less the candidate's stated contribution.

Name of Co-Author	Jiaxin Liu		
Contribution to the Paper	Edited and revised the manuscript.		
Signature		Date	23/04/2023

Name of Co-Author	Dusan Losic		
Contribution to the Paper	Supervised the development of work, edited and revised the manuscript, and acted as the corresponding author.		
Signature		Date	23/04/2023

2

Please cut and paste additional co-author panels here as required.

Name of Co-Author	Jian Wang		
Contribution to the Paper	Edited and revised the manuscript, and acted as the corresponding author.		
Signature		Date	23/04/2023

Name of Co-Author	Haitao Zhang		
Contribution to the Paper	Co-supervised and revised manuscript, and acted as the corresponding author.		
Signature		Date	23/04/2023

Ionic liquid boosting the electrochemical stability of a poly(1,3-dioxolane) solid electrolyte for high-voltage solid-state lithium batteries

Tianhua Chen[a,b], Jiaxin Liu[b,c], Dusan Losic[a]*, Jian Wang[d]*, Haitao Zhang[b]*

[a]*School of Chemical Engineering and Advanced Materials, The University of Adelaide, Adelaide, SA 5005, Australia*

[b]*Institute of Process Engineering, Chinese Academy of Sciences, 100190, Beijing, China*

[c]*College of Chemical Engineering, Shenyang University of Chemical Technology, Shenyang, 110142, P. R. China*

[d]*Helmholtz Institute Ulm (HIU), Ulm D89081, Germany*

Corresponding author email: Dusan Losic, dusan.losic@adelaide.edu.au (D. Losic), Jian Wang, Jian.wang@kit.edu (J. Wang), Haitao Zhang, htzhang@ ipe.ac.cn (H. Zhang)

Abstract

The high-voltage performance of solid-state lithium batteries is severely hindered by poor interfacial contact between solid-state electrolytes and electrodes. To address this problem, a new liquid electrolyte is proposed by in-situ polymerization, with the addition of the FEC (Fluoroethylene carbonate) solvent and ionic liquid PP14TFSI(1-butyl-1-methylpiperidinium bis(trifluoromethylsulfonyl)imide). The incorporation of FEC solvent and $PP_{14}TFSI$ is proposed to have a synergistic effect, resulting in fast Li ion transportation of lithium ions with a transfer number of 0.58 and improved electrochemical performance. The presence of FEC serves to protect current collectors from corroding by $LiPF_6$ salt, and also promotes the formation of a protective interfacial layer at room temperature. Meanwhile, $PP_{14}TFSI$ has a beneficial effect on improving interfacial contact and providing stable components for the interfacial layer. As the electrochemical process takes place, a layer is formed at the interface between the in-situ polymerization electrolyte and electrodes, which consists of composites of fluorine and nitrogen. This layer effectively prevents side reactions from occurring at the interface. The $LiCoO_2$||PPE||Li cell demonstrates strong cycling stability at a high voltage of 4.45 V, maintaining approximately 80% of its capacity after 200 cycles at room temperature with both 0.2 C and 1 C charging rates, and also exhibits a notable increase in coulombic efficiency. Additionally, the NCM811||PPE||Li cell also displays exceptional cycling performance. Overall, the use of in-situ polymerization and coordination of FEC and ionic liquid is a promising approach enabling the design of solid-state lithium metal batteries with high voltage for practical application not achievable before.

Key words: Ionic liquid, FEC solvent, High-voltage, Interfacial layer

1.Introduction

Solid-state lithium metal batteries have been a subject of interest for several years due to their high energy density and safety. They are considered as the next-generation rechargeable batteries.[1] By using solid-state electrolytes (SSEs), these batteries can overcome the safety hazards associated with low thermal stability, leakage, and flammability of organic liquid electrolytes which is significant problem in commercial lithium-ion batteries.[2] However, the performance of high-voltage lithium metal batteries is hindered by interfacial issues,[3] low conductivity at room temperature, and narrow electrochemical windows of the electrolyte.[4]

Interfacial contact is an important factor in evaluating battery performance. One of the main challenges with lithium metal batteries is the formation of dendrites, which are microscopic, needle-like or mossy-like structures that can grow from the surface of the lithium metal electrode and penetrate the separator, causing short circuits and potentially leading to safety issues.[5] There are several factors that contribute to the formation of dendrites, including the uneven deposition of lithium metal on the electrode surface during charging, the formation of a solid electrolyte interphase (SEI) layer on the electrode surface, and the presence of impurities in the electrolyte. To address these issues, researchers are exploring a variety of strategies, including the use of electrolytes with additives that can improve the stability of the SEI layer, the development of new electrode materials that can reduce the formation of dendrites, and the use of advanced characterization techniques to better understand the fundamental processes that occur at the lithium metal-electrolyte interface.[6]

The use of in-situ polymeric electrolytes can result in higher conductivity and a reduction in interfacial impedance. Additionally, the liquid-state monomer (such as 1,3-dioxolane (DOL)[7] and vinyl carbonate[8]) used before polymerization has better wetting properties for the electrodes, improving the contact performance of interfaces and providing efficient pathways for the transmission of lithium ions.[9] To form high-purity solid-state electrolytes in assembled batteries, the liquid electrolytes are polymerized. However, the interface between the monomers and high-voltage cathode/high-capacity anode can cause unexpected side reactions, hindering the matching process.[9] Therefore, further research and improvement are required for the interface contact and high voltage tolerance in order to realize high specific energy LMBs. To address this, researchers have proposed incorporating ionic liquids as high-conductive materials and li quid plasticizers into polymer matrices, which can increase the volume of amorphous regions and improve the electrochemical performance of LMBs.[10] Therefore, it provides pathways for the movement of Li^+ ions between polymer chains at room temperature. $PP_{14}TFSI$, an ionic liquid with a high electrochemical window (5.2V) and high conductivity, has been utilized in rechargeable magnesium batteries, graphite dual-ion batteries, and Li/S batteries.[11] Fluoroethylene carbonate (FEC) can be used as an additive in the electrolyte of lithium-ion batteries. The role of FEC in lithium-ion batteries is to improve the contact between the electrolyte and electrodes, enhancing battery performance and stability. It can form a protective layer to reduce the volatilization and oxidation of the electrolyte, thereby reducing capacity loss and extending the battery life. In addition, FEC can also reduce the formation of SEI film on the electrode surface, improving battery cycling performance and fast charging capability.[12]

In this work, in-situ polymerized poly(dol) fabricated with ionic liquid $PP_{14}TFSI$ and FEC (shorted for PPE electrolyte) has been proposed to improve key performances of Li metal batteries including high conductivity and Li transfer number of 0.58. To improve the energy density, an effective approach is to match high-potential difference and high-capacity cathodes, such as $LiCoO_2$ (LCO), with polymer electrolytes in Li metal batteries (LMBs). To our knowledge, solid-state lithium metal batteries capable of operating at 4.45 V are rarely seen with poly-DOL electrolyte system. The participtaion of FEC and ionic liquid enable stable interfacial layers between PPE electrolyte and electrodes.

2. Experimental section

2.1. Materials

1-butyl-1-methylpiperidinium bis(trifluoromethylsulfonyl)imide ($PP_{14}TFSI$, 99.99%, Lanzhou Institute of Chemical Physics Co., Ltd.). 1,3-dioxolane (DOL, 99.99%, Sigma-Aldrich), 1,2-Dimethoxyethane (DME, 99.99%, Sigma-Aldrich), fluoroethylene carbonate (FEC, 99.99%, Sigma-Aldrich), lithium bis(trifluoromethanesulfonyl)imide (LiTFSI, 99.99%, Sigma-Aldrich), lithium hexafluorophosphate ($LiPF_6$, 99.99%, Sigma-Aldrich). $LiCoO_2$ (LCO, 4.45 V), $LiNi_{0.8}Co_{0.1}Mn_{0.1}O_2$ (NCM811) and $LiFePO_4$ (LFP) materials were bought from Guangdong Canrd New Energy Technology Co. Ltd.

2.2 Preparation of electrolyte, cathode, and assembly of battery

The polymeric electrolyte (PPE) was synthesized by mixing and in-situ polymerization of DOL monomer, 1M/L LiTFSI salt, FEC solvent, DMC solvent, $PP_{14}TFSI$, PP separator, and

1M/L $LiPF_6$ initiator at room temperature. The electrolyte without the addition of ionic liquids and FEC is named PDOL. he electrolyte with the addition of ionic liquids is named PPE electrolyte, and the content of FEC will be indicated as a percentage in front of it. The LCO or the LFP electrode was prepared by spreading a slurry of active material, super P, and polyvinylidene fluoride (PVDF) onto an Al current collector using a blade. The weight ratio of active material, super P, and PVDF was 8:1:1. The electrodes were then vacuum dried at 100 °C for 12 hours, cut into 14 mm diameter disks, and dried again at 100 °C in vacuum for 12 hours. The loading density of active materials on the cathode was 3 ~ 4 $mg \cdot cm^{-2}$. All the electrolyte preparation and battery assembly procedures were carried out at room temperature in an Ar-filled glove box. The cathode, pre-polymerized electrolyte, and Li metal anode were assembled in a CR 2025 coin cell.

2.3 Characterization

The Nicolet Avatar 360 Spectrometer was used to capture Fourier transform infrared spectroscopy (FT-IR) spectra within a range of 4000-500 cm^{-1}. The Haitich SU8020 scanning electron microscope (SEM) and Transmission electron microscopy (TEM, JEM-2100HR, Japan) was used to examine the surface morphology structure of the samples. In order to examine alterations in both the surface and underlying composition of recycled lithium metal and cathode, X-ray photoelectron spectroscopy (XPS) was conducted using the Thermo Fisher Scientific ESCALAB 250 Xi apparatus with Al Ka radiation (hv=1486.6 eV) as the X-ray source. ^{7}Li NMR measurements were conducted on a JNM-ECZ600R with a resonance frequency of 233MHz.

The differential scanning calorimetry (DSC) was performed with a heating rate of 5 °C min^{-1} to measure their thermal properties by thermogravimetric (Setaram Labsys).

2.4 Electrochemical measurements

The constant-currents charge and discharge cycling performances of Li||PPE||LCO/LFP/NCM811 half cells were tested with a LAND test system (CT2001A, China) with a working voltage of 2.5 - 4.45 V, 2.5 - 4.0 V, 2.8 - 4.3V, separately. The Li||PPE||LCO rate test of charge-discharge current was set at the ones corresponding to C/5, 1 C, (1 C=178 mA g^{-1}) without using a constant-voltage mode at both ends of charge and discharge. The Li||PEE||Li symmetric cells were packed with 16 mm Li metal foil, and the tests were operated by Land setting for galvanostatic cycling with current densities of 0.2, 0.5, 1 mA cm^{-2}, respectively. An Li||PPE||stainless steel (ss) asymmetrical cell was employed for linear scanning voltammetry (LSV), with the working electrode consisting of a stainless-steel sheet as the working electrode, Li foil as the counter electrode and reference electrode, in the Autolab (PGSTAT302N) electrochemical workstation at a scanning rate of 1 mV s^{-1}. The LSV were collected in 2.0 - 6.0 V. Electrochemical impedance spectroscopy (EIS) was carried out in the CHI660E under an open circuit voltage, with a frequency range of 10^5 - 10^{-2} Hz and an amplitude of 5 mV. All the above tests were carried out at 25 °C. The electrochemical floating analysis experiment was conducted by performing constant current and constant voltage tests on the NCM622||pDOL-py||Li battery. The battery was charged with a constant current of 0.05mA to 4.0 V initially, then charged with 4.0 V for 10 hours, and continuously charged with a constant current 0.05 mA to 4.1 V and held

for 10 hours. This process was repeated until the voltage reached to 5.0V. All the Li battery cycles and battery cycling performance were conducted on a Xinwei or LAND battery cycler. The EIS was used to measure the ionic conductivity of polymer electrolyte membranes. The ionic conductivity can be determined using the following equation: $\sigma = L/(D * R)$, where R ($\Omega \cdot cm^2$) represents the bulk resistance of the electrolyte, L represents the thickness of the electrolyte, and D represents the effective area. The transference number (t_{Li^+}) of the battery was determined via chronoamperometry using a constant polarization potential of 10 mV at room temperature. The calculating equation of t_{Li^+} is: $t_{Li^+} = [I_S(\Delta V - R_0 I_0)]/[I_0(\Delta V - R_S I_S)]$, where I_o and I_s correspond to the initial and steady-state currents, R_o and R_s represent the interface resistances before and after polarization.

3. Results and discussion

3.1 In-situ polymerization

The liquid-state electrolyte can be infused into porous electrodes via in-situ polymerization, leading to their conversion into solid-state electrolytes (PPE) within porous channels of the electrode, as depicted in Fig. S1. Therefore, the mass percentage of active materials in the electrodes produced by in-situ polymerization is similar to that of traditional liquid-state batterie. The images in Fig. S1a-b display SEM views of the electrode before and after undergoing in-situ polymerization. The images reveal that the LCO electrode was uniformly coated with a layer of PPE, which was not present in the initial LCO electrode.

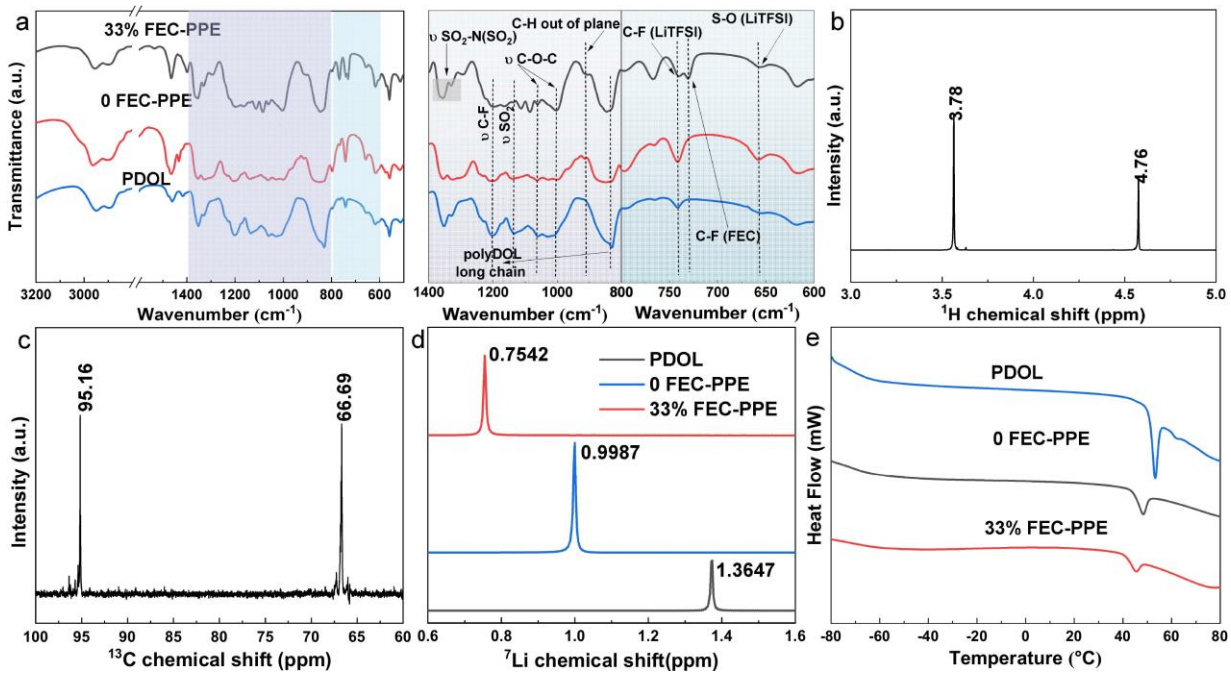

Fig. 1 (a) FTIR spectra of in-situ polymerization (PDOL, PPE electrolyte) samples at room temperature, (b) ^{1}H NMR of in-situ polymerization of PPE, (c) ^{13}C NMR of in-situ polymerization of PPE, (d) ^{7}Li NMR of in-situ polymerization (PDOL, 0 FEC-PPE, and 33% FEC-PPE electrolyte) samples, all the sample were applied deuterated acetone as solvent, (e) DSC curves of PDOL and PPE samples.

Fourier transform infrared spectroscopy (FT-IR) was employed to examine the changes in functional groups of the electrolyte after polymerization, as illustrated in Figure 1a. It seems that the distinct peaks of the cyclic ether in DOL, which were found at 925 and 1096 cm^{-1}, were noticeably absent after the polymerization process.[13] Instead, a sudden appearance of a characteristic peak around 845 cm^{-1} for the O–C–O long chains in PDOL was observed, indicating a successful polymerization process with inevitable DOL monomer retention, as reported.[14] Furthermore, the shifting of the C-O-C vibration at 1010 and 1090 cm^{-1} and the lack

of -CH_2- vibration between 2800 to 3000 cm^{-1} signify that long chain is formed through DOL ring-opening polymerization.[15] The effects of FEC addition on the structure of pDOL segments were investigated in the study. The feature peaks of FEC between 1750 ~ 1800 cm^{-1} illustrates that that there was no chemical reaction between FEC and DOL when undergoing in situ polymerization.[16] The structure and composition information are also confirmed by the ^{1}H and ^{13}C NMR in Fig. 2b-c. It is notable that the hydrogen peaks exhibit chemical shifts after polymerization, the peak at 3.78 and 4.76 ppm corresponds to the H on -O-CH_2-CH_2-O- and -O-CH_2-O- group, respectively.[17] The peaks of ^{13}C NMR at 66.69 and 95.16 ppm corresponds to -O-CH_2-CH_2-O- and -O-CH_2-O- bond, separately. These are consistent with the pDOL structure.[18] Furthermore, the results of FTIR and NMR analyses suggest that there was no chemical reaction between FEC, IL, and DOL during the in situ polymerization of DOL. The incorporation of FEC and IL into the poly-DOL chain framework resulted in the formation of an amorphous region, which led to a reduction in the degree of polymer crystallization. This effect is clearly noticeable in the DSC findings, shown in Fig. 1e. The ^{7}Li NMR carapares the chemical shift of PDOL, 0 FEC-PPE, and 33% FEC-PPE electrolyte sample. The left shift of the peaks represents the increased mobility of Li^{+}, improved the performance of the battery.

3.2 Electrochemical tests of PPE electrolyte

Linear sweep voltammetry (LSV) was applied to examine the electrochemical window of the electrolyte that were polymerized in situ, the results are shown in Figure 2a. It can be observed that the PPE has an electrochemical window wider than 5.2 V. It is obviously that he

addition of FEC and $PP_{14}TFSI$ The Due to the effects of FEC and IL in increasing the operating voltage window of the electrolyte, the electrochemical window of the PPE electrolyte has been significantly enhanced. This is also partly due to the ring-opening polymerization of DOL, which results in the formation of long linear chains.[15] The wider electrochemical window of the PPE suggests that it can be effectively paired with high-voltage cathodes such as LCO and NCM811. The result of the electrochemical floating experiment using NCM622||PPE||Li battery shows that the battery can still operate stably when the voltage reaches 4.6 V (Fig. 2b). When the charge voltage is higher than 4.6 V, which exceeds the voltage window that the electrolyte can withstand, will accelerate the electrolyte decomposition process. Overvoltage charging for the Li anode of the battery means trying to squeeze an excessive number of Li ions into its limited space, resulting in the inability of the Li ions to embed and depositing on the electrode surface, leading to the formation of dendritic growth. As for the cathode, too many Li ions are driven to depart from the cathode lattice structure, affecting the stability of its structure and causing local collapse.

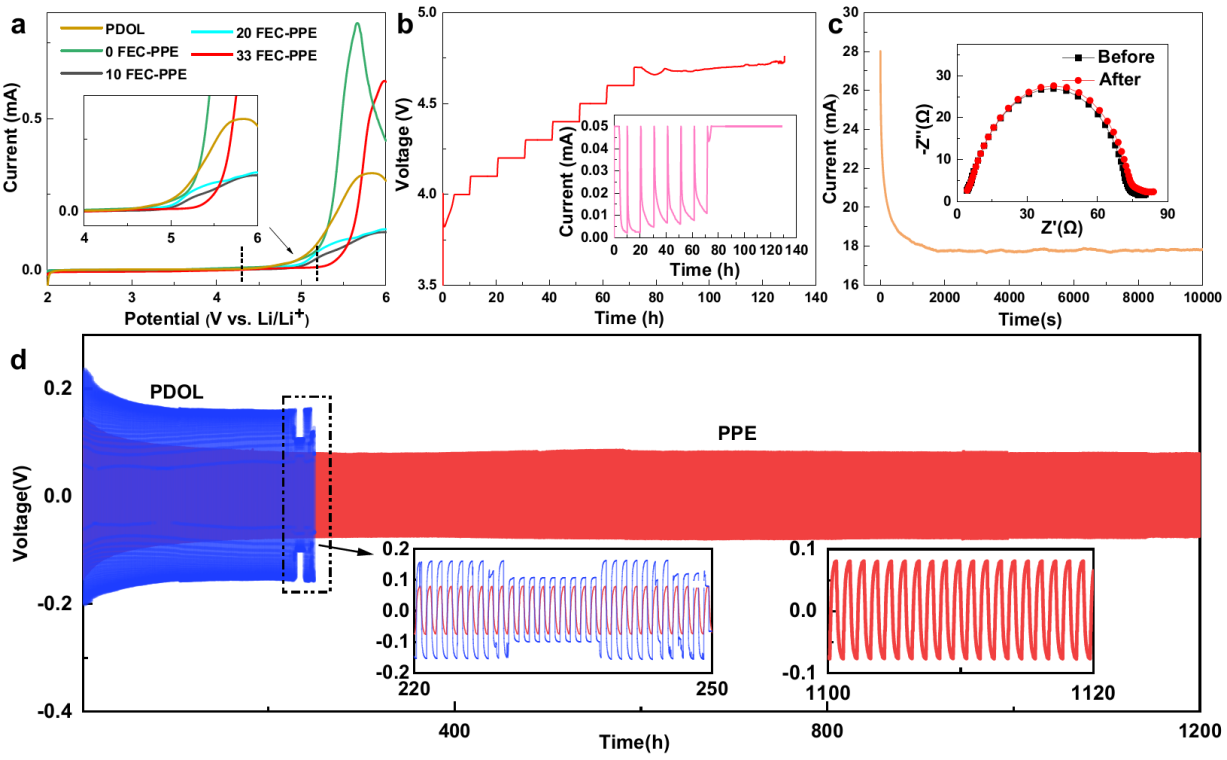

Figure 2 (a) LSV measurements of diffent electrolytes, (b) electrochemical floating analysis of NCM622||PPE||Li battery, (c) current-time curve following DC polarization curves of the PPE electrolyte at room temperature (inset: EIS variation at initial and steady states). (d) Voltage profiles of Li||PPE||Li symmetrical cellat 0.2 mA cm^{-2}, and 0.2 mA h cm^{-2} and room temperature.

The t_{Li^+} value was calculated and the chronoamperometry curves is shown in Fig. 2c, which is 0.58 for the PPE electrolyte, much higher than the PDOL. Effectively increased t_{Li^+} can result in a reduction of concentration polarization for Li^+, prevent the formation of lithium dendrites, and enable faster charging/discharging rates. The enhancement of t_{Li^+} can be attributed to the abundance of free Li ions created by the synergistic effect between the FEC and PP_{14}^+ groups in IL, as confirmed by FTIR, NMR and the following XPS results.

To assess the reversibility of Li plating/stripping in different electrolytes, Li||Li symmetric

batteries were tested at room temperature at different current density, as shown in Fig. 2d and Fig. S2&S3. At a current of 0.2 mA cm^{-2}, the PDOL exhibited a larger initial overpotential about 0.45 V, and underwent a short circuit after 230 h. This implies the unstable interfacial contact, which is caused by the higher polymerization degree of the PDOL. While for the battery with PPE electrolyte, the initial overpotential was about 0.3 V, which slowly reduced to 0.15 V after 100 h, and remained stable for 1200 h. The large initial overpotential maybe caused by the small amount of unpolymerized DOL monomers, which reversed to promote a close interfacial contact, resulting in a stable cycling performance. When the current density increased to 0.5 and 1 mA cm^{-2}, the overpotential increased significantly to 0.2 and 0.3V, separately (Fig. S2 and Fig. S3). The Li||PPE||Li cell demonstrated stable performance at 1 mA cm^{-2}, with no significant increase in polarization even after 100 hours of cycling (as illustrated in Figure S3). This suggests that the system has good compatibility and stability with the Li anode, which is capable of effectively preventing the growth of dendritic lithium.

3.3 Characterization of electrolyte-anode interface

The post-symmetric cells, which contained different electrolytes, underwent 50 cycles at a rate of 0.2 mA cm^{-2} for 0.2 mA h cm^{-2}. Afterwards, the cells were taken apart to observe the surface morphology of the extracted Li metals through SEM, as shown in Fig. 3a-b. It is notable that there was mossy lithium dendrite on the PDOL Li anode, while the surface of PPE cycled Li anode was flat and smooth without lithium dendrite. This phenomenon is consistent with the Li symmetry cycling performance. The chemical composition of the solid electrolyte interphase

(SEI) on Li anode obtained from cycled Li||PPE||Li cells was investigated via XPS. This analysis was carried out after subjecting the cells to 100 hours of cycling at a current density of 0.2 mA cm^{-2}, with PDOL and PPE electrolyte, separately (Fig. 3c-h). The C 1s spectra (shown in Figure 3c) indicate that the SEI layer on Li metal from PDOL battery is responsible for the C-O peak (286.33 eV) and O=C-O peak (289.44 eV). These peaks correspond to the breakdown of DME solvent.[19] The peaks of F 1s at 685.2 and 686.7 eV is assigned to LiF and $Li_xPF_yO_z$, respectively, resulting from the decomposition of $LiPF_6$ salt (Fig. 3e). It has been reported that the SEI layer from a typical $LiPF_6$ system is unstable to support long stability and the $LiPF_6$ corrodes the current collector.[20]

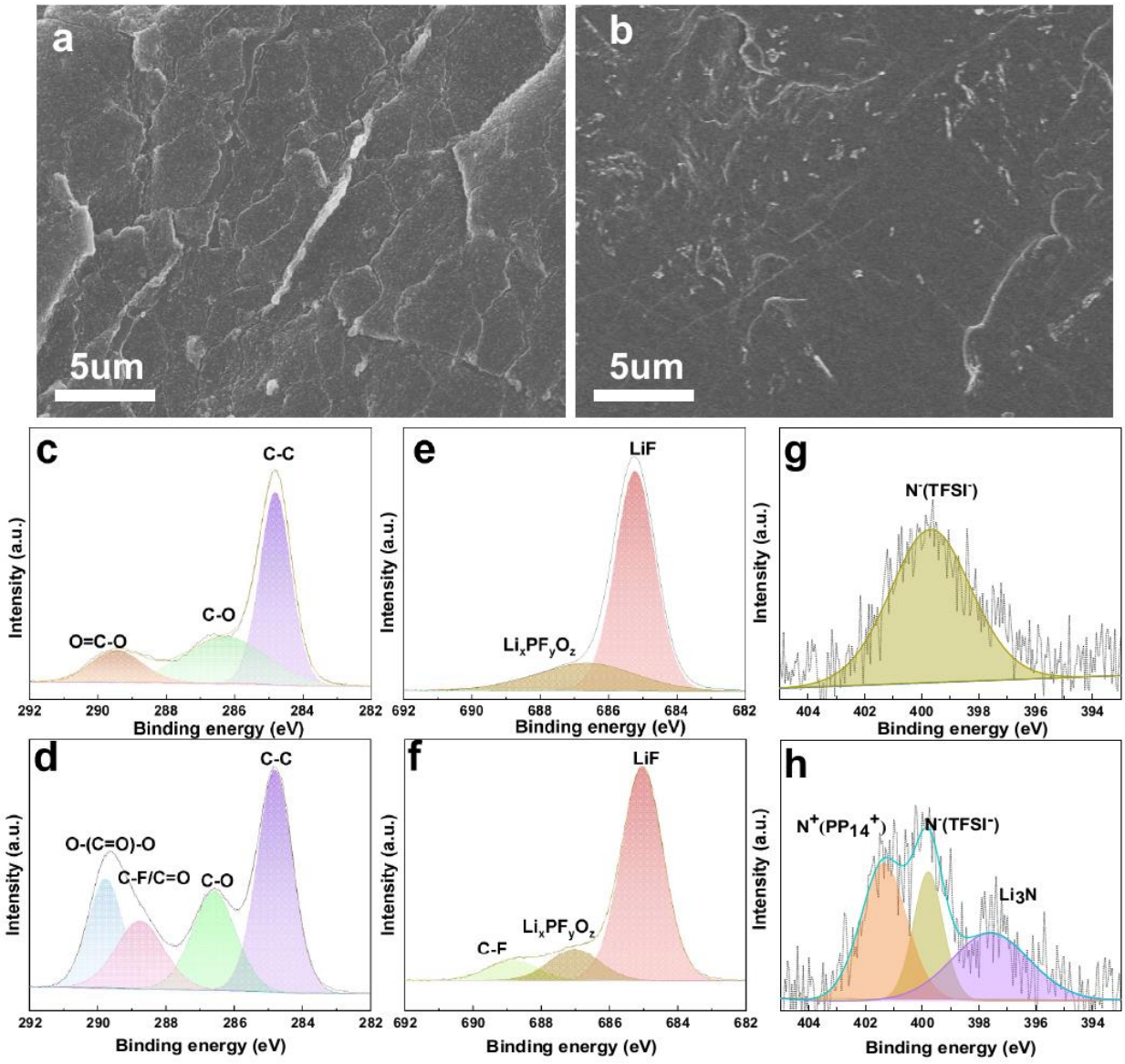

Fig. 3 SEM images of Li anode amphogy with a) PDOL electrolyte, b) PPE electrolyte, XPS spectra (C 1s, F 1s, N 1s) of the Li metal surface from the cycled Li||Li symmetric cells after 50 cycles at 0.2 mA cm^{-2} (c, e, g) PDOL electrolye, and (d, f, h) PPE electrolyte.

FEC has been suggested as a viable electrolyte supplement that boosts the firmness and flexibility of the solid electrolyte interphase (SEI) in Li metal anodes.[21] It has a good ability to stabilize lithium metal negative electrode and can form a dense SEI with high LiF content on the metal lithium negative electrode. Furthermore, adding FEC can alleviate the corrosion of $LiPF_6$

on the battery and help to form stable SEI on the anode and CEI on the cathode.[22] As illustrated in Fig. 3d and f, the existence of FEC leads to the formation of LiF (685.2 eV) and C-F (688.8 eV) coating the surface of Li metal. The LiF found in the solid electrolyte interphase (SEI) layer possesses a high level of mechanical strength and interface energy, which aids in improving the mechanical resilience of the SEI and prevents the growth of lithium dendrites. While too much LiF will lead to the increasement of the interfacial impedance and polarization, the C - F bond has the characteristic of a semi-ionic bond, greatly increasing the electrochemical reactivity and lipophilicity of the electrolyte. In addition, the decomposition of FEC on the Li metal causes the emergence of the C-O peak (286.6 eV), C-F/C=O peak (288.7 eV), and O-(C=O)-O peak (289.9 eV) within the SEI layer, as observed in the C 1s spectra.[12] The result suggest that the stability of the electrode/electrolyte interface in battery with PPE electrolyte was enhanced by the formed LiF riched SEI film.

In N 1s spectra, the peak at approximately 399.8 eV is linked to imide groups found in LiTFSI salt or $PP_{14}TFSI$, as shown in Fig. 3g and h. Meanwhile, the presence of N^- in Li_3N and N^+ in PP_{14}^+ results in two additional peaks at 397.5 and 401.3 eV, separately.[23] As a result, the $PP_{14}TFSI$ ionic liquid in the PPE electrolyte system modifies the SEI layers on the Li metal surface, creating a protective interphase that remains stable during cycling and reduces side reactions between the electrolyte and Li metal. Moreover, PPE electrolyte system promotes the production of Li_3N during cycling, which helps to prevent the growth of Li dendrites. In addition, it can be deduced that the role of $PP_{14}TFSI$ ionic liquid, in this system has the ability to wet the interface, increase the electrochemical window, and reduce the crystallinity of the polymer. The

interface of the electrolytes and electrodes is an important factor in measuring battery performance.

There is no signal indicating the decomposition of DOL monomer, and PDOL which confirms that the SEI rich in LiF resulting from FEC decomposition can effectively prevent the reaction between the electrolyte and lithium metal, ultimately leading to improved electrochemical performance. The improved cycling performance of Li||PPE||Li cells, which have dendrite-free and compact lithium on the lithium metal surface, can be explained by the presence of a stable LiF riched SEI, excellent interfacial contact, and a reduced Li nucleation overpotential. These factors coordinated to protect the lithium anode and prevent the growth of dendritic lithium.

3.4 Cycling performance matched with high-voltage cathodes

With high Li^+ transport and remarkable stability towards lithium metal at room temperature, the PPE electrolyte enable high voltage performance of batteries with different cathodes. Batteries with a high-voltage and capacity $LiCoO_2$ cathode were assembled and tested from 3 to 4.45 V at room temperature. Fig. 4 show the cycling performance of LCO ||PEE||Li batteries with PPE at room temperature (25 °C). After being active for 5 cycles at 0.1 C, the initial discharge specific capacity of $LiCoO_2$||PPE||Li at 0.2 C is 167.5 mAh g^{-1}, higher than that of $LiCoO_2$||PDOL||Li battery (Fig. S4), showing a better compatibility against high-voltage cathodes. And the capacity retain is 78.9% after 200 cycles (88.6% after 100^{th}), with a stable combomlic efficiency. As a contrast, the $LiCoO_2$||PDOL||Li battery decayed sharply and suffered

unstable comlombic efficiency. The discharge specific capacity of $LiCoO_2$||PPE||Li battery is 174.2, 167.5, 154.2, 140.5, and 107.8 mAh g^{-1}, corresponding to 0.1 C, 0.2 C, 0.5 C, 1 C, and 2 C, respectively. Fig. S5 display the TEM image of $LiCoO_2$ cathode after cycled for 20 cycles at 0.1 C, the CEI layer is uniform and with a thickness of 12 nm. The CEI, which is both thin and robust, has the dual capability of inhibiting undesirable reactions between the cathode and electrolyte, as well as lowering the energy barrier for the diffusion of Li ions on the surface.

NCM811 cathode was also applied to test value the PPE electrolyte at room temperature, as depicted in Fig. 5. NCM811||PPE||Li batteries were assembled and tested from 3.0 to 4.3 V at room temperature. The discharge specific capacity of NCM811||PPE||Li cell is 181.9, 162.7, 144.7, 143.6, 117.4 mA h g^{-1}, corresponding to 0.1 C, 0.5 C, 1 C, 2 C, 5 C, respectively (Fig. 5b). With a high and stable Combomlic efficiency, the NCM811||PPE||Li cell exhibits excellent cycling performance at 1 C, from the initial 139.5 mA h g^{-1} to 130.2 mA h g^{-1} after 140 cycles. The capacity retain is 93.3% with slight decay in each cycle, and the average Combomlic efficiency is 99.9%, indicating high compatibility of PPE electrolyte and NCM811 cathode. The TEM image of NCM811 after cycled at 0.1C for 10 cycles demonstrates an even and uniform CEI layer with a thickness of only 8 nm.

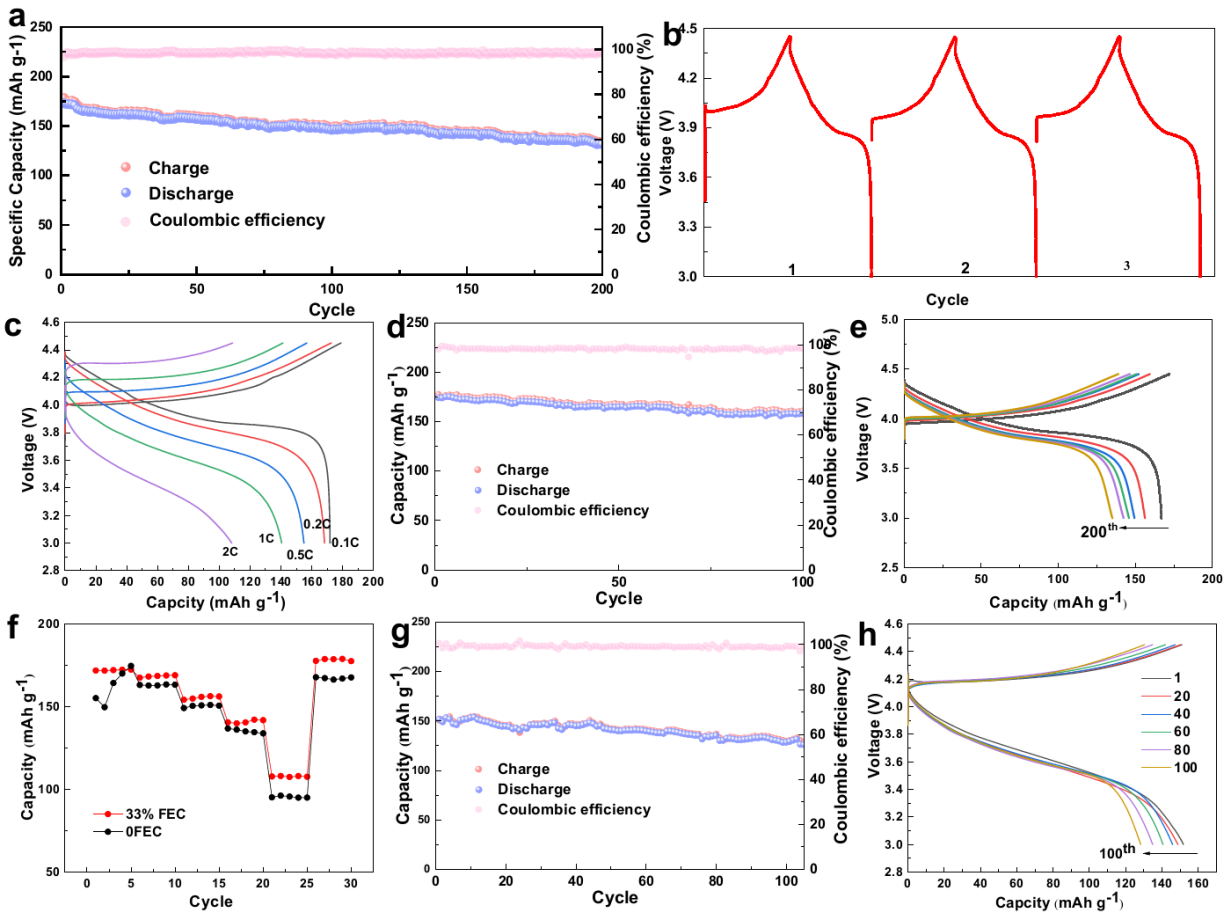

Figure 4 Electrochemical performance of $LiCoO_2$||PPE||Li cells: a) Cycling performance at 0.2 C, b) voltage file, c) galvanostatic charge/discharge curve at different rates, d) cycling performance of at 0.1 C, e) galvanostatic charge/discharge curve at 0.2 C, f) rate performance of, g) at 1 C, h) galvanostatic charge/discharge curve at 1 C. All the tests were conducted at room temperature.

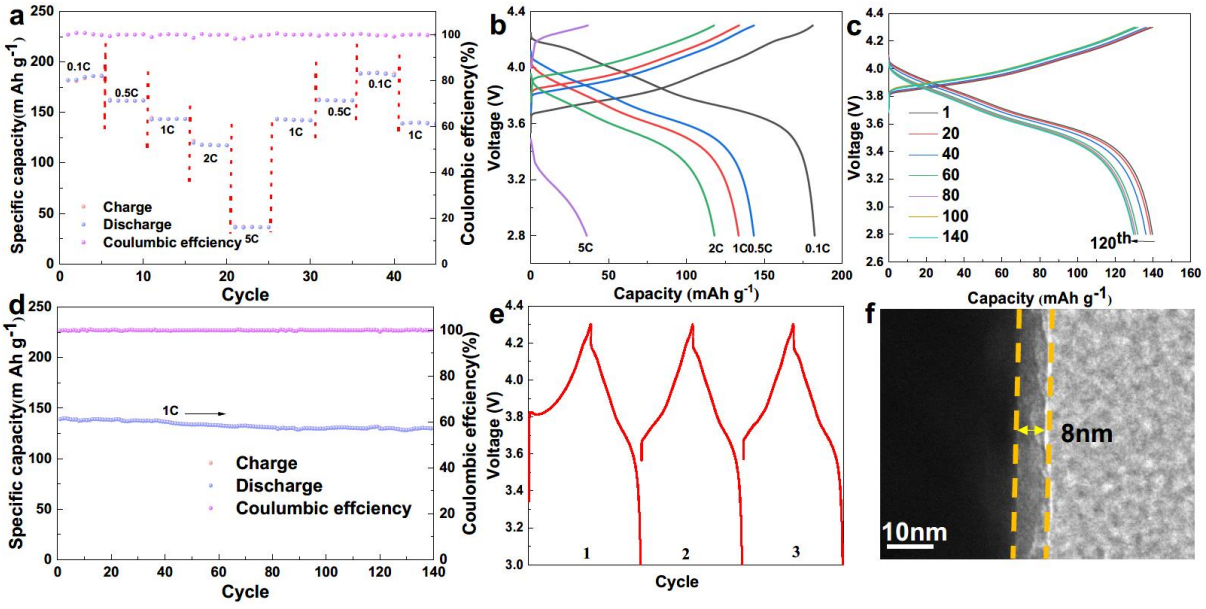

Figure 5 Electrochemical performance of NCM811||PPE||Li cells: a) Rate performance, b) galvanostatic charge/discharge curve at different rates, c) galvanostatic charge/discharge curve at 1C, d) cycling performance of at 1 C, e) voltage file, f) TEM image of NCM811 after cycled at 0.1C for 10 cycles. All the tests were conducted at room temperature.

The PPE has played a crucial role in enhancing the cycling performance of the $LiCoO_2$||Li or NCM811||Li cell by effectively preventing undesirable reactions between the in-situ polymerization electrolyte and electrodes. It was made possible by the presence of the protective interfacial layer consisting of nitrogen and fluorine composites offered by FEC solvent and $PP_{14}TFSI$. The synergistic effect of FEC and ionic liquid $PP_{14}TFSI$ results in the formation of a stable interfacial layer in the battery, thereby leading to excellent electrochemical performance.

4. Conclusion

In summary, a new solid-state electrolyte by in-situ polymerization, which involves the

addition of the FEC solvent and ionic liquid PP14TFSI is developed and demonstrated. The inclusion of FEC solvent and $PP_{14}TFSI$ was shown serve for a multiple purpose in this system, leading to rapid propagation of lithium ions and good electrochemical performance. FEC has the role of impeding current collector corrosion resulting from $LiPF_6$, as well as encouraging the formation of a passivate interfacial layer at room temperature. In other hand, the $PP_{14}TFSI$ has a positive effect on enhancing interfacial contact, and offering stable components for the interfacial layer. During the electrochemical process, an interfacial layer is formed that contains fluorine and nitrogen composites, effectively inhibiting side reactions at the interface between the in-situ polymerization electrolyte and electrodes. The $LiCoO_2$||PPE||Li cell exhibits good cycling performance at a high voltage of 4.45 V, with a capacity retention of around 80% after 200 cycles at 0.2 C and 1 C room temperature, and a significant improvement in coulombic efficiency. The NCM811||PPE||Li cell also conducts excellent cycling performance. Overall, the use of in-situ polymerization and proposed effect of FEC and ionic liquid has the potential to enable the design of solid-state lithium metal batteries with high voltage for practical application.

Declaration of Competing Interest

The authors declare that they have no known competing financial interests or personal relationships that could have appeared to influence the work reported in this paper.

Acknowledgements

The authors thank the Australian Government for providing Tianhua Chen with Beacon of Enlightenment PhD Scholarship to undertake PhD at the University of Adelaide and Institute of

Process Engineering, Chinese Academy of Sciences. This work was partly supported by Australian Research Council (ARC), ARC research Hub for Graphene enabled industry transformation (IH 150100003), ZhongKe-YuNeng Joint R&D center (No. ZKYN2022006), and the International Cooperative Project of CAS (No.122111KYSB20210012).

Reference

[1] J. Liang, J. Luo, Q. Sun, X. Yang, R. Li, X. Sun, *Energy Storage Materials* **2019**, *21*, 308-334.

[2] aY. Zheng, Y. Yao, J. Ou, M. Li, D. Luo, H. Dou, Z. Li, K. Amine, A. Yu, Z. Chen, *Chemical Society Reviews* **2020**, *49*, 8790-8839; bS. Ma, M. Jiang, P. Tao, C. Song, J. Wu, J. Wang, T. Deng, W. Shang, *Progress in Natural Science: Materials International* **2018**, *28*, 653-666.

[3] Q. Yang, J. Huang, Y. Li, Y. Wang, J. Qiu, J. Zhang, H. Yu, X. Yu, H. Li, L. Chen, *Journal of Power Sources* **2018**, *388*, 65-70.

[4] aS. Xu, Z. Sun, C. Sun, F. Li, K. Chen, Z. Zhang, G. Hou, H.-M. Cheng, F. Li, *Adv. Funct. Mater.* **2020**, *30*, 2007172; bY. Wang, Y. Wu, Z. Wang, L. Chen, H. Li, F. Wu, *J. Mater. Chem. A* **2022**, *10*, 4517-4532.

[5] Y.-Y. Sun, F. Li, P.-Y. Hou, *Journal of Materials Chemistry A* **2021**, *9*, 9481-9505.

[6] K. Xu, *Chemical Reviews* **2014**, *114*, 11503-11618.

[7] aJ.-Y. Liang, X.-D. Zhang, X.-X. Zeng, M. Yan, Y.-X. Yin, S. Xin, W.-P. Wang, X.-W. Wu, J.-L. Shi, L.-J. Wan, Y.-G. Guo, *Angew. Chem. Int. Ed.* **2020**, *59*, 6585-6589; bQ. Ma, J. Yue, M. Fan, S.-J. Tan, J. Zhang, W.-P. Wang, Y. Liu, Y.-F. Tian, Q. Xu, Y.-X. Yin, Y. You, A. Luo, S. Xin, X.-W. Wu, Y.-G. Guo, *Angew. Chem. Int. Ed.*, *n/a*; cQ. Liu, B. Cai, S. Li, Q. Yu, F. Lv, F. Kang, Q. Wang, B. Li, *Journal of Materials Chemistry A* **2020**, *8*, 7197-7204.

[8] Q. Zhou, C. Fu, R. Li, X. Zhang, B. Xie, Y. Gao, G. Yin, P. Zuo, *Chemical Engineering Journal* **2022**, *437*, 135419.

[9] Q. Zhao, X. Liu, S. Stalin, K. Khan, L. A. Archer, *Nature Energy* **2019**, *4*, 365-373.

[10] aX. Tang, S. Lv, K. Jiang, G. Zhou, X. Liu, *Journal of Power Sources* **2022**, *542*, 231792; bG. Yang, Y. Song, Q. Wang, L. Zhang, L. Deng, *Materials & Design* **2020**, *190*, 108563.

[11] aW. Ren, D. Wu, Y. NuLi, X. Zhang, J. Yang, J. Wang, *ACS Appl. Mater. Interfaces* **2021**, *13*, 32957-32967; bZ. Zhao-Karger, X. Zhao, D. Wang, T. Diemant, R. J. Behm, M. Fichtner, *Adv. Energy Mater.* **2015**, *5*, 1401155; cJ. Fan, Z. Zhang, Y. Liu, A. Wang, L. Li, W. Yuan, *Chem. Commun.* **2017**, *53*, 6891-6894.

[12] X.-Q. Zhang, X.-B. Cheng, X. Chen, C. Yan, Q. Zhang, *Advanced Functional Materials* **2017**, *27*, 1605989.

[13] H. Yang, B. Zhang, M. Jing, X. Shen, L. Wang, H. Xu, X. Yan, X. He, *Advanced Energy Materials* **2022**, *12*, 2201762.

[14] J. Zhou, T. Qian, J. Liu, M. Wang, L. Zhang, C. Yan, *Nano Letters* **2019**, *19*, 3066-3073.

[15] J. Yu, X. Lin, J. Liu, J. T. T. Yu, M. J. Robson, G. Zhou, H. M. Law, H. Wang, B. Z. Tang, F. Ciucci, *Advanced Energy Materials* **2022**, *12*, 2102932.

[16] Z. Li, W. Tang, Y. Deng, M. Zhou, X. Wang, R. Liu, C.-a. Wang, *Journal of Materials Chemistry A* **2022**, *10*, 23047-23057.

[17] J. Ma, Y. Wu, H. Jiang, X. Yao, F. Zhang, X. Hou, X. Feng, H. Xiang, *ENERGY & ENVIRONMENTAL MATERIALS*, *n/a*.

[18] K. Khan, Z. Tu, Q. Zhao, C. Zhao, L. A. Archer, *Chemistry of Materials* **2019**, *31*, 8466-8472.

[19] Z. Geng, Y. Huang, G. Sun, R. Chen, W. Cao, J. Zheng, H. Li, *Nano Energy* **2022**, *91*, 106679.

[20] C.-C. Su, M. He, R. Amine, Z. Chen, R. Sahore, N. Dietz Rago, K. Amine, *Energy Storage*

Materials **2019**, *17*, 284-292.

[21] T. Hou, G. Yang, N. N. Rajput, J. Self, S.-W. Park, J. Nanda, K. A. Persson, *Nano Energy* **2019**, *64*, 103881.

[22] Q. Wu, M. T. McDowell, Y. Qi, *Journal of the American Chemical Society* **2023**, *145*, 2473-2484.

[23] J. Zheng, M. Gu, H. Chen, P. Meduri, M. H. Engelhard, J.-G. Zhang, J. Liu, J. Xiao, *Journal of Materials Chemistry A* **2013**, *1*, 8464-8470.

Supporting information

Ionic liquid boosting the electrochemical stability of a poly(1,3-dioxolane) solid electrolyte for high-voltage solid-state lithium batteries

Tianhua Chen[a,b], Jiaxin Liu[b,c], Dusan Losic[a]*, Jian Wang[d]*, Haitao Zhang[b]*

[a]*School of Chemical Engineering and Advanced Materials, The University of Adelaide, Adelaide, SA 5005, Australia*

[b]*College of Chemical Engineering, Beijing University of Chemical Technology, Beijing, 100029, China*

[c]*College of Chemical Engineering, Shenyang University of Chemical Technology, Shenyang, 110142, P. R. China*

[d]*Helmholtz Institute Ulm (HIU), Ulm D89081, Germany*

Corresponding author email: Dusan Losic, dusan.losic@adelaide.edu.au (D. Losic), Jian Wang, Jian.wang@kit.edu (J. Wang), Haitao Zhang, htzhang@ ipe.ac.cn (H. Zhang)

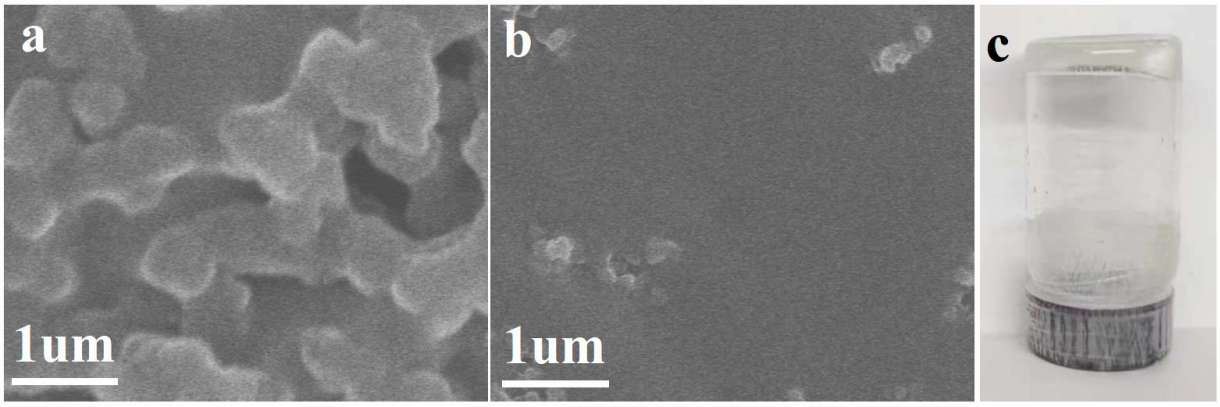

Figure S1 SEM image of surface of (a) blank $LiCoO_2$ electrode, (b) $LiCoO_2$ electrode after in-situ polymerization with PPE electrolyte at room temperature, (c) photograph of electrolyte after in-situ polymerization at room temperature

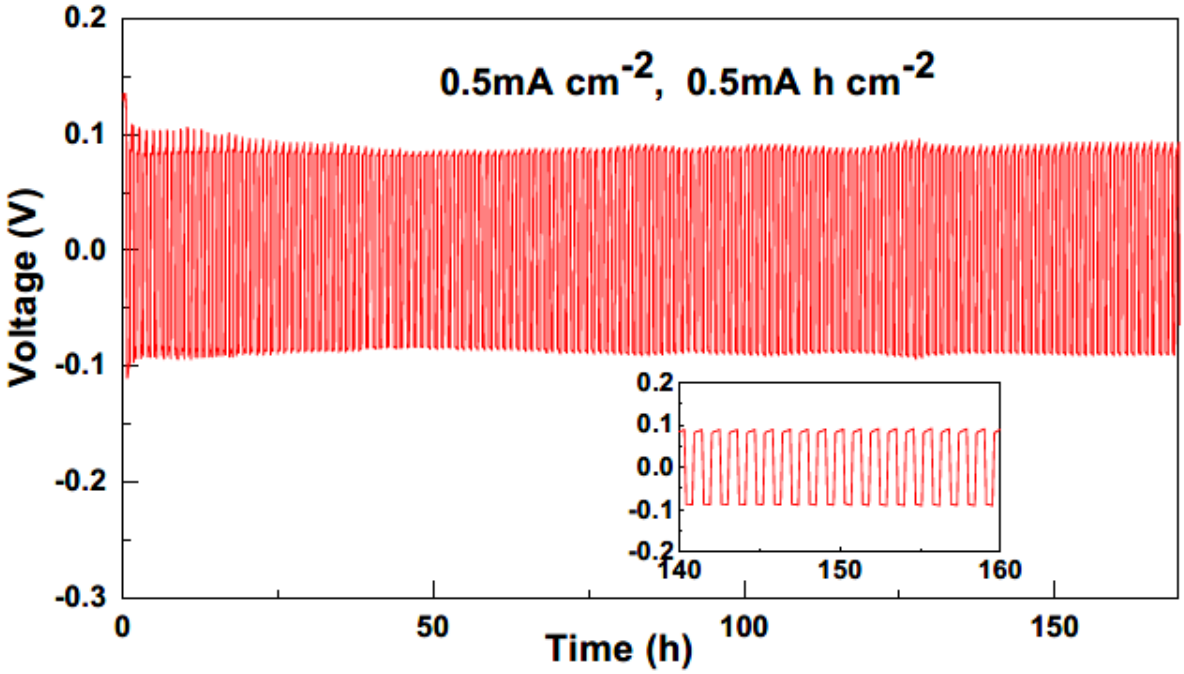

Figure S2 Voltage profiles of Li||PPE||Li symmetrical cell at 0.5 mA cm^{-2}, 0.5 mA h cm^{-2} and room temperature

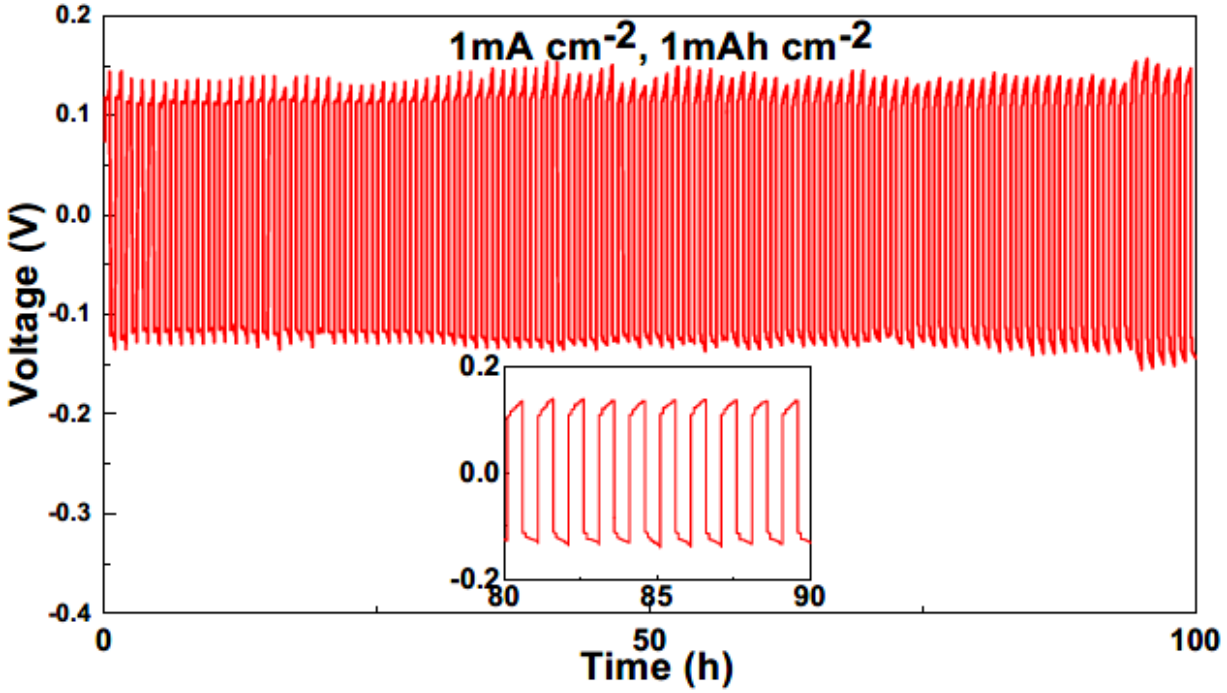

Figure S3 Voltage profiles of Li||PPE||Li symmetrical cellat 1 mA cm^{-2}, 1 mA h cm^{-2} and room temperature

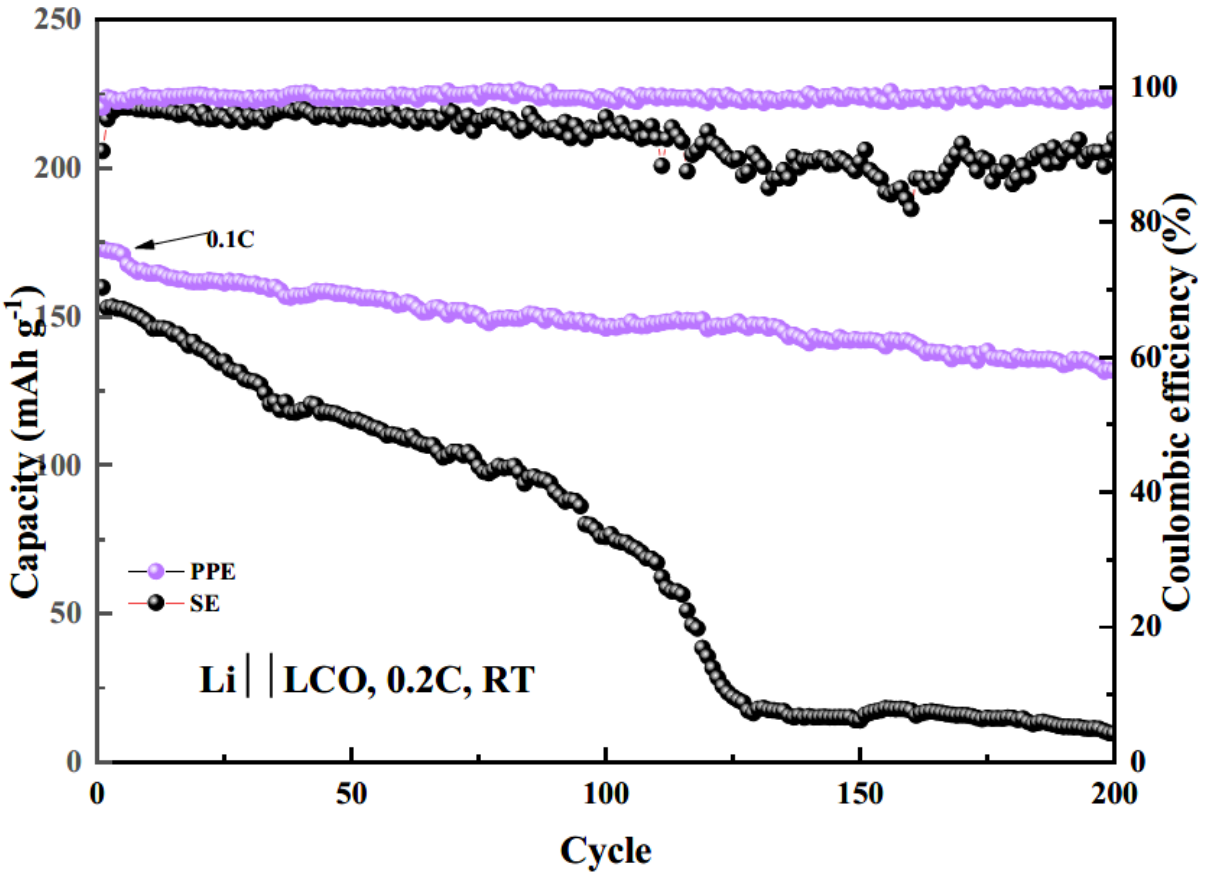

1

2 Figure S4 Comparation of voltage profiles of LCO||PPE||Li and LCO||PDOL||Li cells at 1 C and

3 room temperature

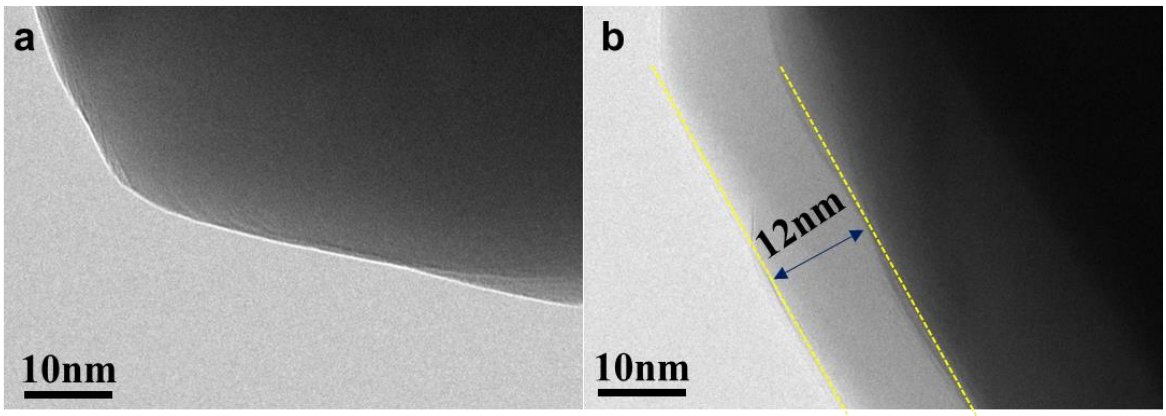

4

5 Fig. S5 TEM images of $LiCoO_2$ cathode: (a) fresh, (b) cycled for 20cycles at 0.1 C at room

6 temperature

CHAPTER 6:

Conclusions and Recommendations

6.1 Conclusions

In this thesis, new perspectives have been presented regarding the utilization of ionic liquids in solid-state electrolytes for the purpose of enhancing the efficiency of solid-state lithium metal batteries. The primary aim of this comprehensive study is to address issues such as the formation and growth of Li dendrite, and to improve the ionic conductivity of polymer electrolytes, as well as to enhance the interface stability between the solid-state electrolyte and electrodes. As a result, the performance of the battery has been greatly improved: the cycle stability of the battery has been significantly enhanced, the operating voltage of the polymer battery has been widened, and the capacity of the polymer solid-state lithium battery has been improved. Based on the research outcomes discussed in this thesis, main contributions can be summarized:

1. Advancing of fundamental understanding the influence of ionic liquids on the performance of solid electrolytes and the structural design of solid electrolytes. This work provides a detailed introduction to the properties of ionic liquids and the problems and challenges faced by solid electrolytes for the solid-state Li metal batteries, as well as the application of ionic liquids in electrolytes. The paper in chapter 2 partly focuses on the review of recent advancements in the utilization of ionic liquids (ILs) and metal-organic frameworks (MOFs) in solid-state electrolytes (SSEs) for various metal batteries including lithium, sodium, magnesium, aluminum, and zinc.

2. By infused the ionic liquid into MOF-5 framework, Chapter 3 showcased a solid-state PIM electrolyte, resulting in a close and nano-wetted interface that facilitates high ionic

conductivity. The IL and MOF were effectively integrated with Li^+ through chemical bonding. The improved lithium transference number of 0.65 was observed as a result of the PIM electrolyte's interfacial contact. The PIM electrolyte proved to be compatible with both the LFP/NCM622 cathode and Li metal anode, displaying uniform Li deposition and stable interfacial contact. The PIM electrolyte also demonstrated high electrochemical activity and capacity retention over long cycling in the LFP||PIM||Li cell at varying rates. The uniform Li deposition was due to the confinement of anions in the MOF host network, which resulted in a thick and uniform CEI layer on the cathode. The study suggests that IL@MOF-based electrolytes have the potential to enhance the performance of Li-based batteries and other energy storage devices by modifying the type of ionic liquid or host material used.

3. A gel electrolyte including an ionic liquid has been developed by in-situ polymerizing on the electrospinning PAN separator. This presented in Chapter 4 results in improved Li^+ transport, high ionic conductivity, enhanced oxidative stability, and an extended operating temperature range, leading to a significant improvement in high cycling performance. The interfacial wettability is also increased by the ionic liquid infusion. The compatibility of the gel electrolyte with Li anode was improved, inhibiting dendrite formation and enhancing long-term cycling stability with LFP cathode. Consequently, the electrolyte can be used in a temperature range of -20 °C to 20 °C. In addition, Li symmetrical cells exhibited stable cycling at different current densities. After 1000 cycles at 2 C, the LFP||pDOL-py||Li cell demonstrated high specific capacity, Coulombic efficiency, and capacity retention. This study presents a convenient approach for achieving wide-temperature applications in solid-

state Li batteries.

4. The application of solid electrolytes in high-voltage batteries such as $LiCoO_2$/Li (4.45 V) and NCM811/Li (4.3 V) presented in Chapter 5 was studied by adding an ionic liquid and FEC. A detailed analysis was conducted on the anode and cathode electrodes of the lithium metal batteries after cycling. The results showed that the electrolyte effectively suppressed the growth of lithium dendrites. Electrochemical test results showed that the battery could cycle stably at high voltage (4.45 V) and could operate at 1 C rate at 4.3 V, due to the excellent ionic conductivity and LiF-riched SEI layer in in this battery system, which is more conducive to the specific capacity of $LiCoO_2$ and NCM811.

5. Ionic liquid in this thesis presented multiple function. Ionic liquids are used as solid-state electrolyte materials to wet the interface, contribute to the SEI film components, and enhance the intension of hydrogen bonding. In addition, by using different types of ionic liquids, the electrochemical window of the battery has been improved to varying degrees, resulting in improved performance and increased Li ion transport and ion conductivity.

6.2 Recommendations for Future Work

The results presented in this thesis have advanced our understanding of the application of ionic liquid participating in solid-state electrolyte in the solid-state Li metal batteries. More research is needed to deep understand the role of ionic liquids on solid-state lithium batteries.

1. Studying the solubility and diffusion coefficient of ionic liquids can optimize the performance of solid-state lithium batteries. The diffusion coefficient refers to the diffusion

rate of ionic liquids in the solid-state electrolyte and is also one of the important parameters of the performance of solid-state lithium batteries. The diffusion coefficient can be obtained through experimental and computational simulation methods. By studying the diffusion coefficient of ionic liquids, we can better understand the transport performance of ionic liquids in solid-state electrolytes and further optimize the performance of solid-state lithium batteries.

2. Establishing a reaction kinetics model between ionic liquids and solid-state lithium battery electrolytes can predict the performance and lifespan of the battery. The reaction between ionic liquids and solid-state lithium battery electrolytes can cause changes in battery performance and lifespan. Therefore, understanding and establishing this reaction kinetics model can predict the performance and lifespan of the battery that is suggested in further studies.

3. By changing the molecular structure and functionalizing of ionic liquids, their performance and application range in solid-state electrolytes can be improved. The properties and performance of ionic liquids depend on their molecular structure and chemical composition, and by changing these factors, their properties and performance can be controlled and improved. Furthermore, by combining them with different solid-state electrolytes, a wider range of applications can be achieved.

4. Developing higher performance ionic liquids is the key to achieving higher performance solid-state batteries. Here are some methods to find ionic liquids with higher ion conductivity,

lower viscosity, and better compatibility with solid-state electrolyte materials:

a. Structural optimization: By designing the structure of ionic liquid molecules, their ion conductivity can be improved. For example, increasing the number of ions in the ionic liquid, changing the size and shape of the ions, etc., can improve the ion conductivity of the ionic liquid.

b. Additives: Adding additives to the ionic liquid, such as small molecule compounds or polymers, can improve its physical and electrochemical properties. Adding additives can reduce the viscosity of the ionic liquid and improve its ion conductivity.

c. Compatibility between ionic liquids and solid-state electrolytes: By selecting appropriate ionic liquids, better compatibility with solid-state electrolyte materials can be achieved. For example, selecting ionic liquids and solid-state electrolyte materials with similar chemical structures can reduce the interactions between the two, thereby improving the ion transport rate.

d. Molecular simulation: Molecular simulation techniques can simulate the interactions between ionic liquid molecules and solid-state electrolyte molecules, predict the properties of ionic liquids, and design higher performance ionic liquids.

e. Discovery of new ionic liquids: High-throughput experimental techniques, such as high-throughput synthesis, screening, and testing techniques, can quickly discover new ionic liquids and accelerate the development of new ionic liquids.

5. Although ionic liquids have great potential in solid-state electrolytes, their production cost is

still relatively high, which limits their commercialization in large-scale production. To overcome this problem, researchers have been looking for low-cost and high-performance ionic liquids.

a. There are several methods to reduce the cost of ionic liquids. For example, renewable resources such as lignin, cellulose, and other biomass can be used to prepare ionic liquids. Alternatively, low-cost raw materials such as waste and inexpensive carbon sources can be used to prepare ionic liquids. In addition, developing more efficient synthetic methods and improving the production process of ionic liquids can also reduce their cost.

b. Another way to address the cost issue is to use ionic liquid mixtures. Mixtures are composed of two or more ionic liquids and have lower cost and better performance. In addition, ionic liquid mixtures can change their properties by adjusting the composition ratio, thereby achieving better performance control.